

Aus der Universitäts-Augenklinik Tübingen
Abteilung Augenheilkunde II
Ärztlicher Direktor: Professor Dr. E. Zrenner
Sektion für Neurobiologie des Auges
Leiter: Professor Dr. F. Schaeffel

**Eye growth, optics and visual performance of the
mouse, a new mammalian model to study myopia**

Inaugural-Dissertation
zur Erlangung des Doktorgrades
der Humanwissenschaften

der Medizinischen Fakultät
der Eberhard Karls Universität
zu Tübingen

vorgelegt von
Christine Maria Schmucker

aus
Weiden i. d. Opf.
2005

Dekan:	Professor Dr. C. D. Claussen
1. Berichterstatter:	Professor Dr. F. Schaeffel
2. Berichterstatter:	Professor Dr. H. - P. Mallot

Contents

I. Introduction	1
1. Refractive errors	1
2. Emmetropization	2
3. The control of axial eye growth by visual signals	4
3.1 Refractive errors induced by imposed defocus	4
3.2 Refractive errors induced by deprivation of sharp vision	5
3.3 Local control of eye growth	6
4. How might the eye know which way to grow?	7
4.1 Trial and error	7
4.2 Magnitude of blur	8
4.3 Possible error signals that guide emmetropization	8
4.3.1 Chromatic aberrations	8
4.3.2 Monochromatic aberrations	9
4.3.3 Accommodation	9
5. Pharmacological prevention of myopia	10
6. Human myopia	10
6.1 Epidemiology of myopia	10
6.2 Genetic control of myopia	11
6.3 Risk factors of myopia	11
6.4 Deprivation myopia in infants	12
6.5 Near work and myopia	12
6.6 Optical aberrations and myopia	13
7. Animal models to study myopia	14
7.1 The model of the chicken	14
7.2 The mouse as a new mammalian model to study myopia	15
7.2.1 Advantages of the mouse model	15
7.2.2 Emmetropization in the mouse eye	15
7.2.3 Deprivation myopia in the mouse eye	16
7.2.4 The retina of the mouse eye	16
7.2.5 Visual performance of the mouse	17

7.2.6 Genetic knock-out models	18
7.2.7 Developmental stages of the mouse	19
II. Purpose of the studies	20
III. Material and Methods	21
1. Animals	21
2. A paraxial schematic eye model for the growing C57BL/6 mouse	22
2.1 Infrared photoretinoscopy	22
2.2 Infrared photokeratometry	24
2.3 Frozen sections	25
2.4 Paraxial ray tracing and schematic eyes	26
3. <i>In vivo</i> biometry in the mouse eye with optical low coherence interferometry	27
3.1 Measurement principle	27
3.2 Measurement procedures in living mice	30
3.3 Measurements in mice with normal vision	31
3.4 Measurements in mice that were deprived of sharp vision (“form deprivation”)	31
3.5 Statistics	32
4. Grating acuity at different illuminances in wild-type mice, and in mice lacking rod or cone function	33
4.1 Development of a behavioral paradigm: the automated optomotor drum	33
4.2 Illumination of the drum	35
4.3 Programming algorithms and measured parameters	35
4.4 Measurement procedure	37
4.5 Statistics	39
5. Contrast thresholds of wild-type mice wearing diffusers or spectacle lenses, and the effect of atropine, a myopia inhibiting drug	40
5.1 Optomotor experiment	40
5.2 Measurements under photopic conditions	40
5.3 Measurements in dim light	41

5.4	Measurements in mice wearing spectacle lenses	41
5.5	Measurements in mice wearing diffusers	41
5.6	Measurements after atropine eye drops	42
IV.	Results	43
1.	A paraxial schematic eye model for the growing C57BL/6 mouse	43
1.1	Development of refractive state and pupil size	43
1.2	Growth of the ocular dimensions	45
1.3	Schematic eye modelling	48
1.4	Image magnification and f/number	49
2.	<i>In vivo</i> biometry in the mouse eye with optical low coherence interferometry	51
2.1	Ocular dimensions in animals with normal vision	51
2.1.1	Variability of axial length measurements and comparisons to data from frozen sections	52
2.1.2	Within-animal variability	53
2.1.3	Peripheral axial eye length	54
2.1.4	Corneal thickness	56
2.1.5	Anterior chamber depth	56
2.2	Effects of deprivation of form vision on refractive development and ocular growth	57
3.	Grating acuity at different illuminances in wild-type mice, and in mice lacking rod or cone function	62
3.1	Baseline variability of the measurement procedure	62
3.2	Spatial vision in wild-type mice	63
3.2.1	Grating acuity as measured in a large optomotor drum	63
3.2.2	Grating acuity as measured in a small optomotor drum	65
3.3	Spatial vision in mutant mice	67
3.3.1	Spatial vision in mice lacking rod function (RHO ^{-/-} and CNGB1 ^{-/-})	67
3.3.2	Spatial vision in mice lacking cone function (CNGA3 ^{-/-})	69
3.3.3	Spatial vision in mice lacking both rod and cone function (CNGA3 ^{-/-} RHO ^{-/-})	70

3.4 Comparisons of optomotor responses in wild-type and mutant mice	70
4. Contrast thresholds of wild-type mice wearing diffusers or spectacle lenses, and the effect of atropine, a myopia inhibiting drug	73
4.1 Contrast thresholds under photopic conditions	73
4.2 Contrast thresholds in dim light	74
4.3 Contrast thresholds in mice wearing spectacle lenses	75
4.4 Contrast thresholds in mice wearing diffusers	76
4.5 Contrast thresholds after atropine eye drops	77
V. Discussion	79
1. A paraxial schematic eye model for the growing C57BL/6 mouse	79
1.1 Refractive state and small eye artifact	79
1.2 Growth rates of the globes in various vertebrates	81
1.3 Growth of the ocular elements in various vertebrates	82
1.4 Homogeneous lens index	83
1.5 Retinal image magnification and brightness	84
1.6 Deprivation myopia	84
1.7 Conclusions	85
2. <i>In vivo</i> biometry in the mouse eye with optical low coherence interferometry	86
2.1 Accuracy of the optical low coherence interferometry	86
2.1.1 Axial eye length	86
2.1.2 Corneal thickness	87
2.1.3 Anterior chamber depth	87
2.2 Myopia and axial elongation during deprivation of form vision	88
2.3 Conclusions	89
3. Grating acuity at different illuminances in wild-type mice, and in mice lacking rod or cone function	90
3.1 Evaluation of the optomotor paradigm	90
3.2 Spatial acuity in wild-type mice, compared with other mammals	90
3.3 Grating acuity at different light levels	92
3.4 Refractive state and visual acuity	93

3.5 Spatial acuity in mutant mice	94
3.6 Conclusions	95
4. Contrast thresholds of wild-type mice wearing diffusers or spectacle lenses, and the effect of atropine, a myopia inhibiting drug	96
4.1 Comparisons to contrast thresholds measured in previous studies	96
4.2 Contrast thresholds in dim light	97
4.3 Refractive state inferred from optomotor experiments with lenses	97
4.4 Contrast thresholds after atropine eye drops	98
4.5 Conclusions	98
VI. Summary	100
1. A paraxial schematic eye model for the growing C57BL/6 mouse	100
2. <i>In vivo</i> biometry in the mouse eye with optical low coherence interferometry	101
3. Grating acuity at different illuminances in wild-type mice, and in mice lacking rod or cone function	102
4. Contrast thresholds of wild-type mice wearing diffusers or spectacle lenses, and the effect of atropine, a myopia inhibiting drug	102
VII. References	104
VIII. Publications and presentations in connection with this research work	118
IX. Acknowledgements	119
X. Curriculum Vitae	120

I. Introduction

1. Refractive errors

The refractive state of the eye is determined by the relationship of axial length and focal length of the refracting surfaces of the eye. Focal length, in turn, is determined by corneal curvature, anterior chamber depth and lenticular power. For optimal vision, the image on the retina must be in best focus which requires a highly precise match between axial length and focal length.

If the image of distant objects is in focus on the retina, without accommodation, the eye is said to be emmetropic. Accommodation refers to the ability of the crystalline lens to increase its optical power by changing its radii of curvature and to focus close objects on the retina. Hyperopia (long-sightedness) results, when the eye is relatively too short for its optical power and the image plane of an object at infinity lies behind the retina. However, in young children, hyperopia of up to 2 to 3 diopters (D) can be tolerated without major vision problems, because the retinal image can be focused with additional accommodation efforts. Due to the large available amplitude of accommodation, the additional 3 D required to focus at infinity may not represent a limitation. Myopia (short-sightedness) occurs when the eye grows too long and the image of an object at infinity falls in front of the retina. Accommodation, therefore, cannot clear the blurred image. Theoretically, myopia could either be caused by an excessive power of cornea and lens, or by increased axial length. However, both population and animal studies showed that increased axial length is the major reason for myopia (e.g. humans, McBrien & Millodot, 1987; chicks, Schaeffel, Glasser, & Howland, 1988; rhesus monkeys, Hung, Crawford, & Smith, 1995). In an average adult human eye, a mismatch of axial length and focal length of 1.0 mm produces a refractive error of about 2.7 D.

Astigmatism is an optical imperfection in which the refractive power of the lens or/and the cornea is not uniform in all meridians. Therefore, light rays entering the eye in different meridional planes are differently focused, making it

impossible to obtain a sharply focussed point of light on the retina from a point source in object space.

2. Emmetropization

The eyes of neonates of a variety of species have refractive errors that tend to decline during postnatal development (e.g. chicks, Wallman, Adams, & Trachtman, 1981; marmosets, Graham & Judge 1999; three shrews, Norton & McBrien, 1992; humans, Pennie, Wood, Olsen, White, & Charman, 2001). Most studies conclude that newborn humans are on average moderately hyperopic, with this hyperopia gradually decreasing during infancy and early childhood (e.g. Chan & Edwards, 1993; Pennie et al., 2001). Figure 1 demonstrates the refractive error distribution for infants (0 – 3 months) and children at the age of six after Gwiazda, Thorn, Bauer, & Held (1993). At birth, the hyperopic refractive error distribution is broad and approximately Gaussian distributed, with a mean value of about 2 D hyperopia (Cook & Glasscock, 1951). At six years of age, when axial eye length has grown from initially 17 mm to about 23 mm (Fledelius & Christensen, 1996), the refractive error distribution becomes leptokurtic, with a peak at a slightly hyperopic status.

Obviously, the development of the refractive state is optimized by a mechanism called emmetropization, which involves an adaptation of the focal length to the axial length of the eye. Why some individuals achieve the remarkable degree of precision required for optimal vision, whereas others develop refractive errors like myopia is not well understood. However, there is some evidence both from human (e.g. Zadnik & Mutti, 1987) and animal (e.g. Schaeffel et al., 1988; Irving, Callender, & Sivak, 1991; Smith, Bradley, Fernandes, & Boothe, 1999; Smith & Hung, 1999) studies that visual experience may play an important role:

- ▷ The development of the refractive state in human neonates and infants is very sensitive to visual disturbance (Chapter I. 6.4).
- ▷ Extensive near work is associated with an increase of myopia (Chapter I. 6.5).

- ▷ If spectacle lenses are placed in front of emmetropic animal eyes so that the focal plane is shifted either behind (hyperopic defocus) or in front of the retina (myopic defocus), the eyes compensate the defocus imposed by the lens by changing their axial growth rates (Chapter I. 3.1).
- ▷ Various animal models develop high amounts of myopia if they are deprived of sharp vision by wearing diffusers in front of the eye (Chapter I. 3.2).

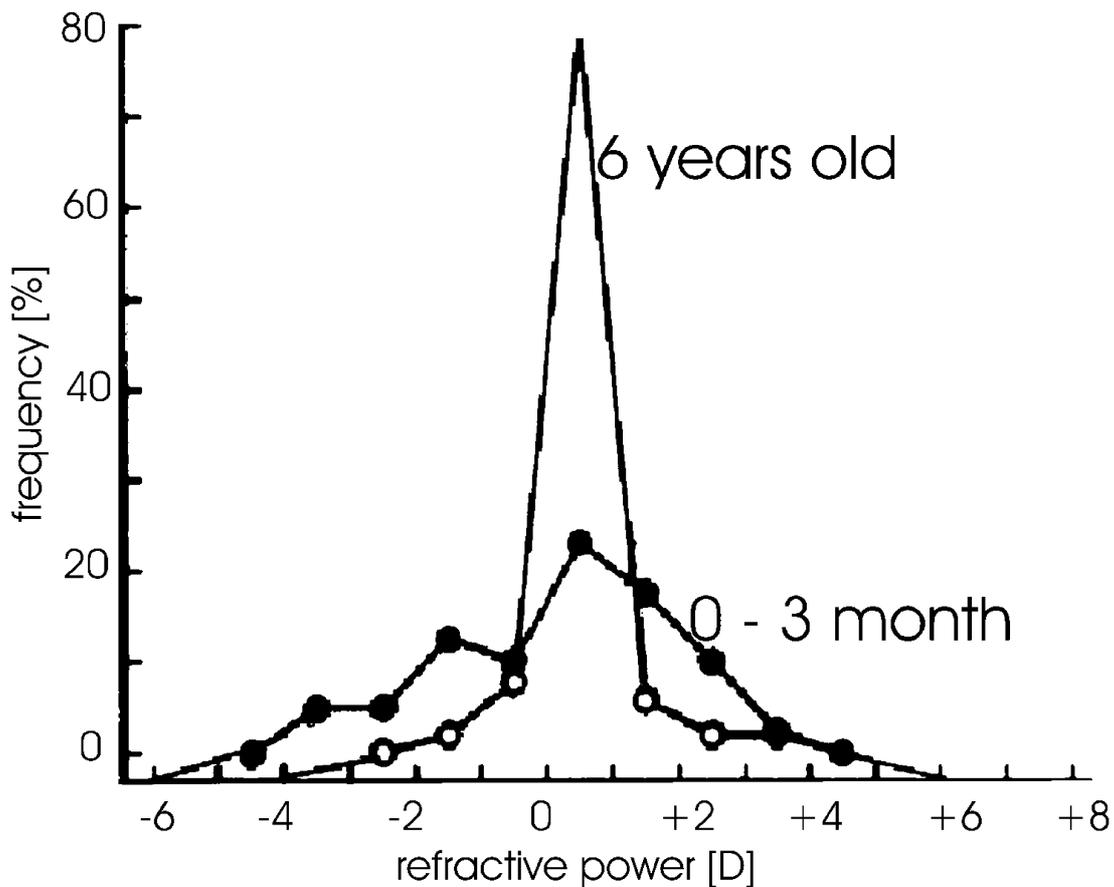


Figure 1. Emmetropization in the human eye (after Gwiazda et al., 1993). After birth, the refractive error distribution is broad and follows about a Gaussian distribution. At the age of six years, refractive errors show a leptokurtic distribution, with a peak around one diopter of hyperopia.

3. The control of axial eye growth by visual signals

3.1 Refractive errors induced by imposed defocus

That the eye uses visual signals to adjust its axial length to the location of the focal plane, has first been shown in the chicken eye by Schaeffel et al. (1988). Subsequently, many experiments were performed in various animal models that confirmed this observation (i.e. chicks, Irving, Sivak, & Callender, 1992; rhesus monkeys, Hung et al., 1995; marmosets, Whatham & Judge, 2001; guinea pigs, Howlett & McFadden, 2002; McFadden, Howlett, & Mertz, 2004).

When positive lenses are placed in front of the eye, the focal plane is shifted in front of the retina, creating a myopic refraction (Figure 2 A). The eye compensates both by expanding the choroid (the vascular layer between the retinal pigment epithelium and the sclera), which pushes the retina forward toward the focal plane, and by slowing ocular scleral growth and elongation (Wildsoet & Wallman, 1995). When eyes are fitted with negative lenses, the focal plane is moved behind the retina, creating a hyperopic refraction (Figure 2 B). To regain sharp focus, the retina needs to be moved backwards to the image plane. This can be done by increasing the growth rate of the eye and thinning the choroid (Wallman, Wildsoet, Xu, et al., 1995; Wildsoet & Wallman, 1995), pulling the retina back towards the focal plane. Once the image is focused on the retina, both the rates of ocular elongation and the thickness of the choroid return to normal (Wallman et al., 1995).

In the chick, the eye can almost completely compensate for lens powers between -10 D and +15 D within a week (Irving et al., 1992), while the monkey can compensate from -3 D to +3 D over several months (Hung et al., 1995; Smith & Hung, 1999), and the guinea pig eye can respond to ± 4 D within six days (Howlett & McFadden, 2002). When chicks wear positive and negative lenses alternately, the effects of both types of lenses do not cancel out each other. Instead, positive lenses create a more powerful inhibitory growth signal (Smith, Hung, Kee, & Qiao, 2002; Winawer & Wallman, 2002), suggesting an asymmetry in the power of both signals.

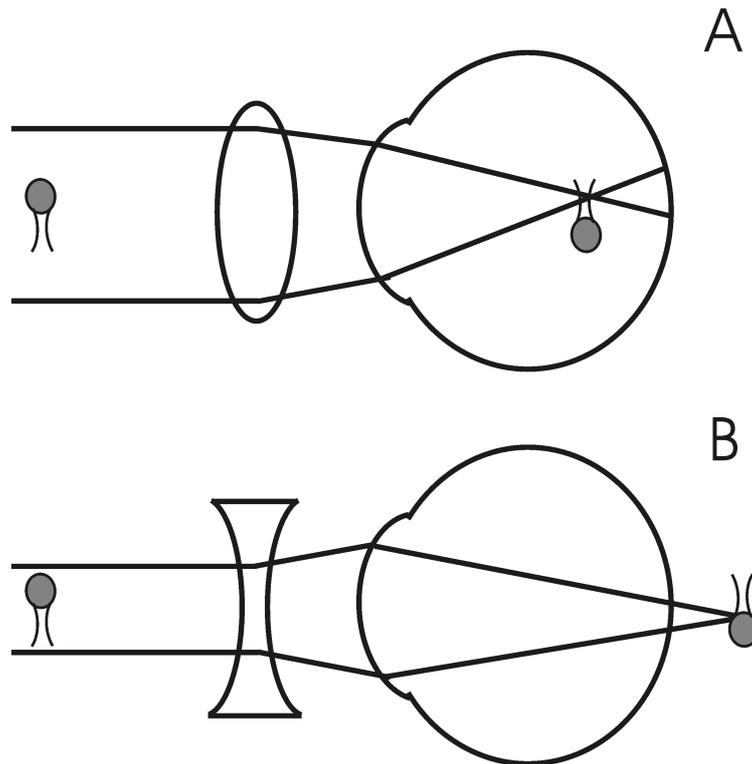


Figure 2. Defocus imposed to an emmetropic eye by positive and negative lenses. A. A plus powered lens moves the focal plane in an anterior direction and myopic defocus is imposed. The eye compensates positive lenses by slowing its rate of elongation and by thickening of the choroid, pushing the retina forward toward the image plane. B. A minus powered lens moves the focal plane in a posterior direction, imposing hyperopic defocus. The eye compensates for negative lenses by increasing the rate of elongation and thinning the choroid, pulling the retina back toward the focal plane.

3.2 Refractive errors induced by deprivation of sharp vision

If the image on the retina is blurred by wearing of frosted diffusers in front of the eye, the eye is deprived of "form vision" (Hodos & Kuenzel, 1984). The reduction of contrast and high spatial frequencies in the image are typical features of this visual manipulation. Form deprivation can also be induced by lid suture. Different from lid suture, diffusers are not in contact with the corneal surface. Therefore, the risk of corneal changes during the deprivation period is reduced.

Deprivation of form vision during a critical period of development has been shown to induce myopia in a wide range of species ("deprivation myopia"). For example in macaques (lid-suture, Wiesel & Raviola, 1977; diffuser, Smith & Hung, 2000), marmosets (lid-suture, Troilo & Judge, 1993; diffuser, Troilo & Nickla, 2002), tree shrews (lid-suture, Sherman, Norton, & Casagrande, 1977; diffuser, Norton, 1990), chicks (lid-suture, Yinon, Rose, & Shapiro, 1980; diffuser, Wallman, Turkel, & Trachtman, 1978), squirrels (lid-suture, McBrien, Moghaddam, New, & Williams, 1993a), guinea pigs (diffuser, McFadden et al., 2004) and, as described most recently, in mice (lid-suture, Beuerman, Barathi, Weon, & Tan, 2003; Tejedor & de la Villa, 2003; diffuser, Fernandes, Yin, Byron, et al., 2004; Schaeffel, Burkhardt, Howland, & Williams, 2004). The degree of myopia and the speed by which the eye elongates vary among species. For example, the chicken has the fastest dioptric growth of almost 3 D per day during the first week after hatching (Schaeffel & Howland, 1988a). Followed by the marmoset at 1.5 D (Troilo & Judge, 1993), tree shrew at 1 D (Norton & McBrien, 1992), and rhesus monkey at about 0.5 D (Bradley, Fernandes, Lynn, Tigges, & Boothe, 1999). Moreover, chicks (Wallman & Adams, 1987), monkeys (Smith, Harwerth, Crawford, & von Noorden, 1987) and tree shrews (Siegwart & Norton, 1998) develop more axial myopia when form deprivation is imposed early in life, while the eye is in its rapid infantile growth phase. It was shown, that form deprivation myopia can be prevented by exposing animals to strobe lightning (Rohrer, Iuvone, & Stell, 1995; Schwahn & Schaeffel, 1997). Removing the diffusers for brief daily periods causes a reduction of the induced myopia and ocular elongation in both the chicken and rhesus monkey (chick: 20 to 30 min per day, Napper, Brennan, Barrington, Squires, Vessey, & Vingrys, 1995; Schmid & Wildsoet, 1997; rhesus monkey: one hour per day, Smith et al., 2002).

3.3 Local control of eye growth

One of the most striking effects of both lenses and diffusers is, that they act locally within the eye. If the optic nerve is severed (Troilo, Gottlieb, & Wallman,

1987; Wildsoet & Pettigrew, 1988) or action potentials of the ganglion cells are blocked (Norton, Essinger, & McBrien, 1994; McBrien, Moghaddam, Cottrill, Leech, & Cornell, 1995), form deprivation myopia remains unaffected. However, spectacle lens compensation still occurs, although it is not completely like normal (Wildsoet, 2003). If diffusers or negative lenses cover half of the retina, only that part of the eye becomes elongated and myopic (Wallman, Gottlieb, Rajaram, & Fugate-Wentzek, 1987; Diether & Schaeffel, 1997). On the other hand, if a part of the eye is covered with positive lenses, axial eye growth is inhibited only in this visual field (Diether & Schaeffel, 1997). Thus, to understand how visual experience affects axial elongation, pathways within the eye from the retina to sclera need to be studied.

4. How might the eye know which way to grow?

There are several ways how the visual system could use blur to direct eye growth to correct refractive errors. Firstly, the eye might grow in a random direction and change direction if the blur gets worse (trial and error). Secondly, the eye might be able to reach emmetropia by elongating proportionally to the magnitude of blur. Since the average blur reaches a minimum when the refraction matches the average viewing distance over the day, this would also "emmetropize" the eye. Finally, the retina could decode the sign of defocus from the retinal image itself, although the underlying image processing is not understood up to now.

4.1 Trial and error

Evidence against a trial and error mechanism was shown by Park, Winawer, & Wallman (2001). In this study spectacle lenses were attached on the chicken eye for 10 min followed by a period of darkness. The chicks increased choroid thickness on positive but not on negative lenses. Because the refractive error

does not change in 10 min, these results show that the eye's initial response to defocus is in the appropriate direction.

4.2 Magnitude of blur

To determine if the magnitude of blur guides lens compensation, Schaeffel & Diether (1999) stimulated the retina of chicks with positive and negative lenses of similar magnitude. The chicks were kept in a restricted environment such that all parts of the visual field were too far away to be focused while wearing a positive lens. Furthermore, accommodation was paralyzed to prevent the eye from reducing the defocus imposed by the negative lenses. If spatial frequency and image contrast were the only cues analyzed by the retina, all chicks should have become myopic. However, the chick's eye compensated in the appropriate direction both for negative and positive lenses, as did chicks in two other studies without cycloplegia (McLean & Wallman, 2003; Park, Winawer, & Wallman, 2003).

4.3 Possible error signals that guide emmetropization

4.3.1 Chromatic aberrations

Chromatic aberrations of the eye arises from the variation in the refraction of different wavelengths of light. When white light is focused through a lens, blue light has a shorter focal distance than red light. The distance between these two foci is known as longitudinal chromatic aberration. In humans, the longitudinal chromatic aberration is about five times larger as the thickness of the retina. Thus, if the eye is myopic, red light will be more in focus than blue light, whereas if it is hyperopic, the reverse will hold. Chromatic aberrations could, therefore, provide information regarding the sign of defocus experienced by the eye. To determine whether or not the sign of refractive error is derived from chromatic aberrations, chicks wearing spectacle lenses were raised in monochromatic light (Schaeffel & Howland, 1991; Rohrer, Schaeffel, & Zrenner,

1992; Wildsoet, Howland, Falconer, & Dick, 1993). These studies showed that the eyes grew in the appropriate direction to correct for the defocus imposed by the lenses, even in absence of chromatic cues.

4.3.2 Monochromatic aberrations

Similar to defocus, other optical aberrations like astigmatism, spherical aberrations and coma blur the image on the retina. It is known, that some higher order aberrations do not cause symmetric distortions of the point spread function for both signs of defocus (humans, Woods, Bradley, & Atchinson, 1996; chicks, Coletta, Marcos, Wildsoet, & Troilo, 2003). Because the retinal images are differently distorted if they are defocused in either direction, it is possible that the retina can extract the sign of spherical defocus from these differences (Wallman & Winawer, 2004). However, an experimental proof for this assumption is still missing.

4.3.3 Accommodation

The average level of accommodation would indicate if an eye is hyperopic (on average, more accommodation) or myopic (on average, less accommodation). Although accommodation would be an useful sensor for the refractive state of an eye, there is little evidence that it is used to guide emmetropization. First, in chicks, spectacle lens compensation is still possible after accommodation has been eliminated by drugs (Schwahn & Schaeffel, 1994), by lesion of the Edinger Westphal nuclei (Schaeffel, Troilo, Wallman, & Howland, 1990) or by ciliary nerve section (Wildsoet et al., 1993). Second, refractive errors can be induced in animals, for example in the grey squirrel, that cannot accommodate (McBrien et al., 1993a). Third, emmetropization can occur locally in the retina (Chapter I. 3.3), whereas accommodation is rotationally symmetric in mammals and birds.

5. Pharmacological prevention of myopia

While the mechanism for emmetropization is still not well understood (Chapter I. 4.), it has been shown that various pharmacological agents are effective at preventing the development of myopia. The muscarinic receptor antagonist, pirenzepine, and the nicotinic antagonist, chlorisondamine, reduce the compensatory response to negative lenses and cause normal eyes to grow slower and become hyperopic (Stone, Sugimoto, Gill, Liu, Capehart, & Lindstrom, 2001; Truong, Cottrill, Gentle, & McBrien, 2002). The non-selective muscarinic receptor antagonist, atropine, reduces myopia in response to lenses or diffusers but has little effect on normal eye growth (Schmid & Wildsoet, 2004). This is true also for apomorphine (Stone, Lin, Laties, & Iuvone, 1989) and reserpine (Ohngemach, Hagel, & Schaeffel, 1997). Although there is no doubt that atropine is currently the most potent drug against myopia development in both humans (Gimbel, 1973; Bedrossian, 1979; Chua, Balakrishnan, Tan, Chan, & ATOM study group, 2003) and animals (chicks: Diether, Schaeffel, Fritsch, Trendelenburg, Payor, & Lambrou, 2004; McBrien, Moghaddam, & Reeder, 1993b; monkeys: Raviola & Wiesel, 1985; Tigges, Iuvone, Fernandes, et al., 1999), the mechanism by which myopia is suppressed is still obscure. A possible target is that atropine increases the contrast sensitivity of the retina, simulating a better image and reducing the error signal that would normally make the eye grow faster. In fact, it was shown that contrast sensitivity in chickens increased after they had received an intravitreal injection of atropine (Diether & Schaeffel, 1999).

6. Human myopia

6.1 Epidemiology of myopia

Although there is general agreement that the growth of the young human eye is regulated by emmetropization (Chapter I. 2.), myopia is one of the most common ocular disorders in humans. Its incidence is approximately 30% of most Western populations and reaches more than 90% in Asian school children

(Rajan, Saw, Lau, et al., 1998). Rural and remote communities show a lower prevalence of myopia than urban areas (6.6% versus 19.3%, e.g. Saw, Hong, Zhang, et al., 2001). Additionally, cultures in which people live mostly outdoors have little myopia (Morgan & Rose, 2005). But when education and other attributes of modern culture were introduced to Inuit or American Indian villages, there was a four-fold increase in the incidence of myopia within one generation (Bear, 1991).

6.2 Genetic control of myopia

Even though there is considerable experimental (e.g. Gwiazda, Hyman, Hussein, et al., 2003) and epidemiological evidence (e.g. Saw, 2003) from human studies that environmental factors play a role, a number of studies demonstrate a strong genetic influence. School-age children with two myopic parents are far more likely to be myopic (62%) than children with one or no myopic parent (19% versus 24%, respectively; e.g. Thorn, Grice, Held, & Gwiazda, 1998). Analysis of extended multi-generation families (Pacella, McLellan, Grice, Del Bono, Wiggs, & Gwiazda, 1999) and twin studies (Hammond, Snieder, Gilbert, & Spector, 2001) provide also convincing evidence of inheritance. Furthermore, it has been speculated that the greater near work demand of the modern societies may have interacted with an underlying genetic susceptibility which results in an increased prevalence of myopia (Rose, Smith, Morgan, & Mitchell, 2001).

6.3 Risk factors of myopia

Although low degrees of myopia (“physiological” or “school” myopia), are generally innocuous, higher degrees of myopia (“pathological” or “degenerative” myopia) may lead to permanent visual impairment and blindness. Pathological myopia often progresses to values greater than 10 D and is associated with a higher risk of additional ocular disorders such as glaucoma (Wu, Nemesure, &

Leske, 1999), cataracts (Wu et al., 1999) retinal degeneration, peripheral retinal changes and retinal detachments (Krumpaszky, Haas, Klauss, & Selbmann, 1997).

6.4 Deprivation myopia in infants

Retrospective analysis have revealed impaired emmetropization in children with various pathological conditions that lead to a degradation of the retinal image quality. Prolonged neonatal exposure to reduced pattern vision, was found to be associated with myopia (Rabin, Van Sluyters, & Malach, 1981). For example, infants with unilateral neonatal eyelid closure are more myopic and have larger axial lengths in the closed eye than in the normal eye (Hoyt, Stone, Fromer, & Billson, 1981). A similar result occurs when a drooping of the upper eyelid (ptosis) or cataract (Rabin et al., 1981) or corneal opacification (Gee & Tabbara, 1988) prevent clear vision.

6.5 Near work and myopia

Occupations that require extended near work, higher levels of education and reading are all associated with an increased incidence of myopia (e.g. Katz, Tielsch, & Sommer, 1997; Al-Bdour, Odat, & Tahat, 2001; Mutti, Mitchell, Moeschberger, Jones, & Zadnik, 2002). Furthermore, a high proportion of young adults who do intensive professional studies became myopic over the few years of studying (i.e. Zadnik & Mutti, 1987).

Wallman & Winawer (2004) suggested that most near tasks, apart from reading, are a combination of hyperopic defocus (at the point of regard) and myopic defocus (from objects in the background). Given the potency of myopic defocus counterbalance the effects of hyperopic defocus in animal studies (Chapter I. 3.1), most near tasks may not interfere with the emmetropization mechanism. Reading, however, is different because the pages occlude most distant objects, and it involves long continuous periods of near-viewing (Wallman & Winawer, 2004). It was also suggested, that the age at which reading starts might

influence the development of myopia (Wallman & Winawer, 2004). Children who start reading earlier or read more (like children in Asia), are better at identifying letters and, therefore, might relax accommodation more often or show insufficient accommodation during reading ("lag of accommodation"). Reduced accommodation is optically similar to wearing a negative lens, and the animal experiments described above have shown that hyperopic defocus is compensated by axial eye elongation (Chapter I. 3.1). On the other hand, if the "lag of accommodation" is corrected by positive lenses like reading glasses, it would be expected that the progression of myopia is reduced. In a multi-center clinical trial (Correction of Myopia Evaluation Trial or COMET), children were assigned to wear either single vision lenses or progressive addition lenses (Gwiazda et al., 2003). Results of this were that progressive addition lenses could, in fact, reduce the progression of myopia. This effect was small if averaged over all 247 children (14% reduction of myopia, or about 0.20 D in the first year of treatment), but the inhibitory effect could become as large as 50% inhibition if the analysis was focused on those children who just started to become myopic.

6.6 Optical aberrations and myopia

The finding that visual deprivation can lead to myopia (Chapter I. 3.2 and 6.4) has led to the hypothesis that the presence of large amounts of higher order aberrations might also predispose an eye to myopia. He, Sun, Held, Thorn, Sun, & Gwiazda (2002) showed that optical quality decreases as myopia increases. However, the increase of aberrations was only observed in highly myopic subjects whereas the aberration level was similar in weakly myopic subjects and emmetropic subjects. These observation exclude that the aberrations are a major reason for myopia development. Furthermore, another large study did not find that higher degrees of monochromatic aberrations were associated with myopia (Cheng, Bradley, Hong, & Thibos, 2003).

7. Animal models to study myopia

7.1 The model of the chicken

Since the mid-1970's, several animal models (mainly chicks, tree shrews, marmosets and macaques) have extended our understanding of the aetiology of myopia. Even though the chicken is phylogenetically distant from humans, it became the most frequently used model for myopia studies. Reasons are that its eyes have a good optical quality and a large accommodation range (about 17 D) (Schaeffel, Howland, & Farkas, 1986), that normal refractive and ocular development is similar to humans, although much faster (Pickett-Seltner, Sivak, & Pasternak, 1988), that visual experience can be easily manipulated and that these changes are extremely effective in introducing refractive errors. Therefore, the chick model has made fundamental contributions to the understanding of myopia in three major areas of research. Firstly, it has helped to better define the retinal image processing that leads to adaptive eye growth (i.e. Schaeffel & Diether, 1999; Wildsoet & Schmid, 2001). Secondly, interactions between accommodation and emmetropization could be better explained (e.g. Schaeffel & Howland, 1988b; Wallman, 1993; Wildsoet & Schmid, 2001). Finally, it helped to identify potential pharmaceutical agents against myopia development (e.g. Stone et al., 1989; Diether & Schaeffel, 1999). However, the avian model also has disadvantages. Compared to mammalian models, information on the chick's genome, transcriptome, and proteome are limited. Although molecular studies on myopia are possible in the chicken (Feldkaemper, Wang, & Schaeffel, 2000), follow-up studies do not have the potential of exploiting large and well-maintained genomic databases (i.e. <http://www.tigr.org/tdb/tgi/gggi/>). Furthermore, there are no transgenic models available and it will be tedious to create them. The knowledge about the biochemistry of metabolic pathways is more restricted than in the rat and the mouse, and there are most likely differences between birds and mammals in the signalling cascades that control axial eye growth from visual cues. For example, all-trans-retinoic acid levels in the choroid increase during induction of myopia in the marmoset but decrease in the chicken (Mertz, Nickla, & Troilo, 2000).

Similarly, a presumably important element of the signalling cascade in the chicken, the glucagon-positive amacrine cell (Bitzer & Schaeffel, 2002) appears not in the mammalian retina. Therefore, drugs that are effective in reducing myopia development in chickens may not be potent in mammals.

7.2 The mouse as a new mammalian model to study myopia

7.2.1 Advantages of the mouse model

The mouse represents the most widely used mammalian model for human diseases since the rediscovery of Mendel's laws in 1900. Both the mouse and human genome is approximately the same size, both contain about the same number of genes, and both show an extensive conserved gene order and conserved gene function (Mouse Genome Sequencing Consortium, 2002). Furthermore, many gene knock-out models are available (e.g. Chapter I. 7.2.6) and mapping of loci that include genes for the control of eye growth and myopia were successful. Zhou & Williams (1999a) used quantitative trait loci (QTL) analysis in mice and Young, Ronan, Drahozal, et al. (1998) used transmission disequilibrium tests (TDT) in humans. Based on the knowledge of loci that are involved in eye size, candidate screening is possible which carries the potential to identify targets for pharmacological intervention of myopia.

Additionally, the mouse is readily available, easy to handle, it grows rapidly and can be easily bred (mice produce five to six pups per litter). On the other hand, the highly inbred laboratory strains preclude selective breeding i.e. for high susceptibility to myopia.

7.2.2 Emmetropization in the mouse eye

The relatively poor optical quality (Artal, Herreros de Tejada, Munoz Tedo, & Green, 1998) and small size of the mouse eye (about 3 mm) may be serious impediments to study the mechanisms of eye growth and refractive error development in this species. Remtulla & Hallett (1985) estimated a depth of focus as large as ± 56 D, based on their eye size and photoreceptor diameter. These authors expressed doubts that the behavioral depth of field can be as

large since, for example in the rat eye, behavioral acuity was about five times higher than predicted ganglion cell acuity (Birch & Jacobs, 1979). If such a factor would also apply to the mouse, this would reduce depth of field to ± 11 D. Mice also seem to lack a ciliary muscle (Woolf, 1956) and are assumed to be unable to accommodate (Artal et al., 1998). In fact, accommodation may be unnecessary in the presence of such a large depth of field. These findings imply that emmetropization may be of minor importance in the mouse model.

7.2.3 Deprivation myopia in the mouse eye

Despite the evidence against the necessity of a tight visual control of eye growth (Chapter I. 7.2.2), recent studies have shown that deprivation myopia can be induced in mice. Schaeffel & Burkhardt (2002) found that the mouse eye responds with deprivation myopia when it is covered with diffusers, and both Tejedor & de la Villa (2003) and Beuerman et al. (2003) induced form deprivation myopia by lid suture. However, the responses to visual manipulation are less reliable than in other animal models (Schaeffel & Howland, 2003; Schaeffel et al., 2004), and the visual parameters that are necessary to induce deprivation myopia are still poorly defined.

Due to the lack of appropriate technologies to measure ocular dimensions, axial length data are either still missing (Schaeffel & Burkhardt, 2002) or have limited reliability because the standard techniques are not sensitive enough (histological techniques, Tejedor & de la Villa, 2003; caliper measurements in excised eyes, Beuerman et al., 2003). Also, the axial length changes calculated from schematic eye models of the adult mouse (Remtulla & Hallett, 1985) were smaller than the changes measured in highly imprecise histological techniques by an order of magnitude (Tejedor & de la Villa, 2003) or even more (Beuerman et al., 2003).

7.2.4 The retina of the mouse eye

The mouse retina, like that of all other mammals, contains a mixture of rods and cones with the latter comprising approximately 3% of the total receptor complement (Carter-Dawson & LaVail, 1979; Jeon, Strettoi, & Masland, 1998).

In general, rods are responsible for vision at low light levels, whereas color vision at daylight is provided by the cones. Similar to many other mammals, the mouse has two types of cone photopigments, a middle wavelength sensitive pigment and a short wavelength sensitive pigment, in this case with maximum absorption in the ultraviolet light (Jacobs, Neitz, & Deegan, 1991). These findings suggest that mice have at least dichromatic vision (Jacobs, Williams, & Fenwick, 2004). It also supports the hypothesis that similar interactions between rod and cone photoreceptors may be present in primates and mice (Sharpe & Stockman, 1999).

7.2.5 Visual performance of the mouse

Although the mouse is not predominantly a visual animal, the advantages of the mouse model prevail and several aspects of visual functions have already been studied. Using a forced-choice behavioral paradigm, visual acuity was assessed in the “visual water task” by Prusky, West, & Douglas (2000a). Using this technique, the effects of environmental enrichment (Prusky, Reidel, & Douglas, 2000b) and visual deprivation (Prusky & Douglas, 2003) on visual acuity were studied, and it was also shown, how the contrast sensitivity is affected by ablation of the striate cortex (V1) (Prusky & Douglas, 2004). A behavioral discrimination test was also applied by Gianfranceschi, Fiorentini, & Maffei (1999) (T-maze behavioral task), to measure visual acuity of wild-type and *bcl2* transgenic mice. Even color vision was studied in a behavioral discrimination test (Jacobs et al., 2004). However, the forced-choice behavioral tasks require extensive training and are demanding. Another technique used in assessing visual function, is the optomotor response to a drifting grating. Sinex, Burdette, & Pearlman (1979) used this method to study grating acuity in the adult house mouse and the reeler mutant mouse. Using an optomotor experiment, it was also shown how spatial vision develops with age (Prusky, Alam, Beekman, & Douglas, 2004) and in 129/SvPas, albino CD1 and *rd1* retinal degeneration mice (Abdeljalil, Hamid, Abdel-mouttalib, et al., 2005). Furthermore, visual capabilities of mice were examined electrophysiologically, (e.g. Porciatti, Pizzorusso, Cenni, & Maffei, 1996; Porciatti, Pizzorusso, & Maffei, 1999; Ridder

& Nusinowitz, 2002), or anatomically, by determining the sampling intervals of the photoreceptors (Hughes, 1977; Martin, 1986).

The visual acuity of the C57BL/6J mouse (the common black or nonagouti mouse strain that was used for the public sequencing effort) found in the above described behavioral and electrophysiological studies was approximately 0.50 cyc/deg. This is similar to the acuity of the honey bee (Oyster, 1999). Mice have roughly one-tenth of the acuity of domestic cats (Waessle, 1971) and merely 1/100 that of emmetropic humans. Furthermore, visual acuity in the mouse eye is far from the diffraction limit at the observed pupil size (diffraction limit for a 1.50 mm pupil is about 47 cyc/deg; Oyster, 1999).

7.2.6 Genetic knock-out models

Transgenic and gene knock-out models can foster a better understanding of the normal visual functions and the effects of gene mutations on visual performance. The Rhodopsin knock-out ($RHO^{-/-}$) mouse (studied in this dissertation) carries a replacement mutation in exon 2 of the rhodopsin gene (Humphries, Rancourt, Farrar, et al., 1997). Rhodopsin, the visual pigment of the rods, initiates the phototransduction cascade but it also serves as a structural protein for the discs in the rod outer segment. Therefore, $RHO^{-/-}$ mice do not build rod outer segments. Within three months, these mice lose all their photoreceptors. However, between postnatal weeks four and six, when cone degeneration is not yet substantial, the mutants can be used to study cone function in isolation (Jaissle, May, Reinhard, et al., 2001).

The photoreceptor membrane potential hyperpolarizes in response to illumination by closure of the cyclic nucleotide-gated (CNG) cation channels (e.g. Biel, Zong, Ludwig, Sautter, & Hofmann, 1999) which, in turn, decrease the synaptic glutamate release. In rod photoreceptors, the CNG channel is formed by the subunits CNGA2 and CNGB1 and, in cone photoreceptors, by CNGA3 and CNGB3. In respective knock-outs of one channel subunit (CNGA3 and CNGB1), both the direct effects of the lack of one of these subunits (especially if they include the pore domain) and indirect effects such as problems with cellular trafficking are believed to cause the electrophysiologically

observed selective functional loss. Consequently, the $CNGB1^{-/-}$ mouse completely lacks rod photoreceptor-mediated vision, but in comparison with the $RHO^{-/-}$ mouse, the rods are physically still present until late stages. The $CNGA3^{-/-}$ mouse, generated by Biel, Seeliger, Pfeifer, et al. (1999), lacks cone-mediated light response which is also associated with a progressive degeneration of cone photoreceptors. Hence, they can be used to dissect rod from cone mediated signaling pathways. There are even double knock-out mice ($CNGA3^{-/-}RHO^{-/-}$) available, lacking both functional cones and rods (Claes, Seeliger, Michalakis, Biel, Humphries, & Haverkamp, 2004). These mice show a progressive degeneration of all photoreceptors within three months after birth. The inner retina remains unaffected. Until postnatal week seven, presynaptic markers and postsynaptic glutamate receptors are expressed, suggesting that neurotransmission can take place (Claes et al., 2004). Panda, Provencio, Tu, et al. (2003) showed that mice lacking rods and cones can still regulate their circadian rhythms via a third retinaldehyde-based visual pigment, melanopsin, which is mostly expressed in a subset of retinal ganglion cells. Furthermore, it has been shown that mice lacking functional photoreceptors in the outer retina still have a light-induced pupil response (e.g. Hattar, Lucas, Mrosovsky, et al., 2003; Barnard, Appleford, Sekaran, et al., 2004) that is mediated by photosensitive ganglion cells containing melanopsin. These double knock-out mice can be used to find out whether the retinal melanopsin system also contributes to spatial vision.

7.2.7 Developmental stages of the mouse

The mouse is a precocial species that matures quickly. In general, mice are weaned at three weeks of age (Sundberg, Smith, & John, 2002). They do not open their eyelids before 12 to 14 days postnatal (Sundberg et al., 2002) and the age of sexual maturity is reached between 40 and 60 days (Zhou & Williams, 1999b). Decline in fecundity takes place between six and eight months of age and progressive changes of ageing develop from 12 months to the time of natural death at approximately 99 weeks (Sundberg et al., 2002).

II. Purpose of the studies

To study the mechanisms of myopia development, mice offer a number of advantages over other animal models, including that knock-out models are available, that they can be easily bred, that their genome is extensively studied and that there is abundant information on their physiology (Chapter I. 7.2). On the other hand, their eyes are small, vision is probably not their predominant sense, and no data are published on the development of its ocular parameters during development. Also, there is a lack of techniques to perform ocular biometry *in vivo*. Finally, little is known about their spatial vision, and the relative importance of rod and cone vision.

To establish the mouse eye as a new mammalian model for myopia studies, several optical and physiological factors must be investigated. Therefore, in the first part of this dissertation a paraxial schematic eye model for the growing C57BL/6 mouse was developed (Schmucker & Schaeffel, 2004a). In the second part, an optical technique was established to measure ocular dimension with very high precision *in vivo* (Schmucker & Schaeffel, 2004b). In the third part, an automated optomotor paradigm was developed, based on the optomotor response, to study how grating acuity changes with illuminance and how the cone and rod system contribute to spatial vision (Schmucker, Seeliger, Humphries, et al., 2005). Finally, it was studied how spatial vision in mice is affected by wearing of spectacle lenses or diffusers, and by atropine eye drops (Schmucker & Schaeffel, 2005).

III. Material and Methods

1. Animals

All experiments were conducted in accordance with the ARVO Statement for the Use of Animals in Ophthalmic and Vision Research. The mouse experiments were approved by the University commission for animal welfare (reference AK3/02). Black C57BL/6 wild-type mice were obtained from Charles River GmbH, Sulzfeld, Germany, and bred in the animal facilities of the Institute. The strains were completely inbred and, with the exception of sex chromosome differences and rare spontaneous mutations, all individuals were isogenic.

RHO^{-/-} (generated by Pete Humphries, University of Dublin, Ireland), CNGB1^{-/-} (generated by Martin Biel, Institute of Pharmacology, University Munich, Germany), and CNGA3^{-/-}RHO^{-/-} mice were bred in Tuebingen and made available by Dr. Mathias Seeliger. CNGA3^{-/-} mice on a matching C57BL/6 background were directly obtained from Dr. Martin Biel. For a more detailed description of the mouse mutants see Chapter I. 7.2.6.

Animals were housed with their mothers until weaning at around postnatal day 21, and then in groups of six to eight in standard mouse cages under a 12 h light/dark cycle. Animals wearing occluders were housed individually in standard mouse cages under the same conditions as untreated mice. Ambient illuminance was provided by incandescent lights and was about 500 lux on the cage floor (measured with a calibrated photo cell [United Detector Technology] in photometric mode). All experimental procedures were conducted under the light phase (between 9 a.m. and 4 p.m.) of the daily cycle.

2. A paraxial schematic eye model for the growing C57BL/6 mouse

2.1 Infrared photoretinometry

As an initial step in this study, refractive state and pupil size of three mice were recorded over the first 100 days by eccentric infrared photoretinometry (the Power Refractor) as described by Schaeffel et al. (2004) (Figure 3). In brief, the slopes of the brightness distributions in the pupil were automatically determined in the digital video images with 25 Hz sampling rate using an image processing computer program written by Frank Schaeffel. Then, the brightness slopes were converted into refractive errors, using a factor that was determined in prior calibrations with trial lenses. The previous study showed that mice could be refracted with a standard deviation from several repeated measurements of ± 2.50 D.

To measure refraction, the mice were placed on a small elevated wooden platform and gently restrained on the platform by holding their tails. The platform was slowly turned until one eye was oriented in the direction of the video camera of the refractor. The program automatically initiated measurements when a stable pupil image was defined. Infrared light had the advantage that the animals were not aware of the measurements, and that the pupil size remained large. Pupil sizes were approximately 2 mm under these conditions, but dropped to less than 1 mm when the room light was turned on (Pennesi, Lyubarsky, & Pugh, 1998).

III. Material and Methods

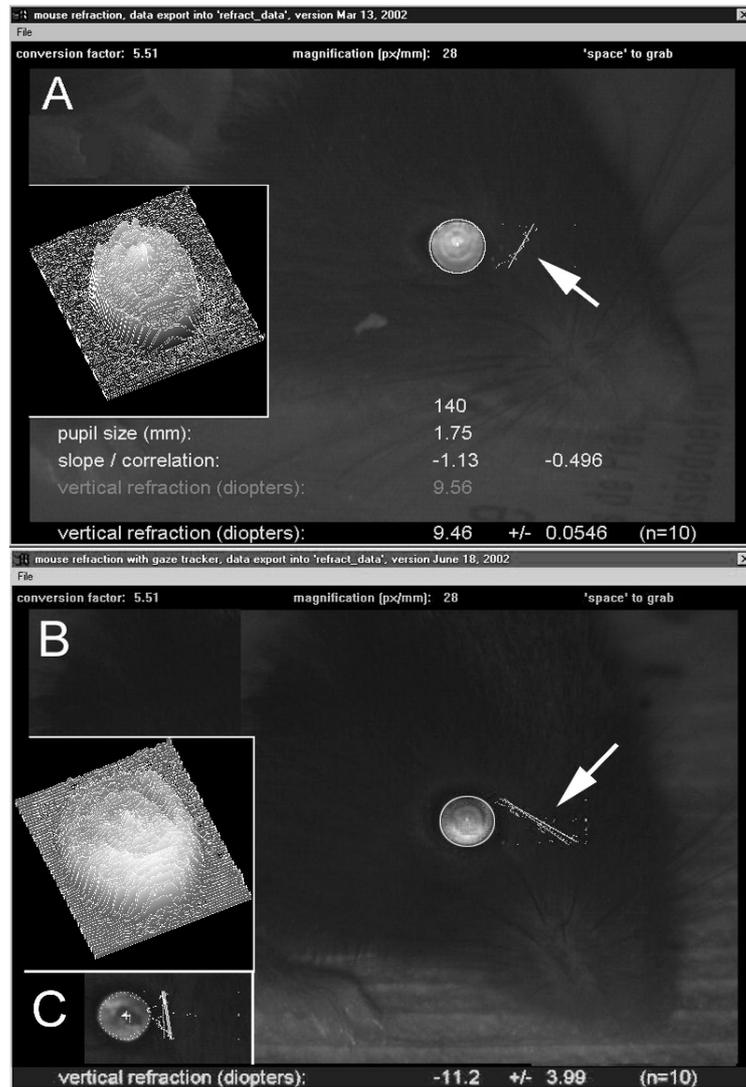


Figure 3. Screen dump of the monitor of the Photorefractor during the measurements of refraction and pupil size in mice. On the left, the brightness distribution in the pupils is shown in a three-dimensional illustration. On the right, the video frame with the mouse is shown, together with the marks that were set by the image processing program. The arrow points toward the regression line that was automatically fit through the brightness distribution in the vertical pupil meridian. The average pixel brightness of the pupil, pupil diameter, the slope of the regression, and the correlation coefficient of the fit are displayed together with the refraction in the vertical power meridian. The number on the bottom represents the average of ten refraction measurements performed in 400 ms. A. Refraction of an untreated control mouse. Note that the pupil is brighter in the top, indicating hyperopia. B. Refraction of a myopic mouse. Note that the pupil is brighter in the bottom, indicating myopia. C. Eye of a mouse with cataract. Figure adapted from Schaeffel et al. (2004).

2.2 Infrared photokeratometry

Corneal radius of curvature was measured *in vivo* by infrared photokeratometry, in 11 mice at the ages of 35, 58 and 75 days. Mice were anesthetized with a subcutane injection of 0.1 to 0.2 ml of a mixture of 1.2 ml 10% ketamine hydrochloride, 0.8 ml 2% xylazine hydrochloride and 8.0 ml sterile saline. After carefully positioning the eye, eight infrared light-emitting diodes (LEDs) arranged in a circle of a diameter of 298 mm created 8 Purkinje images on the cornea (Figure 4). The positions of these reflexes were recorded by an infrared light sensitive video camera equipped with a 210 mm lens and several extension rings, resulting in a highly magnified video image (about 80 pixel/mm). Calculation of corneal radius of curvature from the positions of the infrared light reflexes on the cornea was done following prior calibration and linear extrapolation from measurements on two ball bearings with known radii (3.15 mm and 5.50 mm). The standard deviation from repeated measurements of the radii of curvature in the ball bearings was ± 0.02 mm. In addition to the *in vivo* measurements, corneal radii of curvature were also determined in frozen sections.



Figure 4. Screen dump of the computer monitor during measurements of corneal radius of curvature. An image processing program written in Borland C++ located the first Purkinje images that were created by a circular arrangement of eight infrared LEDs. The radius of curvature was determined by the program, based on a prior calibration of the procedure on surfaces with known curvature. Ten measurements acquired in 0.4 sec had a standard deviation of the radii of curvature of about 15 μm .

2.3 Frozen sections

Freshly excised globes of 20 mice (34 eyes) were placed on the cooled metal platform of a cryostat with defined orientation and immediately embedded in freezing medium (TissueTecTM) at -20°C. Once completely frozen the globes were sectioned in the axial plane until the maximal equatorial diameter was reached and the optic nerve head became visible. Subsequently, three videographs with high magnification (about 150 pixel/mm, achieved with a 135 mm lens and several extension rings) were taken of the frozen block at three different planes with 36 μm distance in depth. After digitization of the video frames, ocular dimensions and radii of curvature of the optical surfaces were determined using Adobe PhotoshopTM. Radii of curvature of cornea, lens and retina were calculated from the equation $r = y^2 / (2*s) + s/2$ with r = radius of curvature, s = sagitta of the chord, y = any chord (Fincham & Freeman, 1974). In each videograph, three measurements were taken at different distances from the estimated optical axis of the eye.

No corrections were made for volume artifacts which were previously shown to be very small (Chaudhuri, Hallett, & Parker, 1983). Furthermore, both Charman & Tucker (1973) and Sivak (1974) observed no significant changes in the dimensions of the anterior chamber or crystalline lens following freezing eyes in the cryostat.

The data on ocular dimensions were plotted versus age and linear regressions were fit to analyze changes over time. Significant developmental changes were identified by significant correlation coefficients. Since no correlation was found between the axial lengths of both eyes in individual animals of the same age

group (Schaeffel et al., 2004), eyes were treated as independent samples even if they originated from the same animal.

2.4 Paraxial ray tracing and schematic eyes

Schematic eyes were developed using both the "OSLO" paraxial ray tracing program (LT Lambda Research Corporation) and a ray tracing program written by Schaeffel & Howland (1988b). The programs were tested against each other and were found to produce identical results. Radii of curvatures and positions of the optical components were taken from the frozen sections. Refractive indices of the optical media in the mouse were taken from the literature for a wavelength of 655 nm (cornea 1.4015, aqueous 1.3336 and vitreous 1.3329, Remtulla & Hallett, 1985). The refractive index of the retina of 1.3510 was taken from a study on the rat eye (Hughes, 1979). The equivalent homogeneous refractive index of the lens was calculated by matching the refractive state of the model eye to the refractions measured with infrared photoretinoscopy. A limitation was then that nothing could be said about off-axis imagery, since this depends heavily on the nature of the refractive index gradient in the lens.

In the present study, the position of the retinal pigment epithelium (RPE) was assumed to be coincident with the photoreceptor plane, as it could be easily identified in the frozen block. The theoretically expected small eye artifact was calculated from the dioptric differences between the photoreceptor plane and the retino-vitreous interface (Glickstein & Millodot, 1970). The paraxial eye model also permitted to calculate the developmental changes in image brightness ($f/\text{number} = \text{posterior nodal distance (PND)}/\text{pupil size}$) and image magnification ($\text{image magnification [mm/deg]} = \tan 1^\circ * \text{PND}$).

3. *In vivo* biometry in the mouse eye with optical low coherence interferometry

3.1 Measurement principle

Biometrical data of living mouse eyes were obtained with a new device based on optical low coherence interferometry (OLCI), the Carl Zeiss "AC Master" (<http://www.meditec.zeiss.com/>). The principle of OLCI is based on a Michelson interferometer (Figure 5). The light source is a low coherence superluminescent laser diode (SLD) that emits an infrared light with a peak emission at 850 nm and a half-band width of 10 nm. Due to the broadened bandwidth, the coherence length is rather short (about 10 μm), compared to standard laser diodes, in which it is about 160 μm . Output energy is 450 μW . The infrared laser beam emerging from the SLD is divided into two perpendicular beams by a semi-silvered mirror. One part is transmitted through the semi-silvered mirror and reaches a stationary mirror (reference beam). The other part is reflected and reaches a mirror that can be moved along the light path with high positional precision (measurement beam). After reflection from both mirrors, two coaxial beams of about 50 μm diameter propagate to the eye, where they are reflected off from the cornea, the lens and the RPE. Interference between both beams can only occur when their optical path lengths are matched within the coherence length. The occurrence of interference is detected by a photo cell and recorded as a function of the displacement of the movable mirror. Due to the usage of coaxial beams, the measurements are largely insensitive against longitudinal eye movements. The scanning time of the movable mirror is about 0.3 sec. The resolution of the system is limited both by the coherence length, which is inversely proportional to the bandwidth of the SLD, and by the precision by which the position of the movable mirror can be controlled. In the human eye, a measurement precision in the range of 2 μm has been described in corneal thickness measurements and of 5 to 10 μm for the anterior chamber depth and lens thickness measurements (R. Bergner, Carl Zeiss, Jena, personal communication 2004).

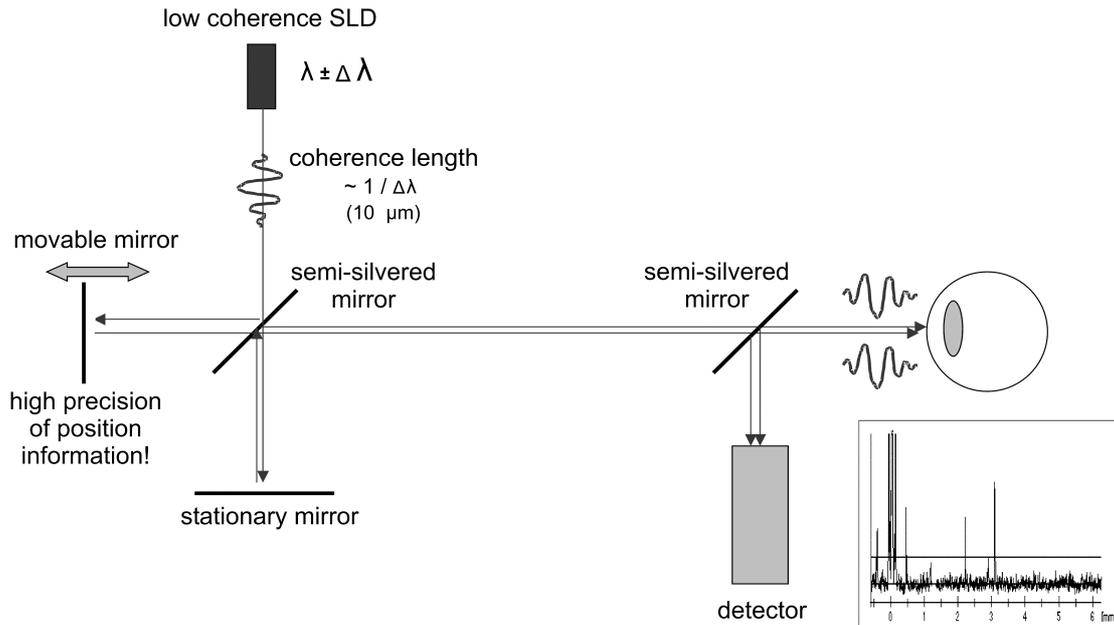


Figure 5. Schematic illustration of the optical low coherence interferometer implemented in the Zeiss "AC Master". SLD: superluminescent diode. The beam emitted from the SLD is either transmitted through the semi-silvered mirror and reflected from a stationary mirror, or reflected at the semi-silvered mirror and then reflected from the movable mirror. Both reflected beams propagate to the eye. If their path length is matched within the coherence length, they display interference. The interference pattern is detected by a detector and displayed on the monitor of the device. The movable mirror is shifted along the measurement axis with very high precision. Once interference is achieved, the corresponding position of the movable mirror provides the information on the position of the respective reflecting surface in the eye.

The major reflections in the eye occur at the anterior corneal surface and at the RPE. Accordingly, the interference signals are most conspicuous at these two layers.

The software of the "AC Master" is designed to measure the anterior segment in human eyes. This means that it expects to find reflecting surfaces at about 0.5 mm behind the anterior corneal surface (which would correspond to the thickness of the human cornea) and a second major reflection between 2 to 5 mm distance (the anterior surface of the human lens). The software could be used to measure mouse eyes because reflecting surfaces were present within the accepted ranges: the distance to the anterior surface of the lens of the mouse eye is in the range of the thickness of the human cornea, and the

III. Material and Methods

distance to the RPE in the back of the eye is in the range of the distance to the anterior lens surface in human eyes. This means that the software had to detect anterior corneal surface, anterior lens surface, and the RPE to provide biometric data (Figure 6). Anterior chamber depth, as plotted below, is defined as the distance from the anterior corneal surface to the anterior surface of the lens. The peak of the posterior lens surface was detected only in a few measurements. Therefore, no data on lens thickness are provided.

To measure corneal thickness in the mouse eye, the cursor that was automatically placed at the anterior lens surface was manually moved anteriorly, to the back of the cornea. The lens surface position was no longer measured in this case. However, the measured axial length was then longer because the length of the path of the light through the optical medium with higher refractive index was shorter (experimental confirmation: Chapter IV. 2.1). The device used a refractive index of 1.3851 for the human cornea and an index of 1.3454 for the aqueous humor. That means that the measurements in the mouse eye are based on an index of 1.3851 for the anterior chamber and/or corneal thickness and an average index of 1.3454 for lens and vitreous humor, which both may not be the best approximation.

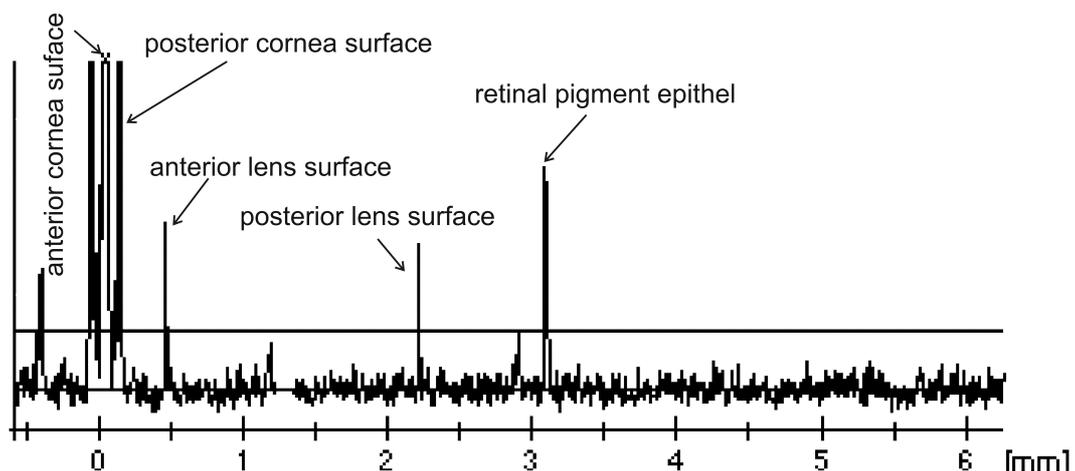


Figure 6. Low coherence interferogram of the mouse eye. The intensity of the peaks is plotted versus the optical path length. The origin of the reflections of the cornea layers, the lens and the RPE are shown. The peak of the posterior lens surface was detected only in a few of the measurements. Therefore, a consistent evaluation of lens thickness was not possible.

3.2 Measurement procedures in living mice

Prior to the measurements, mice were anesthetized with a subcutane injection of 0.1 to 0.2 ml of a mixture of 1.2 ml 10% ketamine hydrochloride and 0.8 ml 2% xylazine hydrochloride, dissolved in 8.0 ml sterile saline. Subsequently, the animals were positioned on a adjustable platform that was screwed to the chinrest of the device (Figure 7 A). The pupil axis of the eye was aligned with the measurement axis, and the distance of the eye to the measurement head was adjusted to approximately 70 mm, using six infrared LEDs arranged in a circle that were imaged on the cornea and focused under high magnification (Figure 7 B). Then, a series of approximately 20 longitudinal scans was performed within a few seconds. All animals recovered from the anesthesia and the measurements without complications.

After completing the measurements, the interferogram was analysed. In some scans, the relevant interfaces were not detected or were ambiguous. Only those scans which showed clear peaks at the cornea, the anterior lens surface and the RPE were used to calculate means and standard deviation of optical eye length, optical corneal thickness and optical anterior chamber depth in each eye.

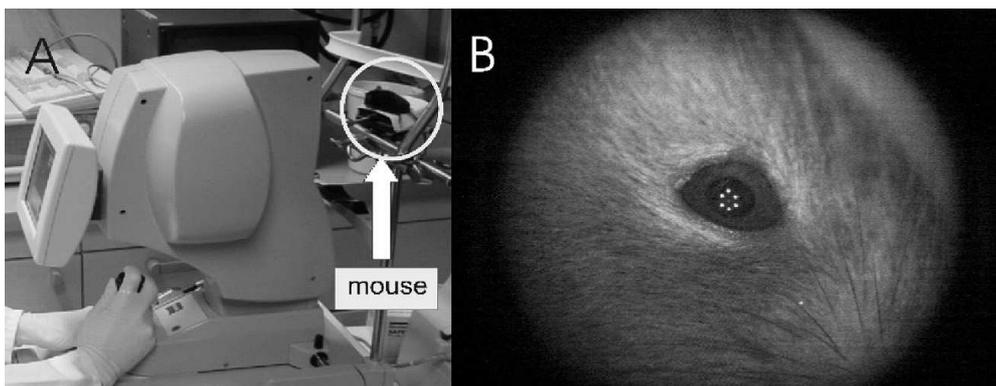


Figure 7. A. The “AC Master” during measurements of a mouse eye. The anesthetized mouse, positioned on an adjustable platform which was attached to the chinrest of the device, is encircled. B. Close-up view of the mouse eye that was used to adjust the eye in the measurement beam. The first Purkinje images of six infrared LEDs are visible, and were used to align the eye.

3.3 Measurements in mice with normal vision

Axial eye length, central corneal thickness and anterior chamber depth were measured in 23 mice with normal visual experience, at the ages of 25, 29, 35, 47 and 53 days. At least three mice were measured in each age group and the means and standard deviation were calculated separately for both eyes in each animal. The data for different age groups were compared to biometric data from the first part of this dissertation in which the ocular dimensions were determined in frozen sections (Chapter III. 2. or Schmucker & Schaeffel, 2004a).

To evaluate the differences between the left and the right eyes, mean values of axial length and their standard deviation from 19 untreated mice at different ages were plotted against each other and the absolute average differences between both eyes was calculated.

To analyze potentially confounding effects of changes in orientation of the eyes during the measurements, the eyes in ten mice were voluntarily rotated in either the horizontal or vertical meridian. In these measurements, the Purkinje image of one of the six LEDs was positioned close to the pupil margin, 0.60 ± 0.06 mm away from its position when the circle (Figure 7 B) was centered in the pupil. With a Hirschberg ratio (= eye rotation necessary to displace the first Purkinje image by 1 mm) of 86.7 ± 3.0 (Schaeffel et al., 2004), the corresponding angles were $52 \pm 6^\circ$ nasally, temporally, superiorly and inferiorly of the pupil axis.

3.4 Measurements in mice that were deprived of sharp vision (“form deprivation”)

One eye in seven mice was occluded by attaching frosted hemispherical thin plastic shells to the fur around the eye (Figure 8). They were hand-made as previously described for chickens (Schaeffel & Howland, 1991), but their radius of curvature was only 8 mm as opposed to 10 mm. Their rim, about 1 mm wide, was glued to the fur around one eye by instant glue (cyanyl acrylate) under light ether anesthesia on postnatal day 27. The rims of the diffusers were far enough away from the eyelids to not interfere with their function. Subsequently, thin plastic collars with an inner diameter of about 1.0 cm and an outer diameter of

III. Material and Methods

about 4.5 cm, were fitted around the neck to prevent mice from removing their diffusers. Food pellets were placed on the floor of the cage to facilitate foraging. The diffusers were removed on day 41. Refractive state, measured by infrared photoretinoscopy (Chapter III. 2.1), and ocular biometry by OLCI, were performed in anesthetized animals both before and after the occlusion period. The number of animals that were covered with diffusers was comparably small; however, previous occlusion experiments in 50 mice had shown that deprivation produces a highly significant change in refractive state in the myopic direction (Chapter V. 2.2).

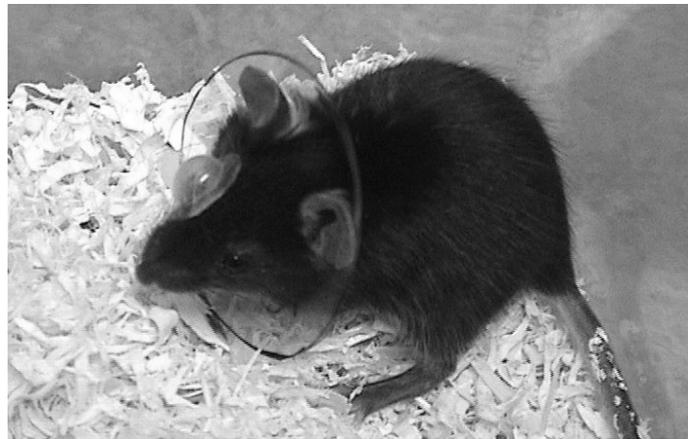


Figure 8. C57BL/6 mouse with a translucent hemispherical plastic diffuser glued to the fur around one eye. A collar, made from a ring of plastic foil, was fitted around the neck to prevent mice from removing the diffuser.

3.5 Statistics

The performance of OLCI was studied in different age groups by analyzing the standard deviations from repeated measurements in the same eyes. To study the effects of eye orientation on the measured axial lengths, a variance ratio test was used. The absolute differences between both eyes in individual animals were analyzed by paired Student's t-tests to estimate the natural variability in eye length. Paired Student's t-tests were also used to compare occluded and open control eyes.

4. Grating acuity at different illuminances in wild-type mice, and in mice lacking rod or cone function

4.1 Development of a behavioral paradigm: the automated optomotor drum

Spatial acuity was measured in an optomotor experiment as shown in Figure 9. During testing, mice were individually placed in a clear transparent acrylic glass cylinder (diameter: 15 cm, height: 18 cm) that was placed in the middle of a rotating drum. Large and small optomotor drums were tested in the experiments to evaluate the effects of target distance and potential refractive errors of the mice. If mice were myopic one would expect a higher grating acuity in the smaller drum, even if the spatial frequencies were adjusted for viewing distance. Furthermore, because the larger drum took more space and was more difficult to handle, a smaller set-up would have been more convenient. In the present study, the large drum had a diameter of 63 cm and a height of 35 cm, and the small one a diameter of 22 cm and a height of 29 cm. Data from the small drum are shown in Figure 28, all other data are from the large drum.

The drums provided the mouse with a drifting vertical square-wave pattern as it rotated in the vertical axis. Spatial frequency could be varied by placing stripe patterns with different width (spatial frequency ranging from 0.03 to 0.60 cyc/deg) inside the drum. Stripe cylinders were made from clear plastic foil on which black stripes were printed with a 1200 dpi laser printer. Since the inside of the drums were covered with white paint, the contrast was determined by the density of the print of the black stripes which was close to 100%.

The cylindrical container in which the mouse was freely moving was placed on a stationary white platform (diameter: 16 cm) in the center of the rotating drum (Figure 9), approximately 2 cm from its bottom. The drum was turned by a electric DC motor (Conrad Electronics, Hirschau, Germany). The direction of rotation could be changed by reversing the polarity of the voltage. The best optomotor responses were obtained for an angular speed of the stripe pattern between 50 and 60 deg/sec. Because the perspex cylinder containing the mouse was closed, it was unlikely that the mouse was stimulated by air currents

III. Material and Methods

that might have been generated by the rotating drum. Furthermore, controls with stationary drums were performed (described later).

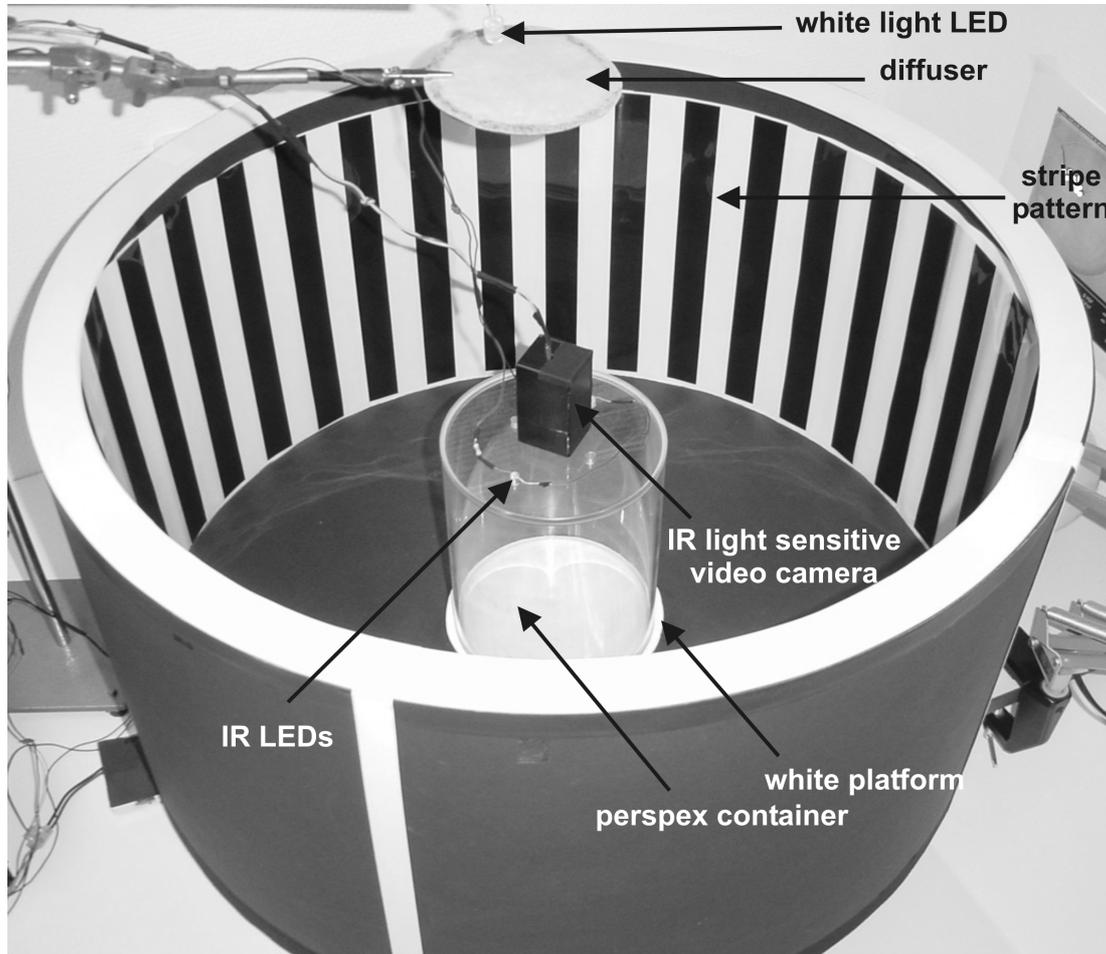


Figure 9. Set-up for the behavioral measurements of grating acuity in mice. Mice were placed individually in the perspex container. To quantify the behavioral responses under dim illumination or in darkness, the mouse was illuminated by two high power infrared light emitting diodes (IR LEDs). An infrared light (IR) sensitive video camera imaged the mouse and, after digitization of the video frames, a screen output as shown in Figure 10 was obtained. The pattern of vertical black and white stripes that was placed inside the drum was made from clear plastic foil. Spatial frequency could be varied by placing stripe patterns with different stripe widths inside the drum. The drum was illuminated either by a light bulb or a white light LED. In the latter case, a frosted diffuser was placed in front of the LED to generate a more homogenous illumination.

4.2 Illumination of the drum

Spatial acuity testing was carried out at different illuminances in the drum (400, 20, 2 and 0 lux, as measured with a calibrated photocell (United Detector Technologies). Measurements with a luminance meter (LS-100 LS-110, Minolta, Japan), positioned at the center of the perspex cylinder at about the height of the mouse and oriented toward the stripe pattern, resulted in readings of 30, 0.1 and 0.005 cd/m² at the three brightness levels mentioned above. An illuminance of 400 lux was generated by a light bulb (Philips, 60 W). Illuminances of 2 and 20 lux were produced by a white light LED (diameter 10 mm, mcd typ 1200, Conrad Electronics, Wernberg-Koebnitz, Germany) that was placed above the cylinder at 48 cm distance from the mouse. A frosted plastic diffuser, placed 2 cm below the LED, generated a largely homogenous illumination. To measure behavioral responses under very dim illumination or in complete darkness, the mouse container was illuminated by two high power infrared light emitting diodes (IR LEDs, VX-301 IR-Sendediode, 80 mW/sr, Conrad Electronics, Wernberg-Koebnitz, Germany), which were inserted in the cover of the perspex cylinder, about 16 cm above the mouse.

The luminance meter was also used to estimate the stripe contrast directly. It was focused either at the black or the white stripes and contrast was calculated by $C = (L_{\max} - L_{\min}) / (L_{\max} + L_{\min})$ with C = contrast, L = luminance of the stripes. The measured contrasts were approximately 90% at 400 lux and at 20 lux, and of 82% at 2 lux.

4.3 Programming algorithms and measured parameters

It was impossible to judge by eye whether the mouse followed a stripe pattern or not, since presumed phases of tracking were interrupted by movements in the opposite direction, or by complete loss of interest as the mouse often engaged in long periods of cleaning behavior. It was, therefore, necessary to automate the movement analysis. At this end, the mouse was imaged by a simple infrared sensitive monochrome miniature surveillance video camera (PAL format, 752 x 536 Pixels, Conrad Electronics, Hirschau, Germany) that

III. Material and Methods

was equipped with a lens with a focal length of 5 mm to achieve a large field of view. The camera was mounted in the center of the top cover of the perspex cylinder (Figure 9). After digitization of the video frames by a standard video board (Matrox Meteor II, TheImagingSource, Bremen, Germany), the video images were processed at 25 Hz by software written by Frank Schaeffel in Borland C++. The following steps were performed:

1. Measurement of the average pixel brightness in each video frame.
2. Detection of all pixels that were > 40% darker than the average brightness.
3. Calculation of the center of mass of these pixels. This procedure reliably marked the center of the mouse body.
4. Measurement of the mouse's angular running speed. Angular velocity (deg/frame) of the center of mass with respect to the center of the cylinder was summed up over time, and the standard deviation of all angular changes was determined after termination of the measurement session (approximately after 20 sec). A one sample t-test was automatically performed to find out whether there was a significant trend of the mouse to move in the direction of the drifting stripe pattern. Because the measurement of angular movement occurred in degrees, the 360° to 0° transition, or vice versa, caused artifactual high speeds. Therefore, the program ignored measurements in which the angular velocity exceeded 2 deg/frame (50 deg/sec).
5. Measurement of the mouse's angular body orientation. Since the mouse also turned its snout-tail axis in response to the drifting stripes, its orientation was also evaluated as a second parameter. An orthogonal regression was fit through the pixels marked in step 3. The changes of the slope of this regression was tracked over time. Again, transitions from 360° to 0°, or vice versa, caused high angular speed as an artifact. This problem was, again, solved by excluding velocities above 2 deg/frame.
6. Because tracking the activity of the mouse was essential for gaining statistically reliable data, the locomotor activity was also recorded. The average absolute angular position change from one frame to the next, as determined in step 4 was taken as a measure of the activity.

III. Material and Methods

The screen output of the software is shown in Figure 10.



Figure 10. Screen dump of the Borland C++ program that tracked the mouse. The program tracked the movement of the center of mass of the mouse, marked by the cross with the circle. The trace of movement is shown on the right. The average angular velocity of the center of mass of the mouse (average running speed) with respect to the center of the container was summed up over time and the standard deviation of all angular changes was calculated after termination of the measurement session (approximately after 20 sec). The angular movement of the snout-tail axis (see dotted line on the mouse image) was also recorded (angular orientation speed). Finally, the average activity was recorded as the average absolute angular position change from one frame to the next.

4.4 Measurement procedure

The behavioral study included 25 black C57BL/6 wild-type mice, three rhodopsin knock-out mice ($RHO^{-/-}$), three rod cyclic nucleotide-gated channel knock-out mice ($CNGB1^{-/-}$), three cone cyclic nucleotide-gated channel knock-

III. Material and Methods

out mice (CNGA3^{-/-}) and three transgenic mice lacking both rod and cone function (CNGA3^{-/-}RHO^{-/-}). Age ranges of the tested animals were between 30 and 40 days.

In most C57BL/6 wild-type mice the directional preference of the movement was correlated with the drift direction of the stripes, immediately after the animal was placed inside the drum. In a few mice, the measurements had to be delayed until the animals had adapted to their new environment and had finished their self-cleaning behavior. To minimize habituation of the optomotor response (Mitchiner, Pinto, Vanable, 1976), the direction of rotation of the drum was reversed approximately every 20 sec. The reversion was repeated five times at each spatial frequency. The initial direction of rotation was randomly chosen. Changing the direction by a mechanical switch on the power supply took about two seconds. Angular running speed, angular orientation speed and locomotor activity were recorded for each direction of rotation. Spatial frequencies of the stripe patterns were exchanged in a random order.

To assess the baseline noise in the measured parameters (i.e. the effects of spontaneous activity of the mouse), it was tested whether how variable the responses of the animals were when no visual stimulus was present. Wild-type mice (C57BL/6) were therefore measured in a drum that was not moving, and in a rotating drum which had no stripe pattern inside.

All mice were tested at seven different spatial frequencies (0.03, 0.05, 0.10, 0.20, 0.30, 0.40 and 0.50 cyc/deg) using the large drum with the diameter of 63 cm. The wild-type mice were tested at four different light levels (see above). For the measurements in darkness, mice were dark adapted for at least 60 min. RHO^{-/-} and CNGB1^{-/-} mice were tested at three light levels (400, 20 and 2 lux) and both CNGA3^{-/-} and CNGA3^{-/-}RHO^{-/-} mice were tested at two light levels (400 and 2 lux).

Furthermore, C57BL/6 wild-type mice were tested in the much smaller drum with a diameter of only 22 cm. Spatial frequencies of 0.03, 0.05, 0.07, 0.10, 0.20, 0.25, 0.30, 0.40, 0.50 and 0.60 cyc/deg were presented, with the stripe width corrected for the shorter viewing distance. However, because the mice could vary their distance to the stripe pattern, the changing viewing angles

introduced large variations in the spatial frequencies. Using this set-up, measurements were performed only at 400 lux.

4.5 Statistics

The *response* of the mouse to different stripe patterns was defined as the difference of its angular movement preference when the drum was rotating clockwise versus counter clockwise. These difference were analyzed both for the angular running speed and angular body orientation speed. The more this value differed from zero or the more it differed from the condition when no visual stimulation occurred, the more important the visual input was to the mouse's behavior.

Mean responses and standard deviations were plotted against spatial frequency. To estimate the cut-off spatial frequency that the mouse could still see, the responses were tested against zero, using paired Student's t-tests.

Furthermore, responses at different spatial frequencies, responses under conditions when no visual stimuli was present, responses at different illuminance, and responses of wild-type and knock-out mice were compared using an analysis of variance (one-way ANOVA). Post hoc analysis (the Dunnett test) was performed on factors that were found to be significant in the ANOVA. The significance level was set at 5%.

Locomotor activity was compared at different illuminances only in C57BL/6 wild-type mice using a variance ratio test. Statistical tests were performed on computer (JMP, version 4 software; SAS Institute, Cary, NC).

5. Contrast thresholds of wild-type mice wearing diffusers or spectacle lenses, and the effect of atropine, a myopia inhibiting drug

5.1 Optomotor experiment

Contrast thresholds were evaluated in an optomotor experiment as previously described (Chapter III. 4.1 or Schmucker et al., 2005). Since the mice were not restrained and could freely move in the acrylic glass container, the angular subtense the stripes was somewhat variable. However, the maximal possible variability in the viewed stripe widths remained below $\pm 24\%$. The angular stripe frequencies are referred to as "spatial frequencies" below, assuming that the fundamental was the limiting Fourier component.

Since it is not possible to judge reliably by eye whether the mouse followed a stripe pattern or not (Chapter III. 4.3 or Schmucker et al., 2005), the mice were tracked by the image processing program as described above. Measurement procedures and data analysis were as described above (Chapter III. 4.4 and 4.5 or Schmucker et al., 2005).

5.2 Measurements under photopic conditions

Optomotor experiments were performed at an average illuminance of the stripe patterns of 400 lux as described above (Chapter III. 4.2).

Contrast thresholds were evaluated in 12 juvenile mice at three spatial frequencies: 0.03 cyc/deg (the lowest frequency tested), 0.10 cyc/deg (the spatial frequency at which the mice displayed the best responses in a previous study, Chapter IV. 3.2.1 or Schmucker et al., 2005) and 0.30 cyc/deg (the highest spatial frequency at which the mice showed significant responses, Chapter IV. 3.2.1 or Schmucker et al., 2005). At spatial frequencies of 0.03 cyc/deg and 0.10 cyc/deg, the stripe patterns were presented with grating contrasts of 91%, 67%, 45%, 24% or 16%. At a spatial frequency of 0.30 cyc/deg, grating contrasts were 91%, 67%, 45% or 24%.

5.3 Measurements in dim light

An average illuminance of the stripe pattern of 20 lux was generated by a white LED (diameter 10 mm, mcd typ 1200; Conrad Electronics) as described above (Chapter III. 4.2). Spatial frequencies of 0.03 and 0.10 cyc/deg were tested at 91%, 67%, 45% or 24% contrast in seven juvenile mice. Mice were dark adapted for at least 60 min before the measurements were performed.

5.4 Measurements in mice wearing spectacle lenses

To evaluate the effects of defocus on contrast sensitivity, ten juvenile mice were tested under photopic conditions at a spatial frequency of 0.03 cyc/deg and maximum contrast (91%). During the optomotor experiment, spectacle lenses were attached to the eyes. Spherical PMMA lenses (obtained from HECHT Contactlinsen, Freiburg, Germany) with a diameter between 10.0 and 12.2 mm and a radius between 7.8 and 8.4 mm were used. The rims of the lens, about 1 mm wide, were attached to the fur around the eyes with ring-shaped double-sided tape (one side: adhesive tape; the other side: Velcro®) with an inner diameter of about 9 mm and an outer diameter of about 13 mm (obtained from Schell Naehzubehoer, Aachen, Germany). The lenses did not interfere with the normal functions of the eyelids. To prevent that the mice could remove the lenses during their cleaning behavior, plastic collars were fitted around their necks as previously described (Chapter III. 3.4). Before the measurements, the mice were adapted to the collars for at least 24 h. Lenses were attached 20 to 30 min before the optomotor experiment started under light ether anesthesia. The same lens powers were used in both eyes. The tested lens powers were +7 D, +25 D, -8 D, -15 D and -25 D. As controls, plano lenses were also tested.

5.5 Measurements in mice wearing diffusers

Four juvenile mice were tested while their vision was blurred with hand-made frosted hemispherical thin plastic shells which served as diffusers (Schaeffel et

al., 2004). The diffusers reduce the contrast of the retinal image over a wide range of spatial frequencies (Bartmann & Schaeffel, 1994). They were attached around the mouse eye in the same way as the spectacle lenses, and plastic collars were applied as described above. Diffusers were tested under photopic conditions, at spatial frequencies of 0.03, 0.10 or 0.30 cyc/deg, and the same contrasts as described above.

5.6 Measurements after atropine eye drops

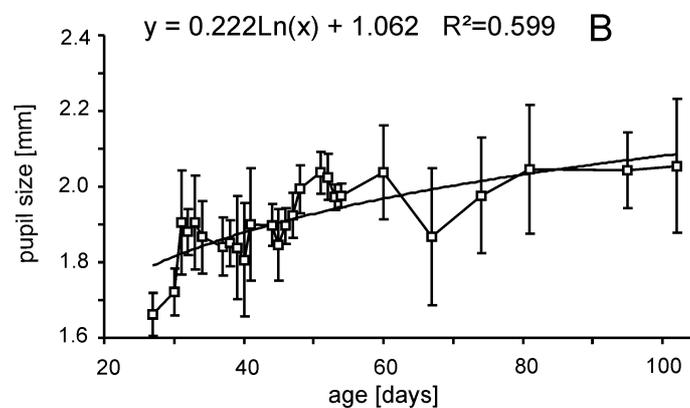
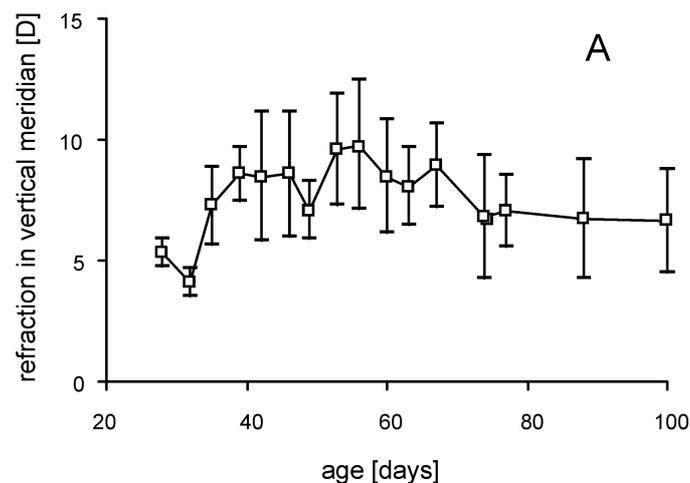
One drop of atropine (1% solution) was instilled in both eyes in five mice. A drop had a measured volume of 33 μ l, and contained 330 μ g atropine sulphate. To verify that the pupils were fully dilated, the light induced pupil responses were studied by video pupillography (Schaeffel & Burkhardt, 2005), before the optomotor experiments, about 20 minutes after atropine instillation. Contrast thresholds were measured under photopic conditions, at spatial frequencies of 0.03, 0.10 or 0.30 cyc/deg, and using the same contrasts as described above.

IV. Results

1. A paraxial schematic eye model for the growing C57BL/6 mouse

1.1 Development of refractive state and pupil size

The refractive development of the mice, as measured with infrared photoretinoscopy, is shown in Figure 11 A. The least hyperopic refractions were measured at day 32 (mean refraction \pm SD: $+4.1\pm 0.6$ D). Hyperopia increased and reached a peak at around day 55 ($+9.8\pm 2.7$ D). From day 70, the measured refractions became stable and levelled off at $+7.0\pm 2.5$ D. Developmental changes in pupil size are shown in Figure 11 B. Pupil diameter increased from about 1.78 mm at day 25 to 2.08 mm at day 100.



IV. Results

Figure 11. A. Development of refractive state (mean \pm SD) in the C57BL/6 mouse, as measured by infrared photoretinography. Averages from three animals are shown. No correction was made for the small eye artifact. Note that, with this technique, the mice reach a final refraction of about $+7.0 \pm 2.5$ D after 70 days. B. Growth of pupil size of the mice over the first 100 days. Error bars denote standard deviations.

The appearance of the brightness distributions of the photoretinoscopic reflexes in the pupils suggest considerable amounts of optical aberrations in the eyes. The ring-shaped areas of higher brightness that are visible (Figure 12) were not detectable in eyes that have good optical quality, like in birds or primates. However, since such brightness distributions were previously observed by Remtulla & Hallett (1985) and were present in most of the mice in the present study, it seems unlikely that these optical aberrations were random. Rather, they might indicate that the crystalline lens of the mouse is multifocal, similar to the lens in fish eyes, as described by Kroger, Campbell, Fernald, & Wagner (1999).

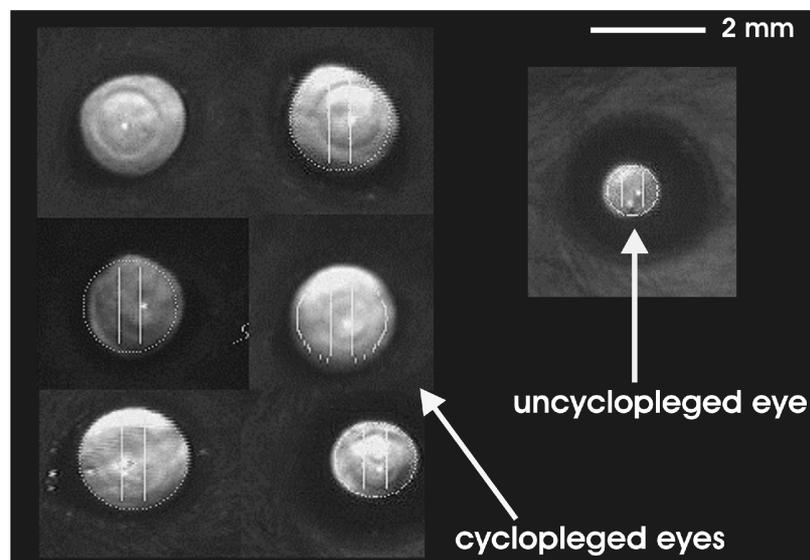


Figure 12. Brightness distributions observed in the pupils of mice during infrared photoretinography. Left column: Appearance of the pupils in six animals under cycloplegia (pupil sizes about 2 mm). Right column: Appearance of a pupil without cycloplegia, refracted at about 2 lux ambient illumination (pupil size about 1 mm). The ring-shaped areas of different brightness may reflect the presence of multifocal lenses as observed by Kroger et al. (1999) in fish eyes.

1.2 Growth of the ocular dimensions

Examples of frozen sections of two mouse eyes are shown for the ages of 23 days and 85 days in Figures 13 A and B, respectively. The sections show that the lens increased considerably in size, resulting in a decline of the vitreous chamber depth.

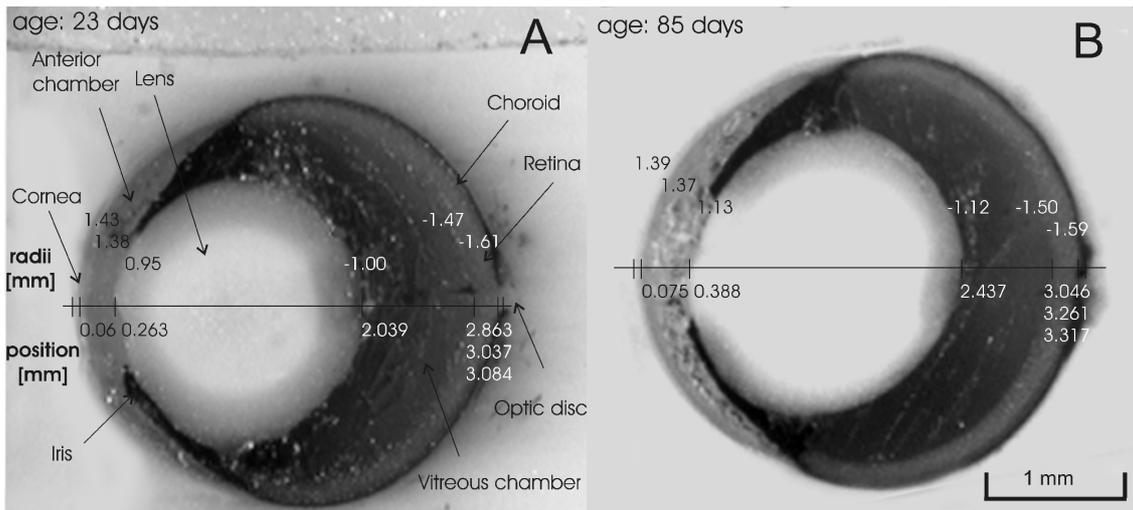


Figure 13. Frozen sections of mouse eyes at two different ages. Radii of curvature (labelled above the optical axis) and positions (labelled below the optical axis) of the optical surfaces were measured in these videographs and used to develop schematic eye models.

Growth curves of corneal thickness, anterior chamber depth, axial lens thickness, vitreous chamber depth, retinal thickness and axial length are shown in Figure 14. The data on the growth of the different components could be fitted by linear regressions. Exponential or logarithmic functions did not increase the quality of the fits. Accordingly, there was no indication that eye growth saturated over the first 100 days. This is a surprising result, given that mice are mature at the age of about 50 days. Axial length (the sum of corneal thickness, anterior chamber depth, lens thickness, vitreous chamber depth and retinal thickness) increased from 3.00 mm at day 22 to 3.34 mm at day 100 (Figure 14 F). Also the lens grew continuously in both axial and horizontal dimensions (axial lens growth is plotted as "lens thickness"), at a constant rate of 5.5 μm per day. Since axial length grew only by 4.4 μm per day, the vitreous chamber depth

IV. Results

declined with age. Figure 14 E shows that retinal thickness (as measured near the optic nerve head) grew from 0.176 mm at day 22 to 0.223 mm at day 100, which was equivalent to a growth rate of 0.6 μm per day.

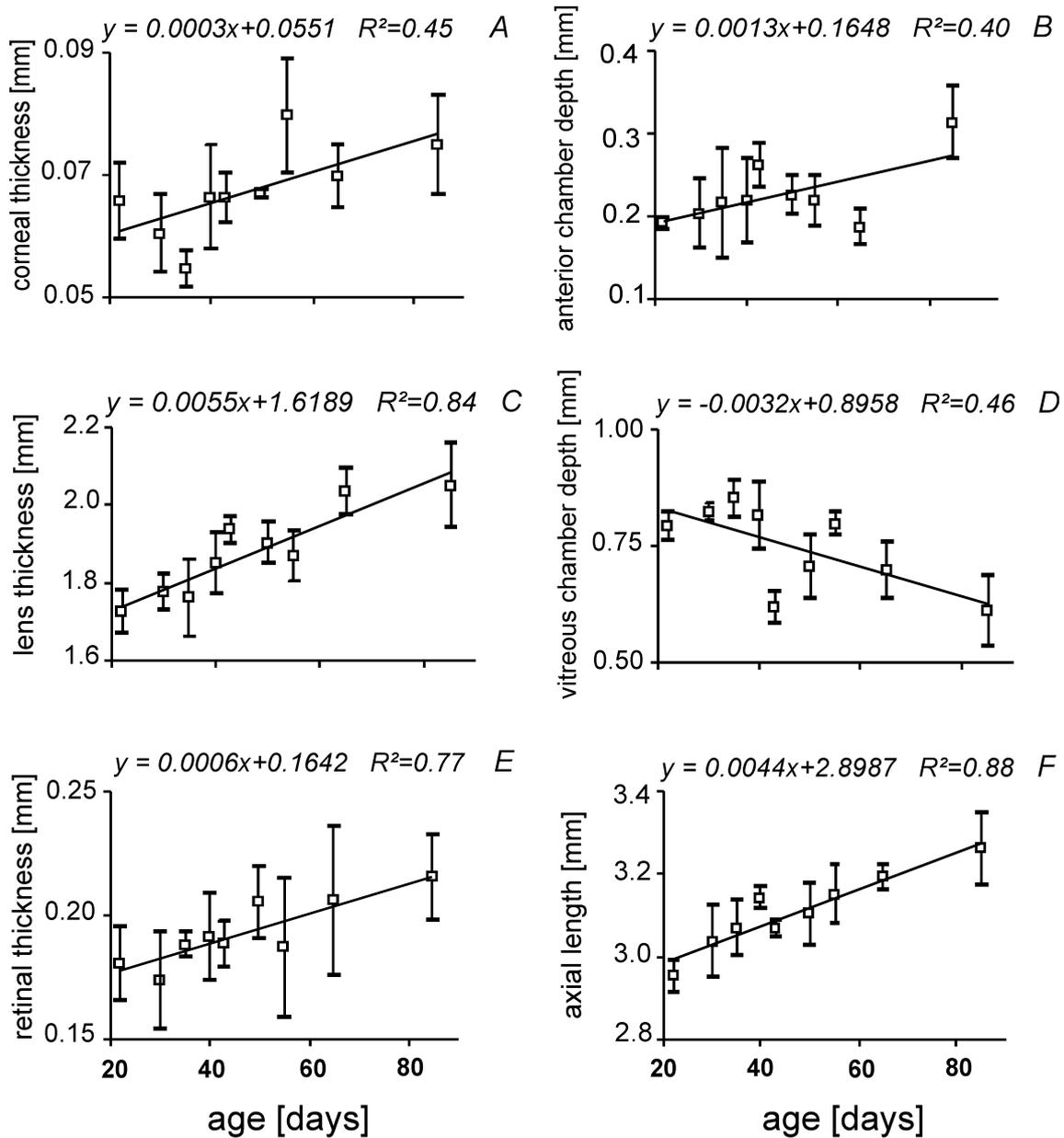


Figure 14. Development of the ocular dimensions of the mouse eye between day 22 and day 100. Axial length (F) is defined as the sum of corneal thickness (A) + anterior chamber depth (B) + lens thickness (C) + vitreous chamber depth (D) + retinal thickness (E). Data are based on frozen sections from 34 eyes (n=3 or more eyes for each age group). Error bars denote standard deviations.

The growth of the radii of curvature of the optical surfaces in the eye is shown in Figure 15. Neither the anterior nor the posterior radius of corneal curvature changed significantly with age (Figures 15 A and B). The averaged radii from all measurements of the anterior surface are 1.414 ± 0.019 mm, and for the posterior surface 1.415 ± 0.044 mm. Photokeratometry *in vivo* gave a slightly flatter anterior surface of the cornea of 1.493 ± 0.080 mm versus 1.414 ± 0.019 mm in frozen sections. The difference became significant due to the large number of samples ($df=66$, $T=5.6$, $P<0.001$, unpaired t-test). The larger standard deviations in the *in vivo* measurements reflect the difficulties in aligning the pupil axis of the mouse eye. It was noted that, if a Purkinje reflex was positioned close to the pupillary margin (due to inherent difficulties in centering), a flatter cornea was measured. This observation is in agreement with findings by Remtulla & Hallett (1985) and suggests an aspherical shape of the cornea. It could also explain that the averaged radii of curvature measured with photokeratometry were larger than with frozen sections. However, both techniques had in common that no changes were detected with age.

Different from the cornea, the radii of curvature of the anterior lens surface increased with age from 0.982 mm at day 22 to 1.208 mm at day 100 (Figure 15 C). The posterior lens showed no significant change in shape if linear regression analysis is used (Figure 15 D). The radius of curvature of the anterior and posterior retinal surface did also not change with age (Figures 15 E and F), with an average radius of curvature of the vitreo-retinal interface of -1.522 ± 0.033 mm and of the RPE of -1.607 ± 0.030 mm.

IV. Results

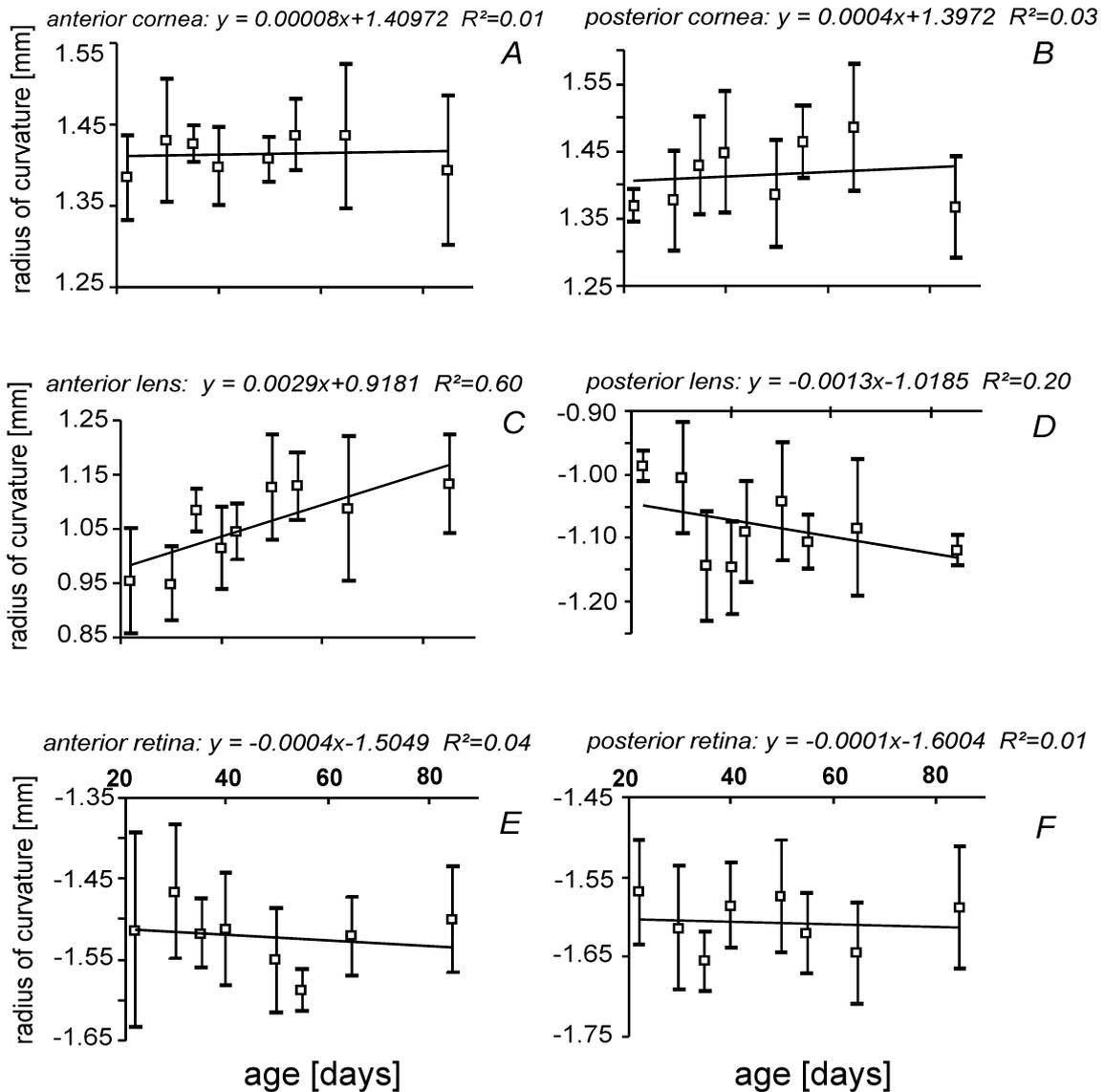


Figure 15. Development of the radii of curvature of the anterior and posterior surface of the cornea (A, B), lens (C, D) and retina (E, F), as determined in frozen sections. Data are based on frozen sections from 31 eyes ($n=3$ or more eyes for each age group). Error bars denote standard deviations.

1.3 Schematic eye modelling

Using the regression analyses shown in Figures 14 and 15, and the measured refractions shown in Figure 11 A, a schematic eye for the age range from 22 to 100 days was developed. The dynamic eye model allowed to construct schematic eyes for all ages between these age limits. The first finding was that

IV. Results

the equivalent lens index was remarkably high and also had to increase linearly with age from 1.579 to 1.657 to reproduce the measured refractions (Figure 16 A). The small eye artifact was calculated as the dioptric difference between the vitreo-retinal interface and the RPE. It ranged from +35.2 D to +39.1 D over the age range considered (Figure 16 B). It was also calculated how much the eye had to elongate to become one diopter more myopic (Figure 16 C). An elongation of 5.4 μm was necessary in a 22-day-old mouse and 6.5 μm was required for the same refractive change in a 100-day-old mouse.

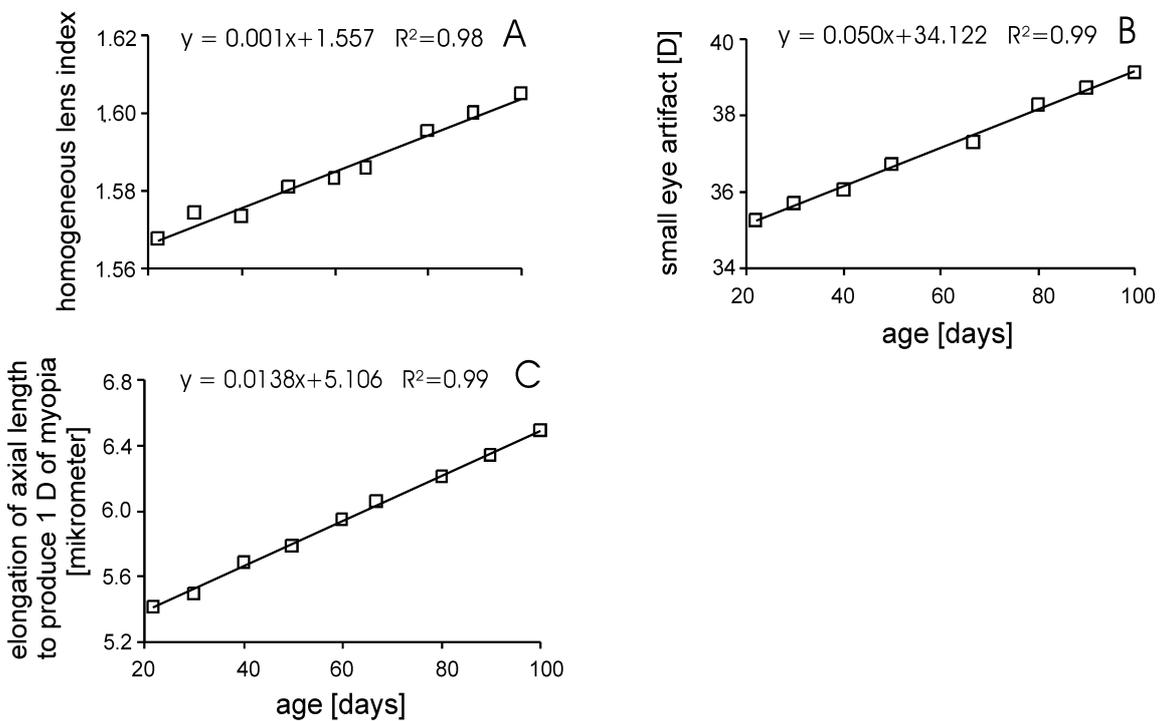


Figure 16. A. The refractive index of the growing lens was adjusted so that the schematic eye matched the refractive state measured by infrared photoretinography. B. The magnitude of the small eye artifact (Glickstein & Millodot, 1970) was calculated from the focal length and retinal thickness. C. Axial elongation necessary to make the model eyes 1 D more myopic, as a function of age.

1.4 Image magnification and f/number

As in other studies (Hughes, 1977), the posterior nodal distance (PND) and hence image magnification were highly correlated with axial length (Figure 17

IV. Results

A). The ratio of PND to axial length provides a further variable that can determine image size at a given eye size (Ott & Schaeffel, 1995). In the schematic eye of the mouse, this ratio changed only little with age (Figure 17 B; from 0.603 to about 0.581). Therefore, the developmental increase in retinal image magnification of about 10%, from 31 $\mu\text{m}/\text{deg}$ in young mice to 34 $\mu\text{m}/\text{deg}$ in adult mice (Figure 17 C) resulted largely from scaling.

The size of the entrance pupil, as measured *in vivo*, was 1.75 mm at day 22 resulting in a f/number of 1.033 (Figure 17 D). The f/number declined slightly with age, resulting in a 10% brighter image at day 100 than at day 22.

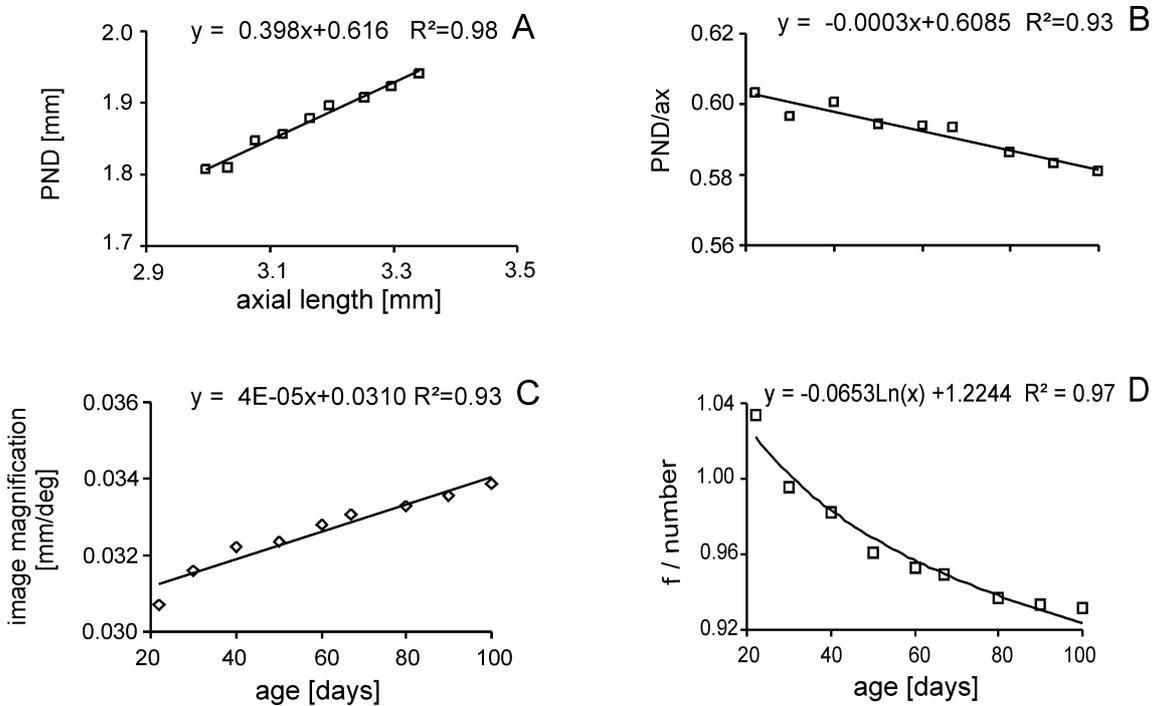


Figure 17. A. Posterior nodal distance (PND) was highly correlated with axial length. B. The ratio of PND to axial length decreased with age and was slightly smaller than in most vertebrates (on average: 0.6, Hughes, 1977). C. Retinal image magnification as a function of age. D. The f/number declined during development resulting in a 10% brighter image at day 100 than at day 22. In this case, a logarithmic function provided the best fit of the data.

2. *In vivo* biometry in the mouse eye with optical low coherence interferometry

2.1 Ocular dimensions in animals with normal vision

Mean values and standard deviations of axial length data, as measured with optical low coherence interferometry are shown in Figure 18. Axial length appeared slightly larger when it was determined after the cursor was manually moved from the anterior lens surface to the back surface of the cornea than when the anterior lens surface was automatically detected by the software. However, this was expected, given that the refractive indices used by the software were adapted for the human eye and were not perfectly correct (Chapter III. 3.1).

Axial length appeared to decline after the age of 53 days (Figure 18). This is in contrast to the previous data from frozen sections (Chapter IV. 1.2 or Schmucker & Schaeffel, 2004a). The cessation must, therefore, rather be due to the fact that mice from different litters were used at each age level.

Due to the satisfactory agreement between manual cursor use and automatic detection by the software (Figure 18), only those data where the cursor was manually moved to the back of the cornea are shown below. A linear regression of axial eye length versus age shows that the eyes grew by 7.3 μm per day ($y = 0.0073 + 2.9614x$, $R^2=0.8613$).

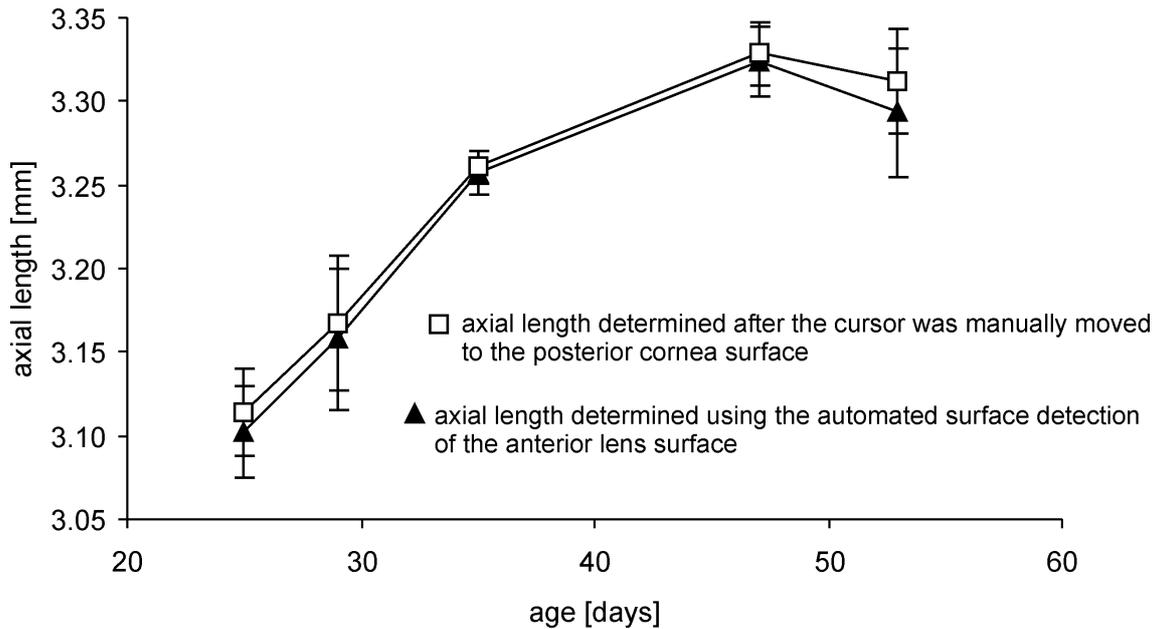


Figure 18. Axial eye growth between day 25 and 53, as measured by OLCI. Axial length was determined either after the cursor was manually moved to the back of the cornea (upper curve) or by using the automated surface detection in the software of the "AC Master" (lower curve). Data from 23 animals contributed to the curves, with three or more animals for each data point. Error bars denote standard deviations.

2.1.1 Variability of axial length measurements and comparisons to data from frozen sections

The average standard deviation for axial length measurements, i.e. the averages of all standard deviations obtained in repeated measurements in individual eyes was $8.0 \pm 2.9 \mu\text{m}$. There were no significant differences among different age groups in this study ($P > 0.05$, variance ratio test).

To determine how well the OLCI data agreed with the data from frozen sections, both data sets are plotted against age in Figure 19. The growth rates determined with OLCI were significantly higher (slope of axial length versus age: OLCI: 0.00728 ± 0.00076 , frozen section: 0.00511 ± 0.00051 , $df=10$, $T=5.5$, $P < 0.001$, variance ratio test; regression equations: OLCI: $y = 0.007x + 2.961$, $R^2=0.861$; frozen section technique: $y = 0.005x + 2.873$, $R^2=0.745$). There was also a consistent overestimation of axial lengths by OLCI by, on average, about $200 \mu\text{m}$ or 6.5%. Both differences trace back to inappropriate assumptions

regarding the refractive indices to convert optical path length into geometrical path length. With an average refractive index of 1.4328 (1.3454 increased by 6.5%) for aqueous humor, lens and vitreous humor, both measurements produce very similar axial length.

The average standard deviations were smaller with OLCI by a factor of 2.7 (average standard deviation of the different age groups: 25 μm in OLCI versus 68 μm in frozen sections).

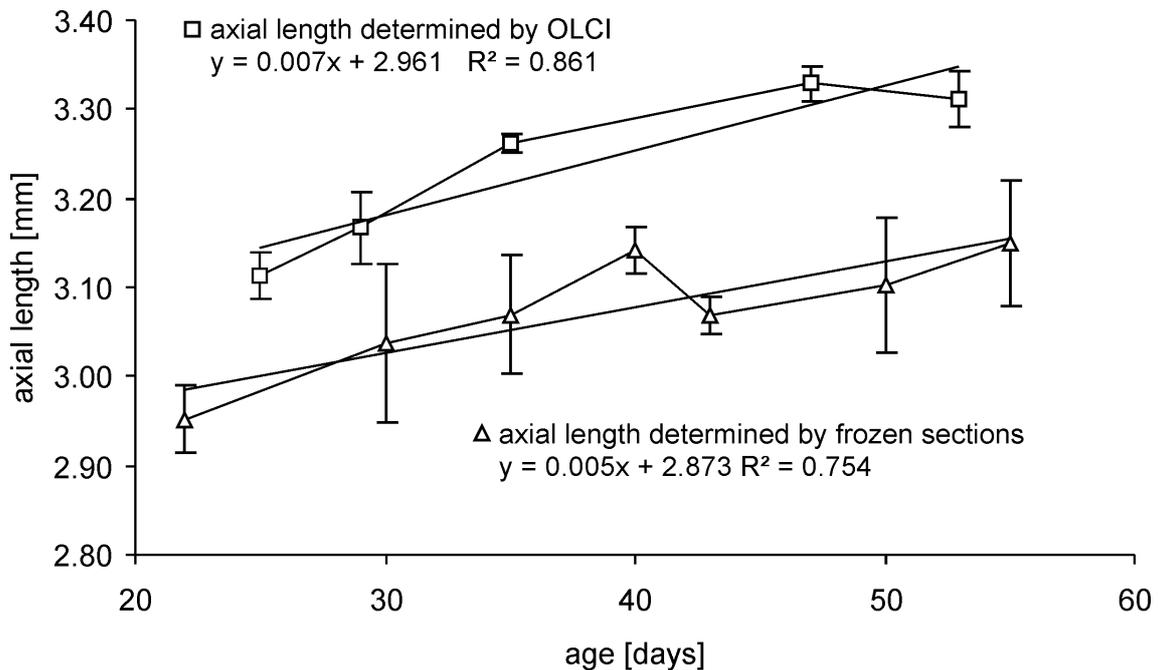


Figure 19. Comparison of axial length measurements by OLCI and by frozen sections (frozen section data are replotted after Chapter IV. 1.2). Axial length determined by OLCI had a lower average standard deviation by a factor of 2.7. Error bars denote standard deviations.

2.1.2 Within-animal variability

To evaluate the resolution of OLCI in detecting differences between both eyes of a mouse, the axial lengths from the left and right eye are plotted against each other (Figure 20). Orthogonal rather than linear regression was applied to study correlations between the eyes, since both data sets represent independent variables, with expected similar variance. First, there was no significant inter-

ocular difference in any of the animals at any age group ($P > 0.095$, paired t-tests). Second, the average absolute differences in axial lengths between both eyes were $17 \pm 18 \mu\text{m}$ and, with the algebraic signs considered, $-9 \pm 23 \mu\text{m}$. The inter-ocular variability in untreated animals shows that monocular deprivation must induce axial length differences of at least $20 \mu\text{m}$ to be detectable by OLCI. This axial length difference is equivalent to a change in refraction of about 4 D (Chapter IV. 1.3 or Schmucker & Schaeffel, 2004a).

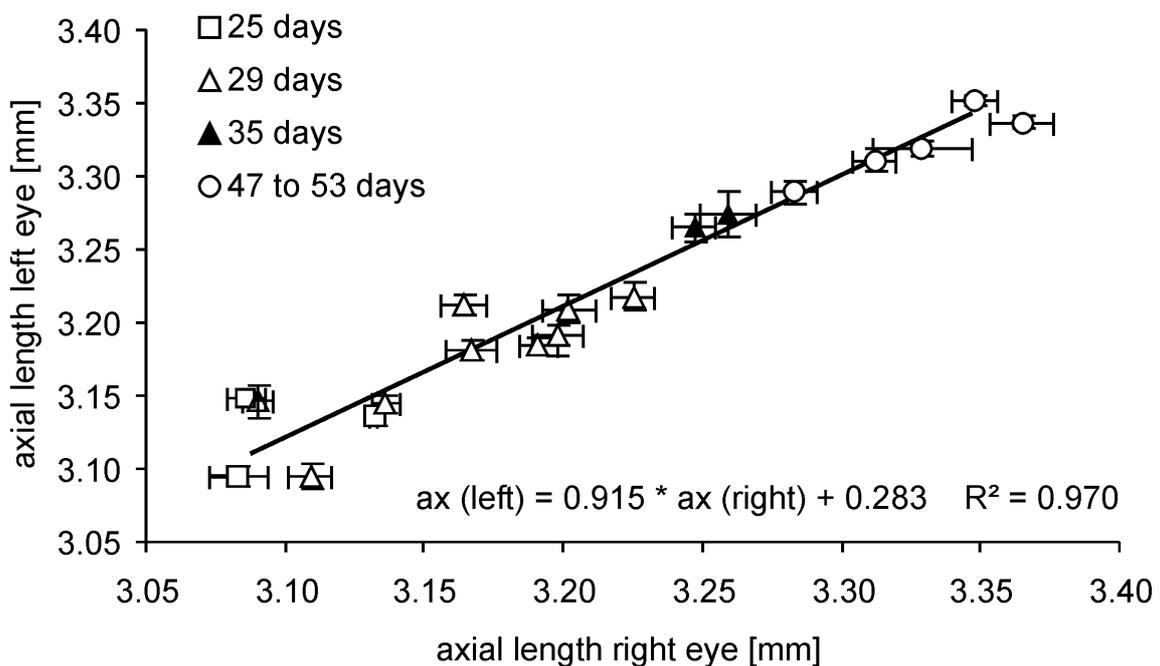


Figure 20. Axial lengths (ax) of left and right eyes of 19 C57BL/6 mice, plotted against each other. Each data point shows the mean value of at least three OLCI scans. Error bars denote standard deviations. The average standard deviation was only $8.0 \pm 4.4 \mu\text{m}$. The equation originates from orthogonal rather than linear regression.

2.1.3 Peripheral axial eye length

Axial length measurements with the pupil axis of the eyes tilted relative to the measurement beam by $52 \pm 6^\circ$ in the nasal, temporal, superior and inferior direction show that there are small, but significant differences in the OLCI scans in the periphery in both meridians (horizontal meridian, Figure 21 A: temporal: -

IV. Results

$8 \pm 21 \mu\text{m}$, $P=0.022$; nasal: $-3.7 \pm 11 \mu\text{m}$, $P>0.05$; vertical meridian, Figure 21 B: superior: $-14.5 \pm 15.3 \mu\text{m}$, $P=0.01$; inferior: $-12.1 \pm 10.6 \mu\text{m}$, $P=0.003$; unpaired t-tests). The average standard deviation obtained in single eyes were $8.0 \pm 2.4 \mu\text{m}$ for the peripheral measurements. This is not different from the standard deviations obtained in the pupil axis. It is clear, however, that variations in angular alignment of a few degrees are not a major contributing factor to the measurement variability.

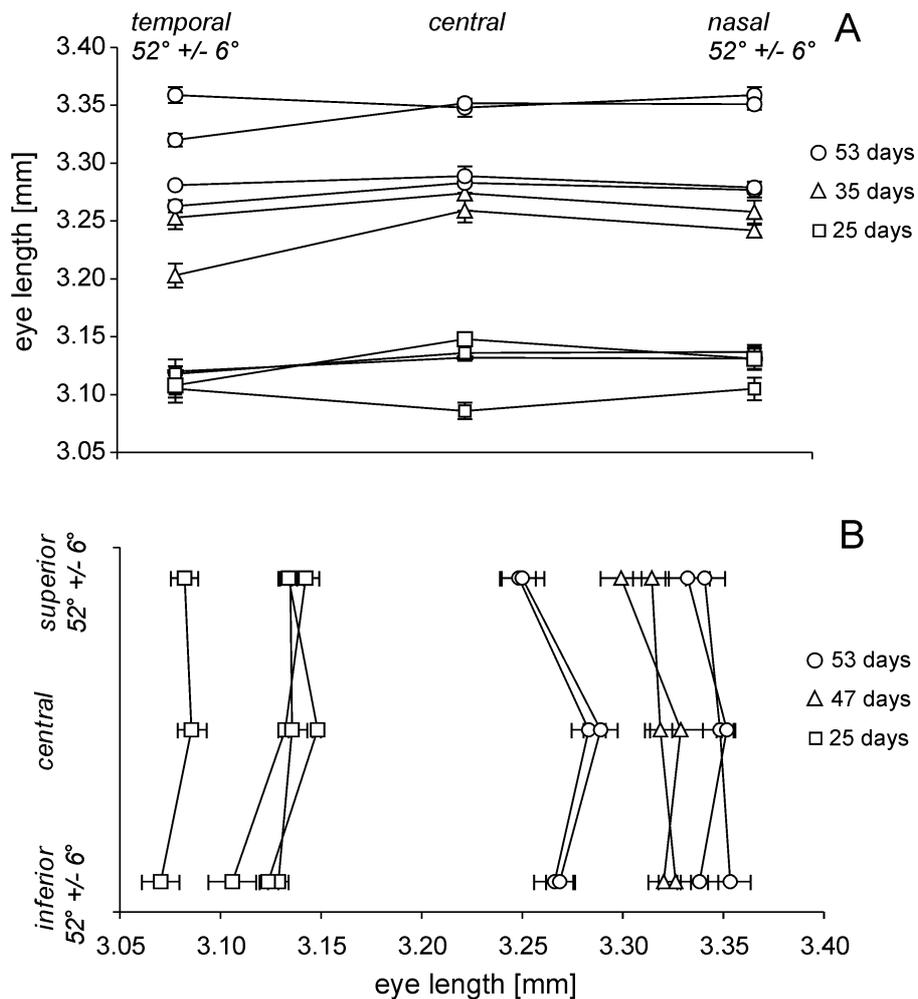


Figure 21. Axial length measured from different angular positions in ten mouse eyes at three different age levels. Each data point represents the mean and standard deviation of at least three OLCI scans in single animals. A. Axial length measurements at three angular positions in the horizontal meridian. B. Axial length measurements at three angular positions in the vertical meridian.

2.1.4 Corneal thickness

A comparison of corneal thickness as measured by OLCI and by frozen sections is shown in Figure 22 A. The average standard deviation is similar with both techniques ($5.0 \pm 2.0 \mu\text{m}$). Thicker corneas were measured by OLCI than in frozen sections by a factor of 1.5, which is too large to be explained by inappropriate refractive indices. The slow growth rate of corneal thickness ($0.4 \mu\text{m}$ per day) was similar with both techniques. The mean absolute difference between corneal thickness in both eyes was $5.14 \pm 4.83 \mu\text{m}$ ($P=0.4$, paired t-test) and, with the algebraic sign considered, $-1.35 \pm 6.92 \mu\text{m}$. The average standard deviation obtained from repeated measurements in individual eyes was $3.5 \pm 2.1 \mu\text{m}$.

2.1.5 Anterior chamber depth

Both techniques show a similar growth rate of the anterior chamber depth ($14 \mu\text{m}$ and $15 \mu\text{m}$ per day, respectively; Figure 22 B). Again, OLCI provides larger anterior chamber depths than frozen sections by a factor of 1.7. The average standard deviation was $20 \pm 6 \mu\text{m}$ in OLCI and $35 \pm 18 \mu\text{m}$ in the frozen sections, with an average absolute difference between both eyes of $16.7 \pm 14.8 \mu\text{m}$ and a difference of $5.4 \pm 22 \mu\text{m}$ with the algebraic sign considered. The average standard deviation obtained from repeated measurements in individual eyes was $10.6 \pm 12.3 \mu\text{m}$.

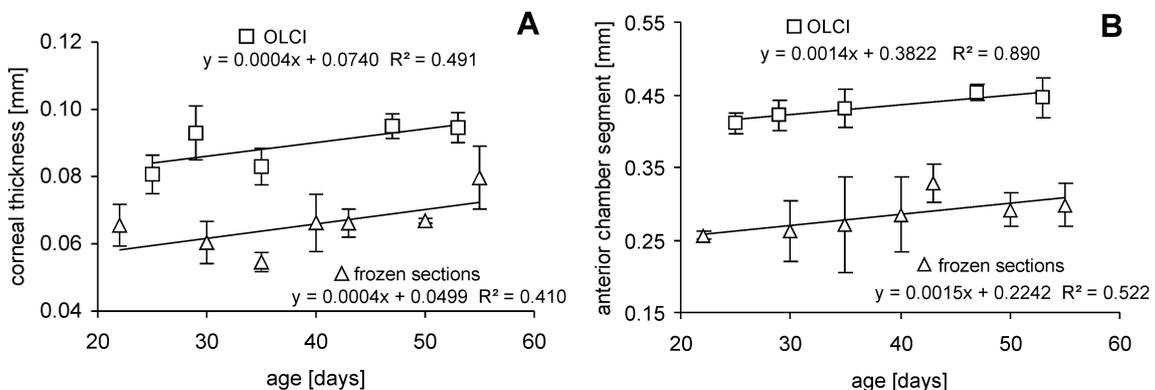


Figure 22. Development of corneal thickness (A) and anterior chamber depth (B) in the growing mouse eye, as determined by OLCI and from frozen sections. Data from frozen sections are replotted from Chapter IV. 1.2. Error bars denote standard deviations. Note that anterior chamber depth includes corneal thickness in both data sets.

2.2 Effects of deprivation of form vision on refractive development and ocular growth

After two weeks of form deprivation, refraction data could be obtained from six animals. In mouse 7, the pupil was too small to obtain reliable refractions. Despite two weeks of deprivation, no significant differences were detected between the refractions of both eyes (deprived: $+6.78 \pm 5.19$ D versus control: $+5.66 \pm 5.27$ D; $P > 0.05$, paired t-test). Refractive development of individual animals are shown in Figures 23 A and B, respectively. In addition, both Figures show the refractive development of untreated mice, replotted from Chapter IV. 1.1. Eyes that were occluded, were more hyperopic at the begin of the experiment than the control eyes ($+6.67 \pm 1.61$ D versus $+3.54 \pm 3.33$ D) and this difference was almost significant ($P = 0.077$, paired t-test). Therefore, the change in refraction during the deprivation period relative to the start-up value was also studied. However, there was still only a tendency to develop relatively more myopia in the occluded eyes (change: $+0.10$ D versus $+2.12$ D in the open eyes) which did not achieve significance ($P = 1.67$, paired t-test).

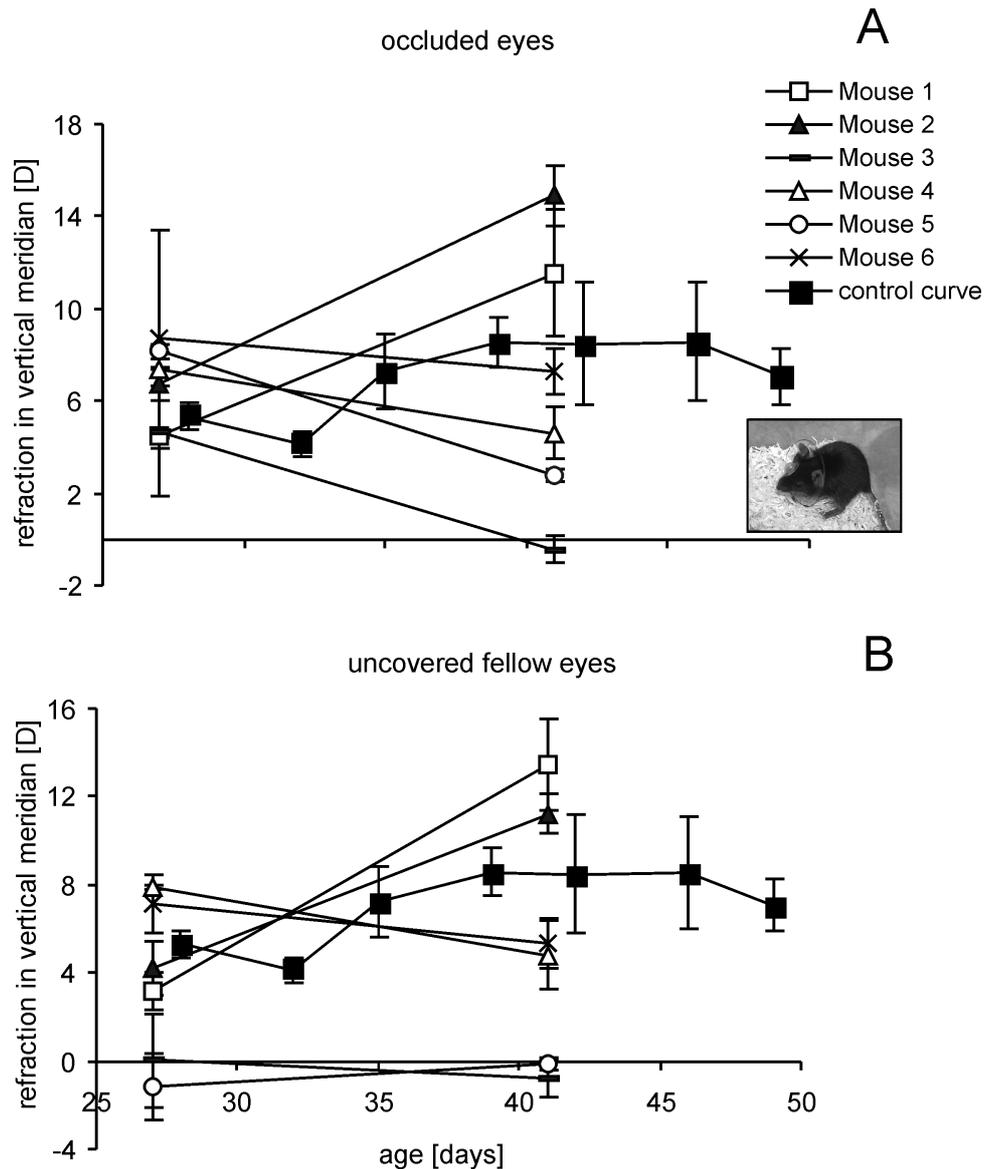


Figure 23. Refractive development in monocularly deprived mice. Refractive error was measured by infrared photoretinoscopy at the beginning of the deprivation period (day 27) and at the end (day 41). The filled squares ("control curve") show the refractive development of three untreated mice from a previous study (Chapter IV. 1.1). A. Refractive development in occluded eyes. B. Refractive development in open fellow eyes. Error bars denote standard deviations.

Axial length data from occluded and open control eyes are shown in Figures 24 A and B. OLCI revealed axial elongation in the occluded eye, compared to the open fellow eye of $38 \pm 36 \mu\text{m}$ ($3.274 \pm 0.027 \text{ mm}$ versus $3.236 \pm 0.039 \text{ mm}$; $P=0.045$, paired t-test). Significance was achieved even though two animals

(mouse 2 and mouse 3) responded in reversed fashion. The average absolute difference between both eyes was $47 \pm 23 \mu\text{m}$, compared to $17 \pm 18 \mu\text{m}$ in untreated animals (Chapter IV. 2.1.2). Even though the changes in eye growth were not always in the direction of more myopia, it is clear that occlusion caused more variability in axial eye growth. On average, the deprived eyes grew 1.16% more than the open fellow eyes.

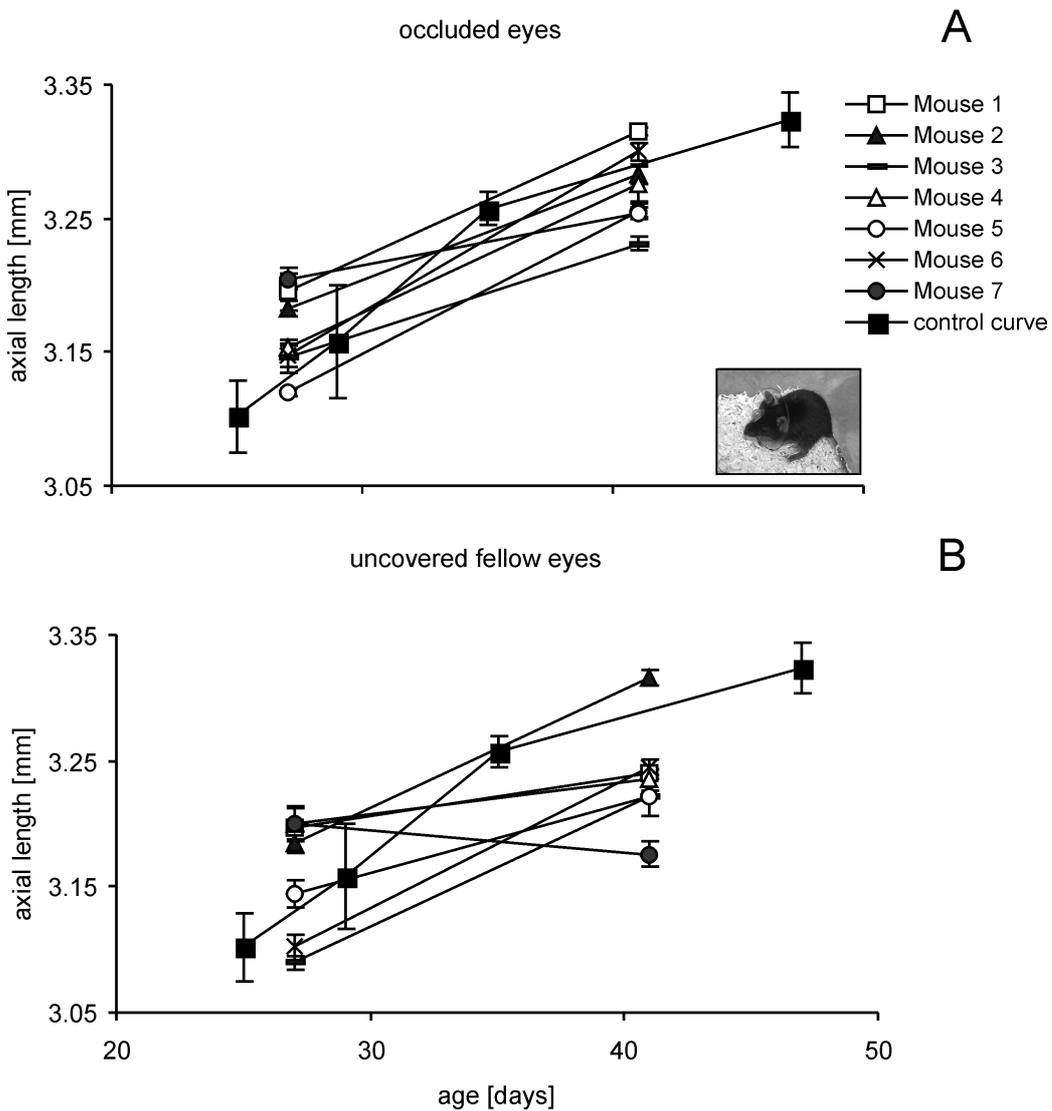
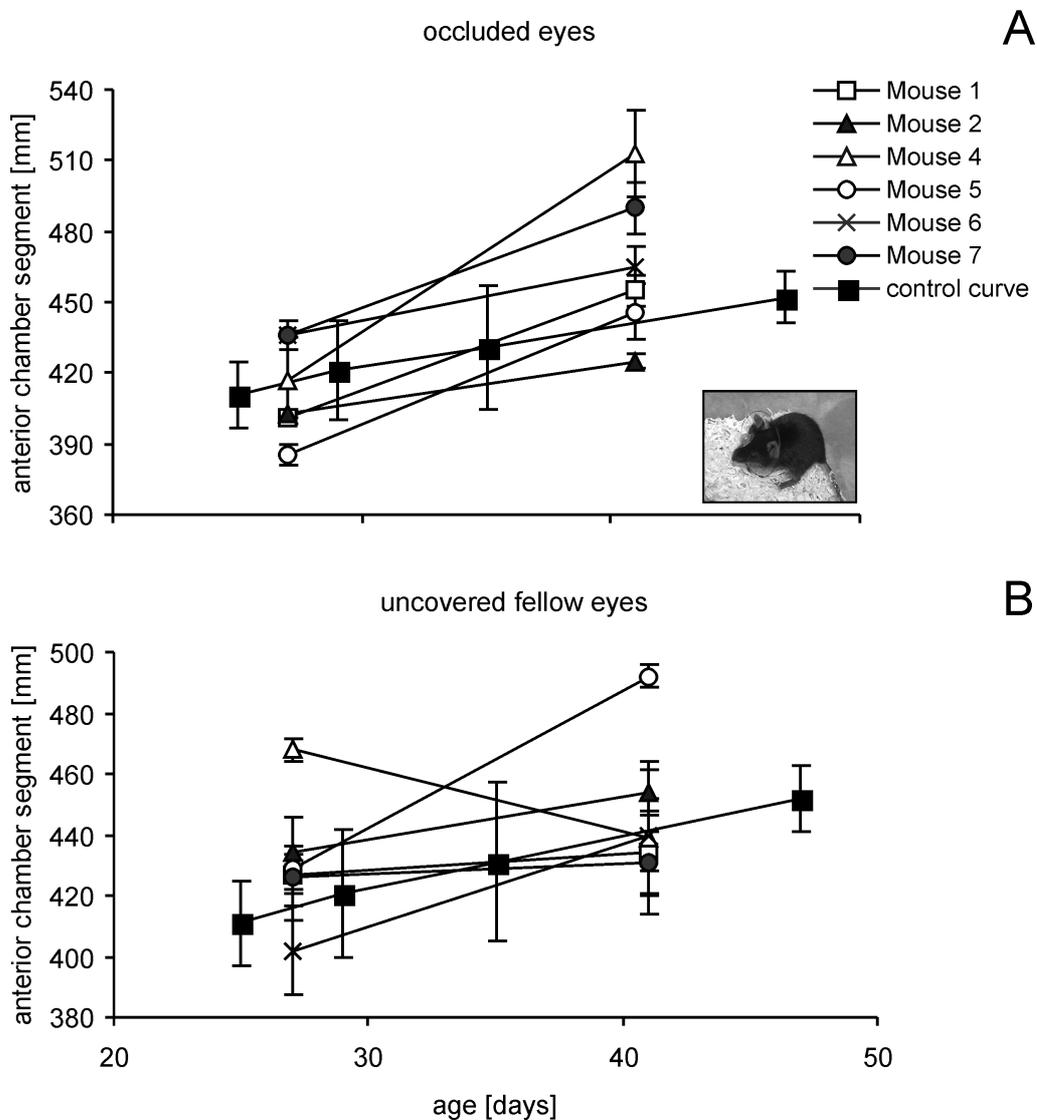


Figure 24. Axial eye growth in the same mice described in Figure 23. Axial eye growth data from 23 untreated control mice (Figure 19) are also shown for comparison. A. Axial eye growth in occluded eyes. B. Axial eye growth in open fellow eyes. Error bars denote standard deviations.

IV. Results

It was striking that no significant myopic shift was induced by form deprivation in this sample (Figure 23), despite that there was significant axial elongation. A possible explanation could be that the dioptric apparatus decreased its refractive power. To increase the focal length, either the cornea could have flattened, the lens could have thinned or the anterior chamber depth could have deepened. On average, there was indeed a tendency of the anterior chamber depth to increase in deprived eyes (Figures 25 A and B) compared to the fellow control eyes ($465.7 \pm 28.8 \mu\text{m}$ versus $448.3 \pm 20.8 \mu\text{m}$). However, a paired t-test did not reveal any significance ($P=0.41$).



IV. Results

Figure 25. Development of anterior chamber depth in the same mice described in Figure 23. In mouse 3, no anterior chamber depth data were obtained, as the anterior lens surface was not detected by the OLCI. Data on the development of the anterior chamber depth in 23 untreated mice is shown for comparison (Figure 22 B). A. Anterior chamber depth in occluded eyes. B. Anterior chamber depth in the open fellow eyes. Error bars denote standard deviations.

3. Grating acuity at different illuminances in wild-type mice, and in mice lacking rod or cone function

3.1 Baseline variability of the measurement procedure

Angular running and orientation speeds and the locomotor activity were studied in the C57BL/6 wild-type mouse in the large drum, either stationary or rotating, without any stripe pattern inside. Figure 26 shows the mean optomotor responses and their standard deviations in both cases. In addition, the effect of variable illuminances was tested. The responses were not significantly different from zero ($P > 0.15$, variance ratio test) both for the stationary and rotating drum, indicating that the movement patterns of the mice were random. For the angular running speed, the response in the stationary drum was $+0.002 \pm 0.002$ deg/frame, and in the rotating drum $+0.008 \pm 0.013$ deg/frame. For angular orientation speed, the response was $+0.020 \pm 0.008$ deg/frame and -0.001 ± 0.030 deg/frame, respectively. The responses were also not different between the stationary and rotating drum without stripe pattern ($P > 0.12$, variance ratio test). Locomotor activity evaluated in the stationary drum was not significantly affected by illuminance (Figure 26 C; $P > 0.10$, variance ratio test). The mean locomotor activity was $+0.298 \pm 0.038$ deg/frame. At each light level, the locomotor activity was significantly different from zero ($P < 0.02$, variance ratio test), indicating that the mice were active.

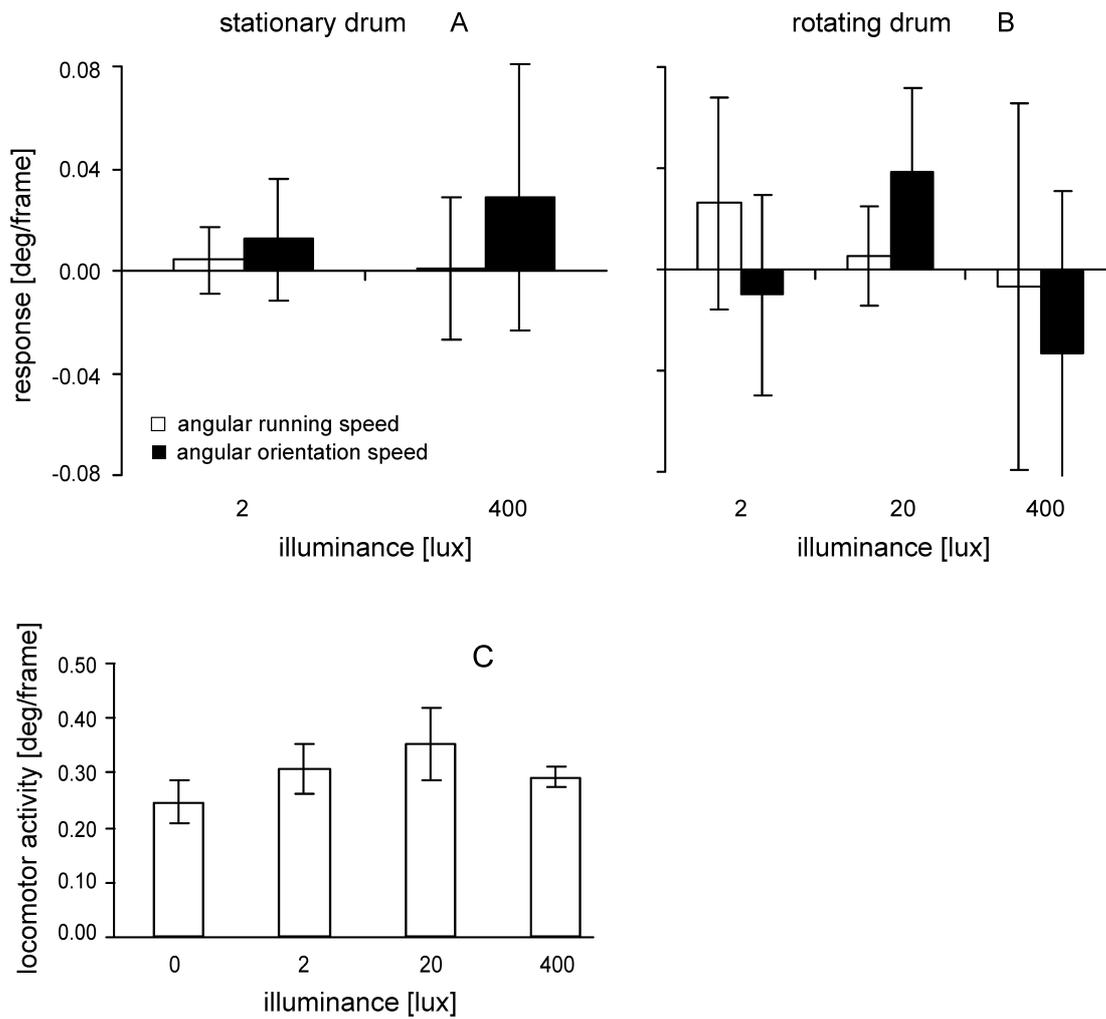


Figure 26. Responses of C57BL/6 wild-type mice in a stationary white drum (A) and in a rotating white drum without stripe pattern inside (B). Note that there were no significant preferences of the mice to move in a certain direction ($P>0.15$, variance ratio test). The locomotor activity of the mice was not significantly different at different illuminances ($P>0.10$, variance ratio test; C: stationary drum without stripe pattern). Each bar graph shows the mean and standard deviation of results from at least three animals.

3.2 Spatial vision in wild-type mice

3.2.1 Grating acuity as measured in a large optomotor drum

Average responses and their standard deviations at different spatial frequencies are shown for both angular running speed and orientation speed in Figures 27 A

and B. Furthermore, Figure 27 shows the possible uncertainty in the spatial frequency variable, resulting from the fact that the mice could move and vary their viewing angles of the stripes. An uncertainty in the spatial frequency variable of approximately $\pm 20\%$ was introduced. On average, the angular running speed was significantly larger than the angular orientation speed and this difference reached statistical significance (difference: $+0.022 \pm 0.031$ deg/frame, $df=40$, $T=2.02$, $P=0.003$, variance ratio test). Apparently, the angular running speed had more descriptive power.

The largest responses were obtained when the drum was rotated at the highest illuminance of 400 lux. At this illuminance, the mice displayed significant responses at spatial frequencies up to 0.30 cyc/deg, compared to the response of zero. When the stripes were smaller, more animals began to move randomly ($P > 0.05$, variance ratio test). Comparing the responses at 400 lux to the responses when no visual stimuli was present (either a stationary drum or a rotating drum without stripe pattern inside, Figure 26 A and B), significant differences were found ($P=0.003$, one-way ANOVA). This confirmed that the mice were able to detect the gratings.

The responses declined when the illuminance was reduced. To estimate the importance of visual input at different illuminances, the responses at all tested spatial frequencies were added up. Using the sum of the responses at 400 lux as a reference, it was found that the importance of visual input declined with declining illuminance (400 lux: 100%, 20 lux: 76.4%, 2 lux: 45.9%, and -9% in complete darkness). The impression was confirmed by a one-way ANOVA which revealed significant differences in the responses at the different illuminances ($P=0.003$). The post hoc analysis revealed no significant difference between the responses at 400 lux and at 20 lux ($P > 0.05$, Dunnett test), but there was a significant difference between the response at 400 lux and 2 lux ($P < 0.05$, Dunnett test) and 400 lux and complete darkness ($P < 0.005$, Dunnett test).

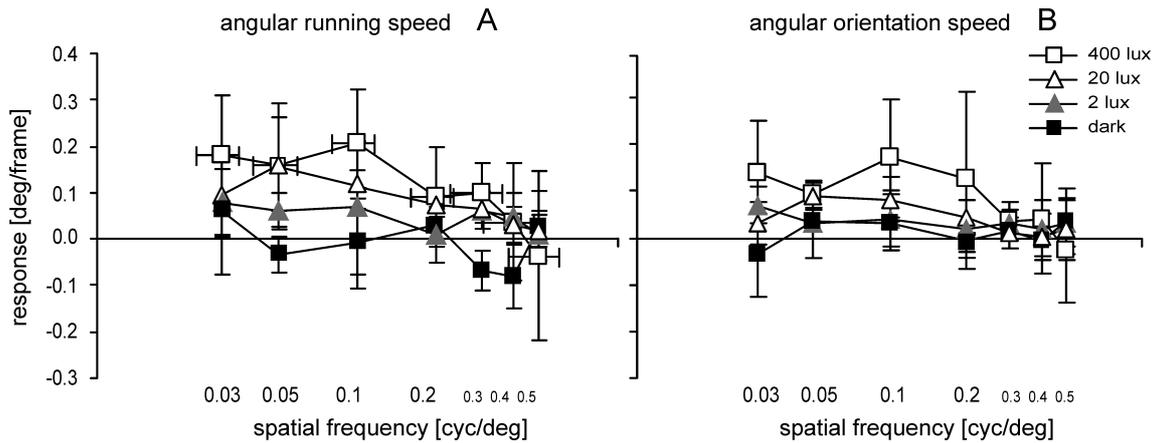


Figure 27. Mean optomotor responses and their standard deviations of C57BL/6 wild-type mice at different spatial frequencies. (A) angular running speed and (B) angular orientation speed. The horizontal error bar illustrates the uncertainty of the spatial frequency variable, resulting from the fact that the mice could change their viewing angle by moving closer to the stripe pattern. Data from seven animals are shown, with three or more animals tested at each data point. Angular running speed had more statistical power ($P < 0.005$, variance ratio test). The responses of the mice were significantly different to the condition where no visual stimuli was present, for spatial frequencies up to 0.10 cyc/deg at 400 lux ($P < 0.05$, Dunnett test). If compared to the null hypothesis, responses were significantly different from zero up to 0.30 cyc/deg ($P < 0.05$, variance ratio test). The responses at 20 lux were decreased, but were not significantly different to the responses at 400 lux ($P > 0.05$, Dunnett test). Responses at 2 lux were significantly different from the responses at 400 lux ($P < 0.05$, Dunnett test). Responses in complete darkness were neither significantly different from zero ($P > 0.05$, variance ratio test), nor significantly different from the response when no stripe pattern was present in the rotating drum ($P > 0.005$, Dunnett test).

3.2.2 Grating acuity as measured in a small optomotor drum

To test whether the viewing distance and, accordingly, refractive state had an effect on the measured grating acuity, wild-type mice were also studied in the small drum.

Figures 28 A and B show the responses of the mice to drifting gratings at 400 lux. As in the large drum, responses reached a peak between 0.07 and 0.25 cyc/deg (angular running speed) or at 0.10 cyc/deg (angular orientation speed). In the small drum, angular running speed was not significantly different

IV. Results

compared to angular orientation speed (difference: $+0.01 \pm 0.04$ deg/frame, $df=18$, $T=2.1$, $P=0.48$, variance ratio test). During these tests, the mice showed responses that were significantly different from zero up to 0.50 cyc/deg ($P < 0.05$, variance ratio test). The response was not significant at 0.40 cyc/deg. Additionally, a one-way ANOVA revealed that the responses were different to the responses without visual stimuli (Figure 26; $P < 0.0001$). The results of the variance ratio test were supported by a post hoc analysis ($P < 0.05$, Dunnett test). The slightly higher spatial acuity obtained in this experiment could either result from myopic refractive errors of the mice, or from the fact that they could move closer to the stripe pattern which increased their viewing angle and reduced the spatial frequency. The uncertainty of the spatial frequency variable was calculated by simple geometry and is plotted as horizontal error bars in Figure 28.

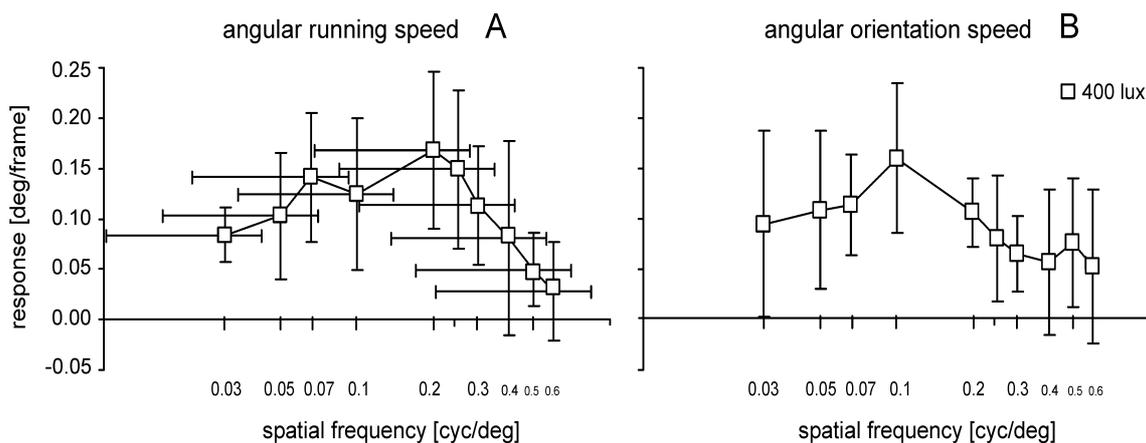


Figure 28. Optomotor responses of C57BL/6 wild-type mice at different spatial frequencies, for angular running speed (A) and angular orientation speed (B). Error bars as in Figure 27. Data from fifteen animals contributed to the curve, with five or more animals for each data point. Mice showed significant responses for spatial frequencies up to 0.50 cyc/deg. Eight out of ten responses were significantly different to zero ($P < 0.05$, variance ratio test) and significantly different from the responses when no visual stimuli were present ($P < 0.05$, Dunnett test).

3.3 Spatial vision in mutant mice

3.3.1 Spatial vision in mice lacking rod function ($RHO^{-/-}$ and $CNGB1^{-/-}$)

Figures 29 A and B show the grating acuity in rhodopsin knock-out ($RHO^{-/-}$) mice at three different light levels. Different from wild-type mice in the large drum, there was no significant difference between angular running and angular orientation speed (difference: -0.05 ± 0.07 deg/frame, $df=38$, $T=2.0$, $P=0.78$, variance ratio test). Comparing the responses of the $RHO^{-/-}$ mouse to the responses when no visual stimulation was present (Figure 26), significant differences were revealed ($P=0.002$, one-way ANOVA). The Dunnett test showed that significant responses at 0.03, 0.05 and 0.10 cyc/deg were only elicited at 400 lux ($P<0.05$). The conclusion was similar when the responses were tested against zero ($P<0.05$, variance ratio test).

A one-way ANOVA was also performed to identify differences between the responses of the $RHO^{-/-}$ and the wild-type mice ($P=0.007$). The post hoc analysis showed that there was no difference between the two strains in the responses at 400 lux ($P>0.05$, Dunnett test). However, the $RHO^{-/-}$ mouse showed a reduced response at both 20 lux and 2 lux ($P<0.005$, Dunnett test).

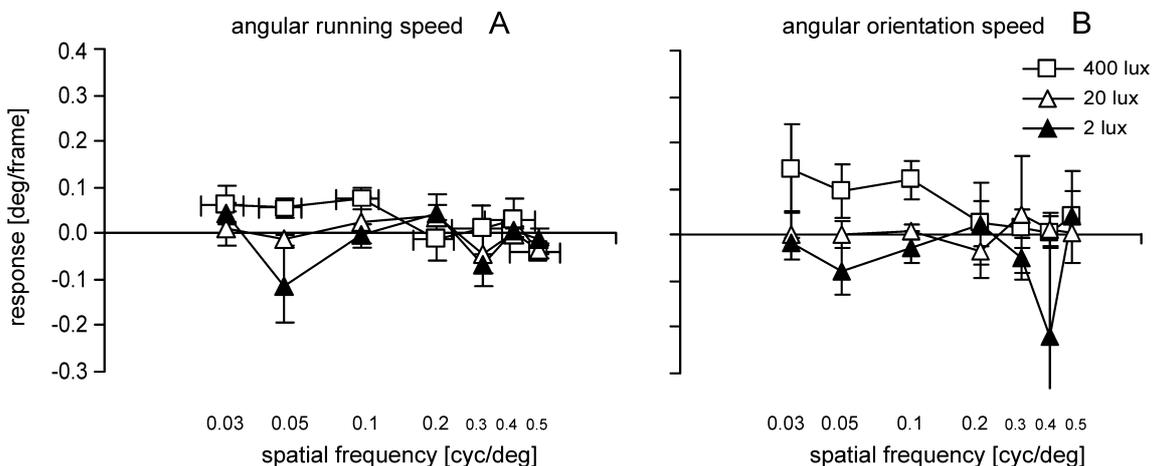


Figure 29. Optomotor responses of rhodopsin knock-out ($RHO^{-/-}$) mice are plotted against spatial frequency for angular running speed (A) and angular orientation speed (B). Error bars as in Figure 27. At 400 lux, the mice showed significant responses up to 0.10 cyc/deg ($P<0.05$, Dunnett test). At 20 and 2 lux, response was randomly distributed and neither significantly

IV. Results

different from zero ($P>0.05$, variance ratio test) nor significantly different from the response when no visual stimuli was present ($P>0.05$, Dunnett test).

Grating acuity in the second model lacking rod-mediated vision (the $CNGB1^{-/-}$ mouse) is shown in Figures 30 A and B for three light levels. As in the $RHO^{-/-}$ mouse, significant responses were only elicited at 400 lux. Again, there was no significant difference between angular running speed and angular orientation speed (difference: -0.01 ± 0.02 deg/frame, $df=40$, $T=2.0$, $P=0.36$, variance ratio test).

These mutants showed significant response to gratings of 0.03, 0.05 and 0.20 cyc/deg at 400 lux ($P<0.05$, variance ratio test). In comparison to the responses when no visual stimuli was present (Figure 26), significant responses were observed at 0.03 cyc/deg and 0.05 cyc/deg ($P<0.05$, Dunnett test).

To uncover differences between the responses of the $CNGB1^{-/-}$ and the wild-type mice, a one-way ANOVA was performed ($P=0.001$). Similar to the $RHO^{-/-}$ mouse, the post hoc analysis showed no difference between the responses at 400 lux ($P>0.05$, Dunnett test). Again, the responses at 20 lux and 2 lux were significantly reduced ($P<0.005$, Dunnett test). A one-way ANOVA did not reveal any differences between the two knock-out models lacking rod function ($P=0.4$).

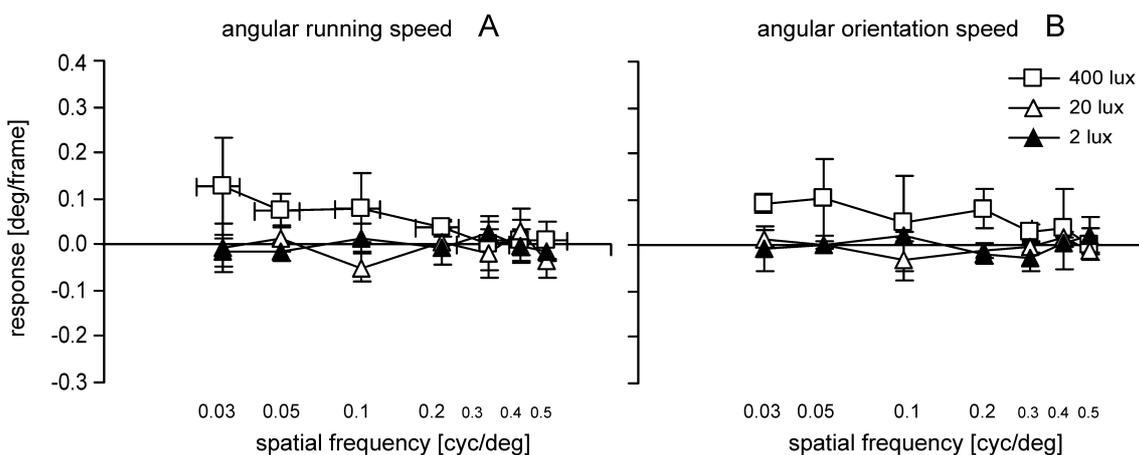


Figure 30. Optomotor responses at different spatial frequencies are shown for mice lacking rod function ($CNGB1^{-/-}$), for angular running speed (A) and angular orientation speed (B). Error bars as in Figure 27. At 400 lux, the mice showed significant responses at 0.03 cyc/deg and 0.05

cyc/deg ($P < 0.05$, Dunnett test). At both 20 and 2 lux, the responses were random ($P > 0.05$, Dunnett test).

3.3.2 Spatial vision in mice lacking cone function (CNGA3^{-/-})

Data from mice lacking cone function are presented in Figure 31. On average, angular orientation speed was significantly larger than angular running speed and this difference reached statistical significance (difference: -0.05 ± 0.05 deg/frame, $df = 26$, $T = 2.1$, $P = 0.0007$, variance ratio test). Surprisingly, both at 400 lux and at 2 lux, the CNGA3^{-/-} mice performed in the optomotor task comparable to the wild-type (no significant difference, $P > 0.08$, one-way ANOVA).

Student's t-test showed significant responses up to 0.10 cyc/deg at 400 lux ($P < 0.05$, variance ratio test). Comparing the responses of the mouse lacking cone function to the responses when no visual stimuli was present (Figure 26), a one-way ANOVA revealed significant differences ($P < 0.0001$). The most compelling result of the post hoc analysis was that spatial frequencies up to 0.20 cyc/deg were resolved at 400 lux ($P < 0.05$, Dunnett test).

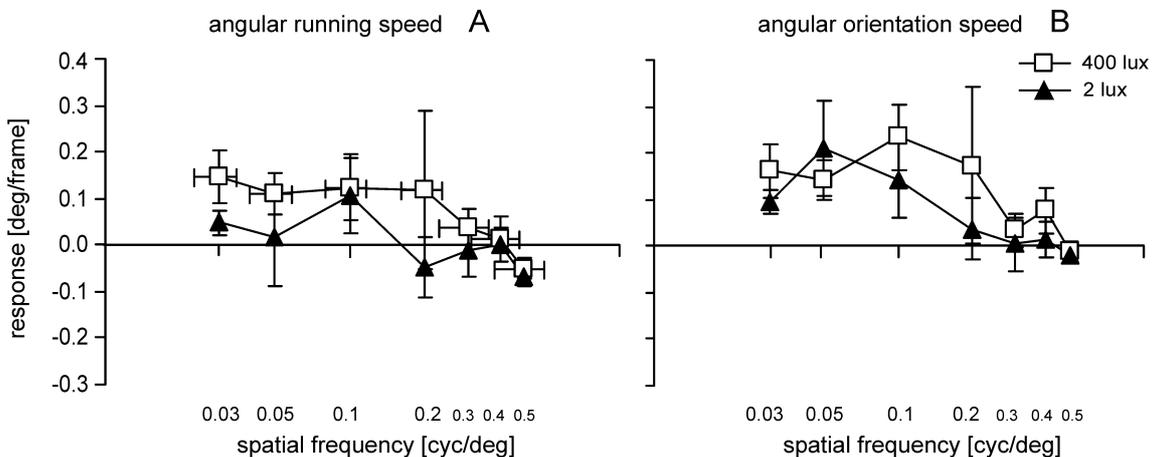


Figure 31. Optomotor responses of mice lacking cone function (CNGA3^{-/-}) are plotted against spatial frequency for angular running speed (A) and angular orientation speed (B). Error bars as in Figure 27. In this mutant, the angular orientation speed provided higher significance ($P = 0.0007$, variance ratio test). At 400 lux, the mice showed significant responses up to 0.20 cyc/deg ($P < 0.05$, Dunnett test). At 2 lux, the mice showed significant responses up to 0.10 cyc/deg ($P < 0.05$, Dunnett test).

3.3.3 Spatial vision in mice lacking both rod and cone function (CNGA3^{-/-}RHO^{-/-})

The optomotor responses of mice lacking both rods and cones are shown in Figure 32. Different from C57BL/6 mice, but similar to mice lacking rod function, there was no significant difference between angular running and orientation speed (difference: -0.01 ± 0.36 deg/frame, $df=26$, $T=2.1$, $P=0.59$, variance ratio test). Responses were neither significantly different from the null hypothesis ($P>0.05$, variance ratio test) nor from the responses without visual stimulation ($P=0.55$, one-way ANOVA). In conclusion, these animals were obviously not able to distinguish the black and white stripes.

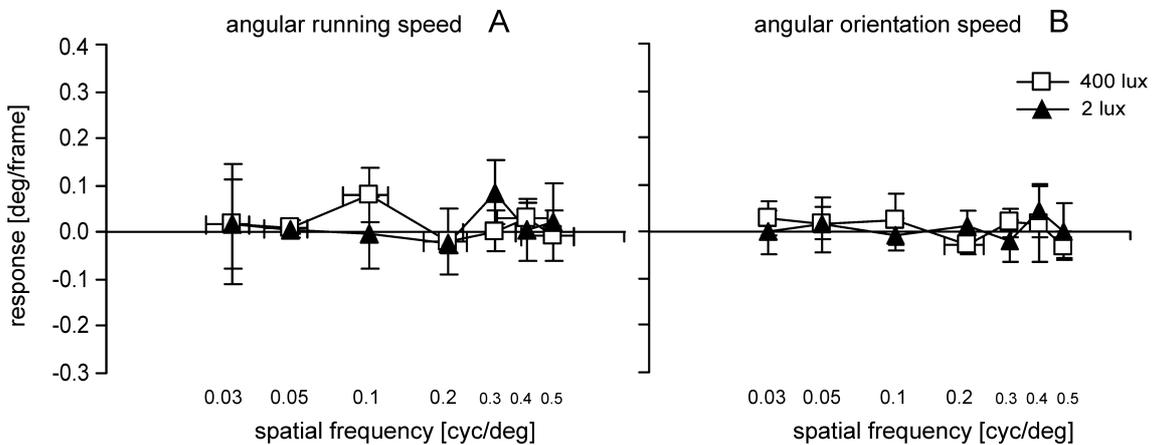


Figure 32. Optomotor responses of mice lacking both rod and cone function (CNGA3^{-/-}RHO^{-/-}) are plotted against spatial frequency for angular running speed (A) and angular orientation speed (B). Error bars as in Figure 27. Both at 400 and 2 lux, the responses were randomly distributed and neither significantly different from zero ($P>0.05$, variance ratio test), nor significantly different from the responses without visual stimulation ($P>0.05$, Dunnett test).

3.4 Comparisons of optomotor responses in wild-type and mutant mice

To quantify the importance of spatial vision in the wild-type and knock-out models, the responses obtained at different spatial frequencies were added up, providing a number that reflects the importance of spatial visual input. This summation was performed at all tested illuminances and the results are shown

IV. Results

in Table 1 (response refers to angular running speed) and Table 2 (response refers to angular orientation speed). The sum of the responses of the wild-type mice at 400 lux were used as reference and set to 100%. The Tables illustrate that the importance of visual input declines monotonically with decreasing illuminance. In mutant mice lacking rod function ($RHO^{-/-}$ and $CNGB1^{-/-}$), no visual input was detected at all at dim light (20 lux and 2 lux). At 400 lux, the optomotor response was still 24% to 41% of the wild-type when angular running speed was evaluated, and between 60% and 74% when angular orientation speed was evaluated. Mice lacking cone function ($CNGA3^{-/-}$) displayed an optomotor response that was even larger than that in wild-type mice. Also, in this mutant, the angular orientation speed achieved higher statistical significances. The responses of the double knock-out mice ($CNGA3^{-/-}RHO^{-/-}$) did not differ from the noise levels found in the wild-type in complete darkness.

Table 1. Relative responses in terms of angular running speed in wild-type and knock-out mice.

	<i>response</i>	<i>response</i>	<i>response</i>	<i>response</i>	<i>response when no visual stimuli was present (rotating drum)</i>	<i>response when no visual stimuli was present (stationary drum)</i>
	400 lux	20 lux	2 lux	0 lux		
<i>wild-type</i>	100%	76%	46%	-9%	18%	3%
$RHO^{-/-}$	24%	-1%	-14%			
$CNGB1^{-/-}$	41%	-11%	-4%			
$CNGA3^{-/-}$	70%		8%			
$CNGA3^{-/-}RHO^{-/-}$	15%		15%			

The sum of the responses at the different measured spatial frequencies of the wild-type (C57BL/6) mice at 400 lux was used as reference (100%). In mice lacking functional rods ($RHO^{-/-}$ and $CNGB1^{-/-}$), spatial vision was detectable only at 400 lux. In mice lacking cone function ($CNGA3^{-/-}$), spatial vision was still 70% of the wild-type at 400 lux. The double knock-out mice ($CNGA3^{-/-}RHO^{-/-}$) had no detectable spatial vision. Since the addition of responses measured at different spatial frequencies, each with a defined standard deviation, caused complex patterns in error progression, standard deviations were omitted. It is clear however that

IV. Results

negative response values do not indicate that the animals moved, in fact, into the direction opposite to the stripes, but rather reflect statistical variability.

Table 2. Relative responses in terms of angular orientation speed in wild-type and knock-out mice.

	<i>response</i>	<i>response</i>	<i>response</i>	<i>response</i>	<i>response when no visual stimuli was present (rotating drum)</i>	<i>response when no visual stimuli was present (stationary drum)</i>
	400 lux	20 lux	2 lux	0 lux		
<i>wild-type</i>	100%	48%	41%	12%	-29%	33%
<i>RHO^{-/-}</i>	74%	7%	-53%			
<i>CNGB1^{-/-}</i>	60%	-7%	-3%			
<i>CNGA3^{-/-}</i>	139%		82%			
<i>CNGA3^{-/-}RHO^{-/-}</i>	24%		24%			

Data analysis as in Table 1. In mice lacking functional rods (*RHO^{-/-}* and *CNGB1^{-/-}*), the importance of visual input was reduced at the brightest illumination 400 lux, but still significant. No signs of visual input were observed at 20 and 2 lux. Surprisingly, mice lacking cone function (*CNGA3^{-/-}*) showed an even better optomotor response both at 400 and at 2 lux than the wild-type. Similar to Table 1, there was no indication that the double knock-out mice (*CNGA3^{-/-}RHO^{-/-}*) had any spatial vision.

4. Contrast thresholds of wild-type mice wearing diffusers or spectacle lenses, and the effect of atropine, a myopia inhibiting drug

4.1 Contrast thresholds under photopic conditions

Average responses for three spatial frequencies and their standard deviations at different contrasts are shown for both angular running speed and orientation speed in Figure 33. There was no significant difference between angular running speed and angular orientation speed (difference: $+0.00 \pm 0.04$ deg/frame, $df=26$, $t=2.06$, $P=0.10$, variance ratio test).

The largest responses were obtained at the lowest spatial frequency that was tested (0.03 cyc/deg). At this spatial frequency, the mice displayed a significant response at 91%, 67%, 45% and 24% contrast. Below 24% contrast, more animals began to move randomly ($P>0.05$, variance ratio test). At a spatial frequency of 0.10 cyc/deg, no significant response could be elicited at a contrast lower than 45% ($P>0.20$, variance ratio test). At the highest spatial frequency tested (0.30 cyc/deg), significant responses were measured only at the maximum possible contrast ($P=0.03$, variance ratio test).

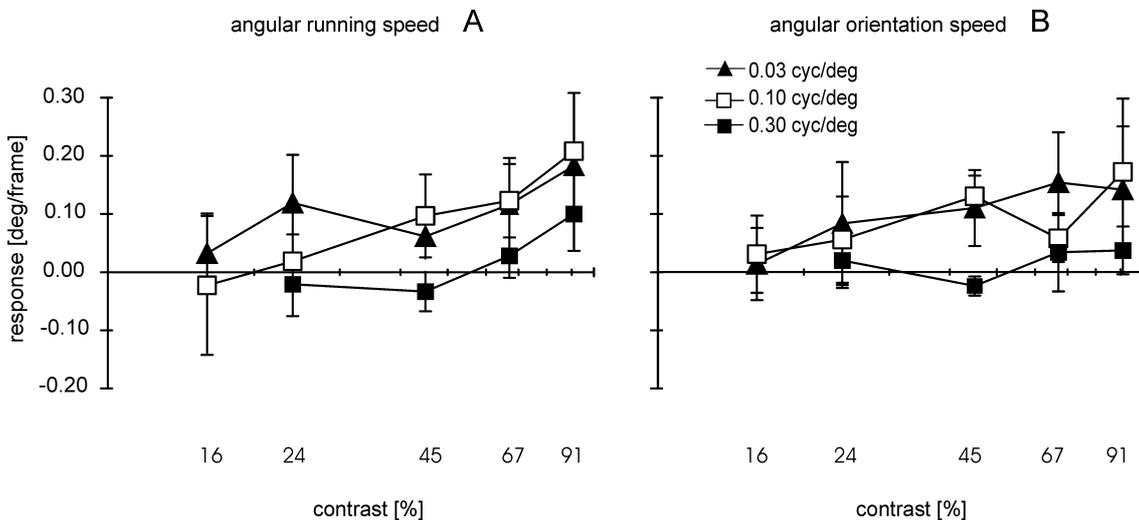


Figure 33. Optomotor responses and their standard deviations of C57BL/6 mice at three spatial frequencies. Responses are plotted against grating contrast, for both angular running speed (A) and angular orientation speed (B). Average illuminance of the stripes was 400 lux. Data on responses at maximum contrast (91%) originate from Chapter IV. 3.2.1. Averages from 12

IV. Results

animals are shown, with four or more animals tested at each data point. Responses were significant at 24% contrast or higher at a spatial frequency of 0.03 cyc/deg, at 45% or higher at 0.10 cyc/deg and only at 91% at 0.30 cyc/deg ($P < 0.05$, variance ratio test).

4.2 Contrast thresholds in dim light

Figure 34 shows the optomotor responses of the mice at a illuminance of 20 lux, for spatial frequencies of 0.03 cyc/deg and 0.10 cyc/deg. In these experiments, angular running speed was slightly higher than angular orientation speed (difference: $+0.03 \pm 0.03$ deg/frame, $df=14$, $t=2.12$, $P=0.05$, variance ratio test). In dim light, significant responses were only obtained at the maximum stripe contrast (91%), both at 0.30 cyc/deg and 0.10 cyc/deg ($P < 0.02$, variance ratio test). At lower contrasts, the movements of the mice in the drum were random ($P > 0.20$, variance ratio test).

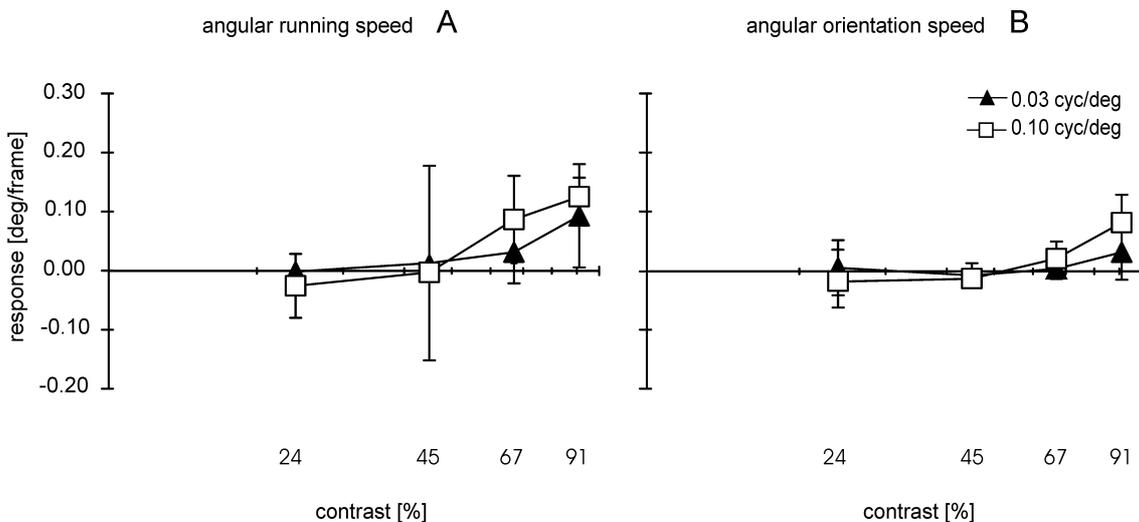


Figure 34. Optomotor responses in dim light (20 lux). Angular running speed (A) and angular orientation speed (B) are shown at two spatial frequencies. Data on the responses at maximum contrast (91%) originate from Chapter IV. 3.2.1. Data from seven animals are shown, with three or more animals tested at each data point. In dim light, optomotor responses reached significance only at the highest stripe contrast ($P < 0.05$, variance ratio test).

4.3 Contrast thresholds in mice wearing spectacle lenses

Figure 35 shows optomotor responses of mice to a grating with 0.03 cyc/deg and with 91% contrast, when they were wearing spectacle lenses of various powers. In these experiments, the angular orientation speed was slightly higher than the angular running speed, although statistical significance was not reached (difference: -0.01 ± 0.02 deg/frame, $df=10$, $t=2.23$, $P=0.44$, variance ratio test).

The largest optomotor responses were found when the mice had either plano lenses, or +7 D lenses (Figure 35; mean angular orientation speed: $+0.06 \pm 0.07$ deg/frame and $+0.06 \pm 0.06$ deg/frame, respectively). However, because the standard deviations were so large, none of these responses achieved significance ($P=0.08$ and $P=0.09$, respectively, variance ratio test). With -15 D lenses, the mice were still able to resolve the grating (angular orientation speed: $+0.05 \pm 0.03$ deg/frame; $P=0.01$, variance ratio test). With +25 D or -25 D lenses, the optomotor responses were no longer different from zero ($P>0.16$, variance ratio test).

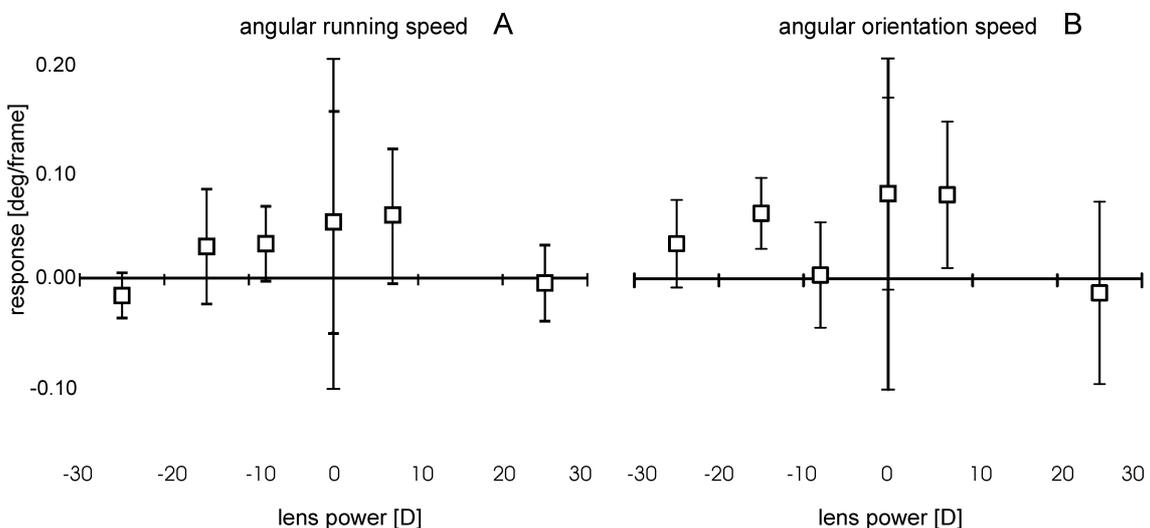


Figure 35. Optomotor responses with the equally powered spectacle lenses in front of both eyes, for angular running speed (A) and angular orientation speed (B). Data from ten animals are shown, with three or more animals tested at each data point. Measurements were performed at 400 lux. The optomotor responses decreased with increasing lens power, for both positive and negative lenses. Due to the large standard deviation, significance was not achieved

IV. Results

with plano lenses and with +7 D and -8 D lenses, although the responses were significant with the -15 D lenses in the case of angular orientation speed ($P < 0.05$, variance ratio test). Responses were not different from zero with +25 D or -25 D lenses.

Locomotor activity was significantly increased in mice wearing spectacle lenses ($+0.29 \pm 0.03$ deg/frame versus $+0.20 \pm 0.02$ deg/frame; $P = 0.001$, variance ratio test). The increase in activity could either be due to the attempts of the mice to remove the lenses, or due to light ether anesthesia that was necessary to attach the lenses, about 30 min before the measurements started.

4.4 Contrast thresholds in mice wearing diffusers

Figure 36 shows the optomotor responses of mice wearing translucent diffusers over both eyes. There was no significant difference between angular running and orientation speed (difference: $+0.00 \pm 0.05$ deg/frame, $df = 24$, $t = 2.06$, $P = 0.82$; variance ratio test). The optomotor experiment showed that spatial vision was largely abolished since the optomotor responses became random ($P > 0.05$, variance ratio test).

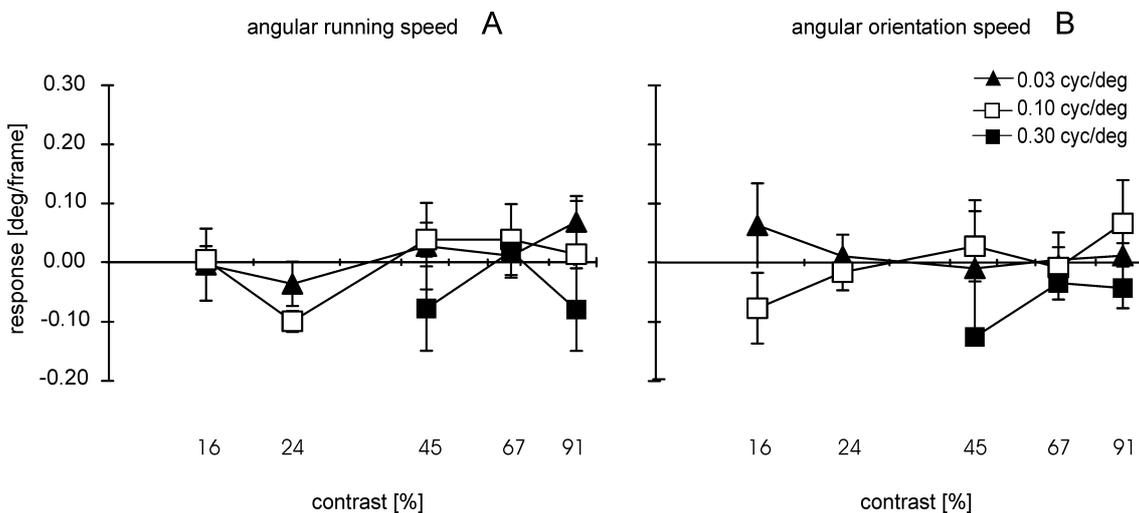


Figure 36. Optomotor responses with diffusers in front of both eyes, measured at different grating contrasts. Angular running speed (A) and angular orientation speed (B) were measured at a illuminance of 400 lux. Data from four animals are shown, at least three mice were tested at

each data point. Responses were not significantly different from zero, indicating that spatial vision was largely abolished ($P>0.05$, variance ratio test).

As with the spectacle lenses, the locomotor activity increased at 0.03 cyc/deg ($+0.36\pm 0.04$ deg/frames versus $+0.20\pm 0.02$ deg/frames, $P=0.001$, variance ratio test). However, there was no significant increase at 0.10 and 0.30 cyc/deg ($P=0.10$, variance ratio test). Since significant optomotor responses were observed in the case of the lenses (Figure 35), the lack of significant optomotor responses cannot be attributed to extensive cleaning behavior and neglect of the presented stripe patterns.

4.5 Contrast thresholds after atropine eye drops

After atropine application, the pupil sizes increased by on average of 0.40 mm, over 20 minutes (1.62 ± 0.10 mm versus 2.02 ± 0.07 mm). Atropine also completely suppressed light induced pupil responses, in line with observations by Schaeffel & Burkhardt (2005).

Optomotor responses for three spatial frequencies and different contrasts are shown in Figure 37. There was no significant difference between angular running speed and angular orientation speed (difference: $+0.01\pm 0.04$ deg/frame, $df=26$, $t=2.06$, $P=0.41$, variance ratio test).

Surprisingly, but similar to previous findings in chickens (Diether & Schaeffel, 1999), atropine increased contrast sensitivity, at least at the lowest spatial frequency that was tested (0.03 cyc/deg). Here, the mice displayed significant optomotor responses down to contrasts of 16% ($P=0.02$, variance ratio test). At higher spatial frequencies, there was no difference to the responses of untreated mice, measured under photopic conditions ($P>0.60$, variance ratio test).

IV. Results

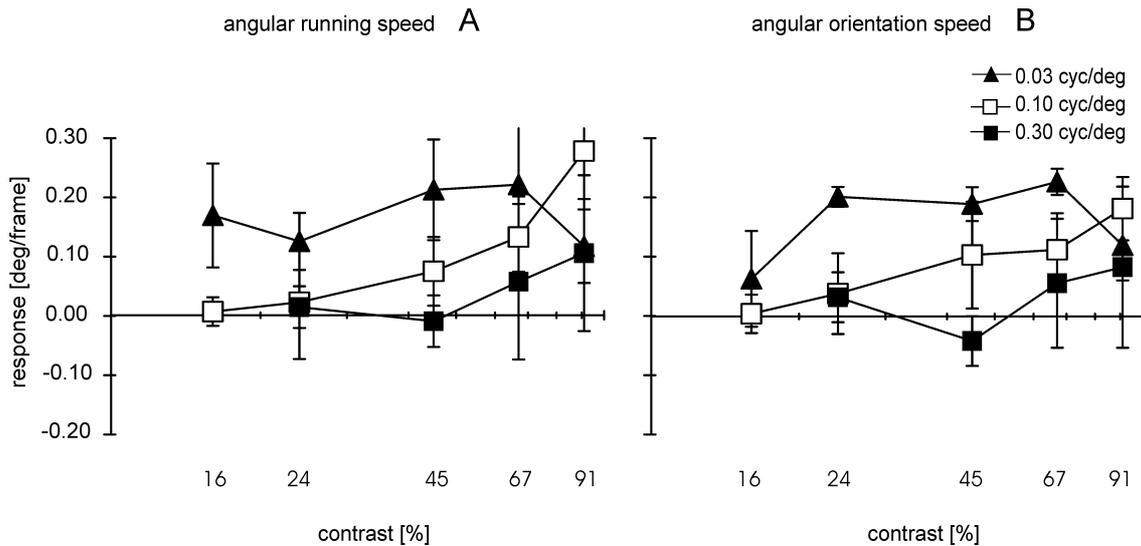


Figure 37. Optomotor responses after application of atropine. Angular running speed (A) and angular orientation speed (B), measured at a illuminance of 400 lux, are plotted against grating contrast. Averages of data from five animals are shown, with three or more animals tested at each data point. Significant optomotor responses were elicited down to grating contrasts of 16%, at a spatial frequency of 0.03 cyc/deg, of 45% at 0.10 cyc/deg, but only of 91% at 0.30 cyc/deg ($P < 0.05$, variance ratio test).

It was excluded that the increase in contrast sensitivity was due to increased locomotor activity. At the lowest spatial frequency tested, locomotor activity was only slightly increased, compared to untreated mice but this difference did not achieve significance ($+0.24 \pm 0.03$ deg/frame versus $+0.20 \pm 0.02$ deg/frame, $P = 0.07$, variance ratio test). At the other spatial frequencies tested, there was not even a trend to an increase of the locomotor activity ($P > 0.91$, variance ratio test).

V. Discussion

1. A paraxial schematic eye model for the growing C57BL/6 mouse

1.1 Refractive state and small eye artifact

Refractive state seems to reach a constant value of approximately $+7.0 \pm 2.5$ D at the age of 70 days which could indicate that a stable refraction is reached only after sexual maturity. As in many other studies (e.g. Norton, Wu, & Siegwart, 2003), an unknown factor is the contribution of the small eye artifact which pretends a more hyperopic refractive state than actually present, because the light used for the measurement is reflected predominantly at the vitreo-retinal interface, rather than at the photoreceptor layer. However, it is the position of the photoreceptor layer relative to the focal plane that determines the physiologically relevant refractive state. Therefore, the true refraction of the mouse is likely to be more myopic than measured here. However, comparison of refractive state using both retinoscopy and visually evoked potentials (VEPs) in various animals (rat, Mutti, Ver Hoeve, Zadnik, & Murphy, 1997; pigeon, Millodot & Blough, 1971; ground squirrel, Gur & Sivak, 1979) suggest that the light reflection may not only occur at the vitreo-retinal interface because the small eye artifact would then be much larger and many animals should then, in fact, be quite myopic. An example is the mouse: if the light reflected from the fundus would come only from the vitreo-retinal interface, the small eye artifact would amount to more than 30 D and, based on the measurements of refractive state in this study, the mice would be more than 20 D myopic. A new study (Norton et al., 2003) suggests that tree shrews which are measured with streak retinoscopy at +7.0 D and with an autorefractor (using infrared light) at about +4.0 D, are in fact about emmetropic when measured with VEPs. Thus, it is likely that the reflecting layer(s) must be closer to the photoreceptor layer than assumed in the original paper on the small eye artifact (Glickstein & Millodot, 1970).

The refractive errors measured with infrared light in the present study were less hyperopic than those in other studies, in which white light was used. Tejedor & de la Villa (2003) measured hyperopia of approximately +13.5 D in 30-day-old mice and Beuerman et al. (2003) found a refractive error of more than +15.0 D in adult Balb/CJ mice. A possible reason for this discrepancy is chromatic aberration which renders an eye more hyperopic in the red end of the spectrum. To test this hypothesis the infrared LEDs of the Power Refractor were replaced with yellow LEDs with a peak emission at 550 nm. However, the cyclopleged mice were still not more hyperopic. The average slope of the brightness profile in the pupil was 0.71 ± 0.24 (five measurements in one untreated animal), which converts into a refractive error of about +8.0 D. It is therefore likely that the infrared light penetrates deeper into the fundus before reflection than the visible light. One should also consider that it is very demanding to perform streak retinoscopy in an eye with a very small pupil. To evaluate this factor, refractive errors were measured with streak retinoscopy and compared to infrared photoretinoscopy in anesthetized mice (Figure 38). Because the mouse has a very sensitive pupil response to light (Pennesi et al., 1998), measurements without cycloplegia are almost impossible (pupil sizes approximately 1 mm). The measurements with streak retinoscopy and infrared photoretinoscopy were not even correlated (refraction measured with streak retinoscopy = $0.276 * \text{refraction measured with infrared photoretinoscopy} + 15.988$, $R^2=0.047$).

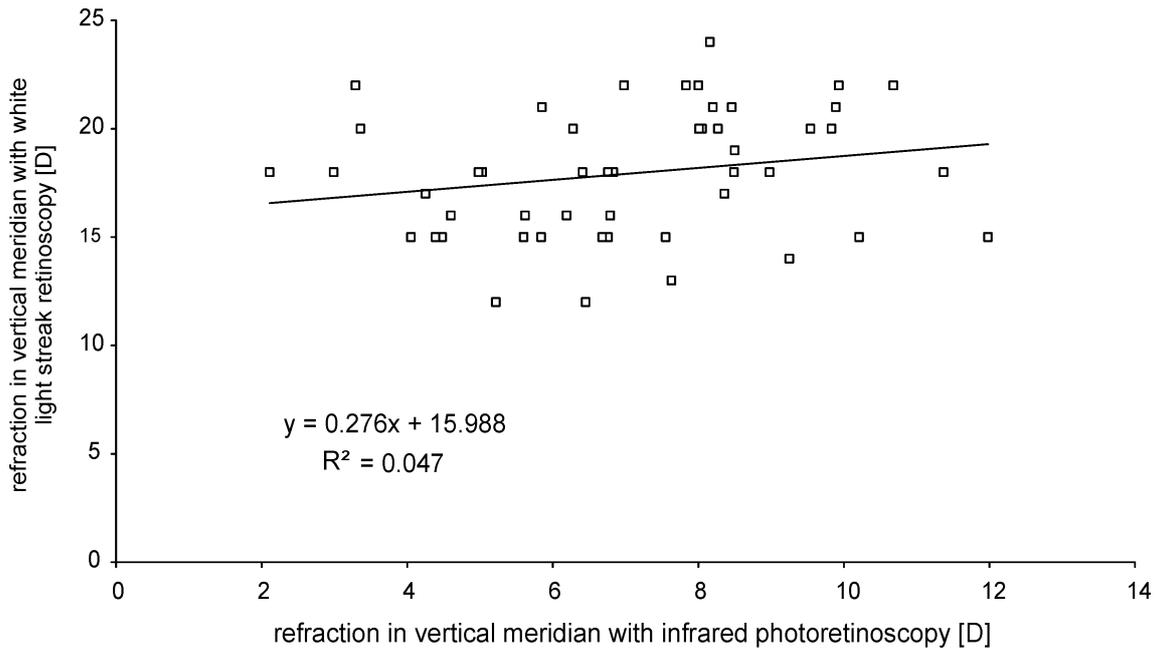


Figure 38. Refraction in vertical meridian, as measured with white light streak retinoscopy (ordinate) and infrared photoretinoscopy (abscissa). Measurements were performed in 52 anesthetized mice, without cycloplegia. There is no correlation between the two methods indicating that streak retinoscopy is not a reliable technique to measure refractive errors in mouse eyes.

1.2 Growth rates of the globes in various vertebrates

A striking feature of the mouse eye is its slow but long-lasting and linear growth rate between day 22 and day 100. During this time, the lens grew at a rate of 5.5 μm per day and the globe length at a rate of 4.4 μm per day. Zhou & Williams (1999b) examined eye weights in 507 mice from 50 different strains and also found that growth continued long after sexual maturity. In their study, the eye weight data could be best fit by linear regression when they were plotted versus the logarithm of age. There are also data on prenatal eye growth in the CD 1 mouse (E8 to E19), measured by ultrasound biomicroscopy (Foster, Zhang, Duckett, Cucevic, & Pavli, 2003). Already before birth, the globe and the lens appear to grow linearly at a rate of 122 μm and 68 μm per day, respectively. At birth, the axial length should then be about 1.32 mm, about 40% of the value at 100 days. When the mice are weaned (around day 22), the globe

has already reached about 90% of its size at 100 days, and 95% when sexual maturity is reached. The growth pattern in the mouse eye is similar to other species where also a period of rapid axial growth during early infancy (in mice: from birth to approximately day 22), is followed by a period of slower growth when the animals become juvenile (rhesus monkey, Bradley et al., 1999; marmoset, Graham & Judge, 1999; tree shrew, Norton & McBrien, 1992; chick, Irving, Sivak, Curry, & Callender, 1996). Also the human eye shows a biphasic growth curve (Larsen, 1971a; Gordon & Donzis, 1985). In comparison to the chick and tree shrew, the relative elongation of the mouse eye is approximately five times less. Between day 22 and 46, the mouse eye grew approximately 0.11 mm (~3.5%). The chicken eye elongated approximately 1.80 mm (~19%) over the same time period (Schaeffel & Howland, 1988a). In the tree shrew, the eye grows more like in the chicken, about 19% over the same age range (Norton & McBrien, 1992).

1.3 Growth of the ocular elements in various vertebrates

In 22-day-old mice, corneal radius of curvature had almost reached its final value. Such early completion of corneal development has also been observed in cats (Thorn, Gollender, & Erickson, 1976), three shrews (Norton & McBrien, 1992) and humans (Oyster, 1999). Different from corneal curvature, anterior chamber of the mouse eye increased continuously with age (between day 22 and 100: 1.3 μm per day). This is similar in macaques (Kiely, Crewther, Nathan, Brennan, Efron, & Madigan, 1987) marmosets (Graham & Judge, 1999), tree shrews (Norton & McBrien, 1992) and humans (Larsen, 1971b).

A developmental decline in vitreous chamber depth, due to the prominent growth of the lens, has been described before only once in the tree shrew eye (Norton & McBrien, 1992). On the other hand, that the lens grows continuously over the life span is more common (i.e. tree shrews, Norton & McBrien, 1992; kittens, Thorn et al., 1976). Also in humans, the lens continues to grow during adulthood (Cook, Koretz, Pfahnl, Hyun, & Kaufman, 1994), although there is a phase in late childhood between the age of six and ten years (Zadnik, Mutti,

Fusaro, & Adams, 1995), where the lens actually thins. It is not known whether it also reduces its volume.

Remtulla & Hallett (1985) analysed 41 eyes from C57BL/6J mice between 98 and 203 days and described no age related changes of the optical components. In this study, corneal thickness (0.093 mm) and anterior chamber depth (0.452 mm) were slightly larger compared to the values of 100-day-old mice in the present study (0.085 mm and 0.293 mm, respectively). Furthermore, Remtulla & Hallett (1985) described a thinner lens for adult mice (2.032 mm; 100-day-old mouse: 2.169). However, posterior chamber depth (0.558 mm; 100-day-old mouse: 0.572) and total axial length (3.372 mm; 100-day-old mouse: 3.339) were nearly equal in both studies. These minor differences trace most probably back to strain differences or differences in the rearing conditions.

Retinal thickness (near the optic nerve head) is comparable in human (0.23 mm) and mice (100-day-old mouse: 0.22), in line with a notion by Glickstein & Millodot (1970) that retinal thickness is similar among different species of mammals, no matter of the absolute eye size.

1.4 Homogeneous lens index

The presence of a refractive index gradient in the lens is common to all vertebrate eyes (Campbell, 1984), but its structure is difficult to describe in detail (Acosta, Vazquez, Smith, & Garner, 2003), in part because the index gradient is very variable among individual eyes (Artal, Berrio, Guirao, & Piers, 2002). In the present study, the description of the lens had to be confined to the paraxial region and no attempt was made to study the structure of the gradient index. It is clear that the equivalent homogeneous index is only a theoretical number which is much higher than what is biologically possible (<1.55 , Hughes, 1979). However, the equivalent homogeneous indices in this study match the values found in other studies (chicken, Pickett-Seltner, Weerheim, Sivak, & Pasternak, 1987; Schaeffel & Howland, 1988a). Also in the only published paraxial schematic eye model of the adult mouse (Remtulla & Hallett, 1985), the

equivalent refractive index of 1.659 is in agreement with the findings in the present dissertation (100-day-old mouse: 1.657).

1.5 Retinal image magnification and brightness

The difference in retinal magnification between a 22 and 100-day-old mouse was only about 10% but this value matches the changes expected from axial eye growth. The image magnification found in the 22-day-old mouse eye (31 μm per deg) was in agreement with the value that was previously published for adult mice (31 μm per deg at 550 nm, Remtulla & Hallett, 1985). This agreement is due to the paraxial focal length which matches the value for young mice in the present study.

In the present study, the f/number of the adult mouse eye (0.93) was much lower than in humans (about 4.5, Schaeffel & Wagner, 1996), diurnal birds (60-day-old chick: 1.35, Schaeffel et al., 1986; pigeon: 1.98, Marshall, Mellerio, & Palmer, 1973) or in nocturnal birds (barn owl: 1.13, Schaeffel & Wagner, 1996). With a f/number ≤ 1.0 , the retinal image in the mouse eye is probably among the brightest of all vertebrates. Furthermore, the f/number declined slightly with age, resulting in a 10% brighter image at day 100 than at day 22. This change is less than in the chick (50 versus 1 day of age: +49%, Schaeffel et al., 1986), toad (adult toad versus tadpole: +350%, Mathis, Schaeffel, & Howland, 1988) or barn owl (60 versus 10 days: +30%, Schaeffel & Wagner, 1996).

1.6 Deprivation myopia

The mouse eye turned out to be a demanding model to study deprivation myopia (Tejedor & de la Villa, 2003; Schaeffel et al., 2004). Degrading the retinal image with diffusers or lid-suture induced a shift in refractive state in the myopic direction but the anatomical correlate, an increase in axial length, was unconvincing (Schaeffel & Howland, 2003). Assuming that the dioptric amount of myopia that can be induced depends on the natural dioptric growth rate of the

eye, 0.80 D of myopia could be induced per day in a 22-day-old mouse. Since the dioptric growth rate declines with age (from -0.80 D at day 22 to -0.68 D at day 100), an occlusion period of at least 12 days is necessary to produce approximately 10 D of myopia, equivalent to a change of axial length of 55 μm . Compared to other animal models, the mouse eye shows a smaller dioptric growth rate per day. A 20-day-old chick grows approximately -1.75 D per day (Schaeffel & Howland, 1988a). Troilo & Judge (1993) suggested a dioptric growth rate of -1.25 D per day in the 20-day-old marmoset. However, in these animals the growth rate levels off more rapidly. In the chicken eye, it is less than -0.50 D at day 80 post-hatching and the marmoset eye has already stopped growing.

1.7 Conclusions

The most striking features of the schematic mouse eye were, that linear growth was slow but extended far beyond sexual maturity, that the corneal curvature did not increase with age, and that the prominent lens growth caused a developmental decline of the vitreous chamber depth. Furthermore, a calculated axial eye elongation of 5.4 to 6.5 μm was sufficient to make the schematic eye 1 D more myopic. Thus, techniques with high spatial resolution are necessary to uncover visually induced growth changes in the eye.

2. *In vivo* biometry in the mouse eye with optical low coherence interferometry

2.1 Accuracy of the optical low coherence interferometry

2.1.1 Axial eye length

Axial length could be determined with a mean standard deviation of $8.0 \pm 2.9 \mu\text{m}$, which is equivalent to a refraction change in a mouse eye of about 2 D (Chapter IV. 1.3 or Schmucker & Schaeffel, 2004a). Therefore, OLCI represents a significant improvement in performance over current techniques to measure small eyes (caliper measurements in excised eyes, Beuerman et. al., 2003; biometry in frozen sections, Remtulla & Hallet, 1985, Chapter IV. 1.2 or Schmucker & Schaeffel, 2004a), or measurements in standard histological sections of fixated tissues (Tejedor & de la Villa, 2003).

Axial length was previously measured in emmetropic human subjects by laser doppler interferometry, using partially coherent light, with a standard deviation of $\pm 30 \mu\text{m}$ (about $\pm 0.1\%$) by Hitzenberger (1991). In a mouse eye, a standard deviation of $8.0 \mu\text{m}$ is equivalent to about $\pm 0.25\%$ which is only slightly worse than in a human eye which has much better optics.

Biometric data of axial length from OLCI and from frozen sections were highly correlated (regression line: OLCI data = frozen section data * 1.173 - 0.354, $R^2=0.870$). The consistent offset of about $200 \mu\text{m}$ between both techniques is explained from the fact that frozen sections provide data on geometrical length and OLCI technique on optical path length. To convert one into the other, the refractive indices along the optical path must be known. The major source of error must be the lens which has a much higher refractive index than the default index that is used by the software in the "AC Master". The lens makes up approximately 60% of the total path length when the measurement beam travels through the eye (Chapter IV. 1.2 or Schmucker & Schaeffel, 2004a). Even though the measurement beam is aligned with the optical axis of the lens, the refractive index gradient in the lens, common to all vertebrate eyes (Campbell, 1984), determines the average index along the optical path. The internal structure of the refractive index gradient is difficult to measure in detail (Acosta

et al., 2003) and it is also variable among individual eyes (Artal et al., 2002). Therefore, the effective lens index can only be estimated by searching the best match of both sets of axial length data. This was achieved with an average refractive index of $n = 1.433$.

2.1.2 Corneal thickness

Recently, Schulz, Iliev, Frueh, & Goldblum (2003) have measured corneal thickness using optical low coherence reflectometry (OLCR) in mice *in vivo*. They found a mean corneal thickness of $106.00 \pm 3.45 \mu\text{m}$ in eight four-month-old male mice of the balb-c inbred strain. Jester, Lee, Li, et al. (2001) measured corneal thickness in adult transgenic mice using contact *in vivo* confocal microscopy and found a corneal thickness of $112.9 \pm 7.0 \mu\text{m}$ in eight non-treated PEPCK-TGF β over-expressing mice. The measurements in frozen sections (Chapter IV. 1.2 or Schmucker & Schaeffel, 2004a) provided a corneal thickness of $91 \mu\text{m}$, and the OLCI technique a corneal thickness of $122 \mu\text{m}$, both at the age of four month. Schulz et al. (2003) reported that corneal thickness could be measured with a standard deviation of $3.5 \mu\text{m}$. They also found that corneal thickness did not differ significantly in the right and left eye (mean difference: $-0.84 \pm 4.57 \mu\text{m}$). This is similar to the findings in the present study (mean standard deviation: $3.5 \mu\text{m}$; mean difference between right and left eye: $-1.35 \pm 6.92 \mu\text{m}$).

2.1.3 Anterior chamber depth

The average standard deviation of anterior chamber depth measurements was $10.6 \pm 12.3 \mu\text{m}$. Drexler, Baumgartner, Findl, Hitzenberger, Sattman, & Fercher (1997) measured the anterior chamber depth in the human eye by partial coherence interferometry and obtained a standard deviation of $8.7 \mu\text{m}$ (range: $3.9 \mu\text{m}$ to $16.8 \mu\text{m}$) for non cyclopleged eyes and $1.9 \mu\text{m}$ (range: $1.7 \mu\text{m}$ to $2 \mu\text{m}$) for cyclopleged eyes. These results showed that the variability of OLCI measurements of anterior chamber depth in human eyes can be reduced by a factor of five under cycloplegia. However, since there is no convincing evidence

for accommodation in mice (Artal et al., 1998), it is unlikely that cycloplegia would have reduced the variability in mice very much.

2.2 Myopia and axial elongation during deprivation of form vision

In the current sample, no significant refractive changes could be detected after 14 days of form deprivation. It was previously observed that mice do not always develop myopia in response to deprivation (Schaeffel et al., 2004; Fernandes et al., 2004). An extended analysis of data from 50 mice that were studied earlier in our lab by Eva Burkhardt, and for which no OLCI data are available, shows that the myopic shift in occluded eyes is highly significant, but variable and not very large (Figure 39). Therefore, the lack of a significant shift of refractive state in the myopic direction in the seven mice studied with the OLCI is not so unexpected. That there was an increase in axial length in the deprived eyes is in line with results from other animal models. That it was not accompanied by a shift in refraction, implies that other biometric changes occurred in the eyes that counterbalanced the effects of axial elongation. There was, on average, an increase in anterior chamber depth of $17.33 \pm 43.16 \mu\text{m}$. Paraxial ray tracing predicts that the shift in lens position would produce an increase in hyperopia of about 1.7 D. Although this cannot fully counterbalance the expected shift in the myopic direction, it has some compensatory effect.

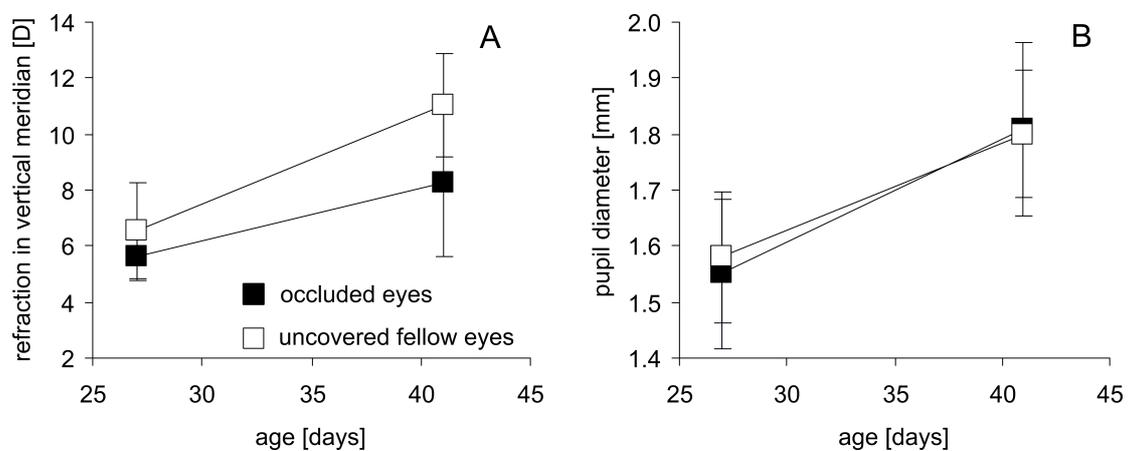


Figure 39. A. Average refractive development in 50 mouse eyes that were covered by diffusers from day 27 to day 41 (filled squares), compared to the refractive development in their open fellow eyes (open squares). Note that the average difference in refractions after two weeks is small (2.77 ± 3.33 D) but is still highly significant ($P < 0.0001$, paired t-test). B. Since pupil size may be a confounding variable in measurements of refractive state (Schaeffel et al., 2004), it was verified that the pupil sizes did not differ in both eyes. The plot includes previously published (Schaeffel et al., 2004), and unpublished new data.

2.3 Conclusions

OLCI had sufficient resolution in living mice to detect axial length changes *in vivo* that were equivalent to a dioptric change of 2 D. Using this technique, it was confirmed that the mouse eye responds to form deprivation with axial elongation, similar to the eyes of other animal models. The lack of a myopic shift in this sample, despite the axial elongation, demonstrates that biometric data are particularly important when the mouse eye is used as a model to study myopia. Further studies are necessary to determine whether the relatively poor optical quality (Artal et al., 1998) and/or the rod dominance in the retina may be other complicating factors.

3. Grating acuity at different illuminances in wild-type mice, and in mice lacking rod or cone function

3.1 Evaluation of the optomotor paradigm

The optomotor response to a moving grating can be used to evaluate the spatial acuity in mice as suggested by the following observations:

1. Most mice showed a preference to move in the direction of the stripe pattern.
2. There was no preference when the drum was rotated without the stripe pattern inside or when it was not rotated at all.
3. The movements of the mice were also random in complete darkness.
4. The differences in movement preferences were not explained by light dependent activity changes, since the locomotor activity did not change with illuminances ($P > 0.10$, variance ratio test).

Even though the behavioral procedure offers the advantages that the animals can be tested without prior training and while they are freely moving, a source of noise was that they could vary their distance to the stripe pattern and were, therefore, exposed to variable spatial frequencies.

To measure the responses of a mouse to stripe patterns with different spatial frequencies takes about 45 min. Hence, relatively rapid screening for spatial vision in mice can be performed, and the only action of the experimentator is to place the mouse in the perspex container in the center of the rotating drum.

3.2 Spatial acuity in wild-type mice, compared with other mammals

In primates, foveal visual acuity is limited by the density of cones as they have a one-to-one ganglion cell connection in the center of the fovea (Perry & Cowey, 1985). In lower mammals, the upper limit is imposed by the peak density of the retinal ganglion cell (RGC) mosaic as there is a significant degree of convergence (Pettigrew, Dreher, Hopkins, McCall, & Brown, 1988). Gianfranceschi et al. (1999) estimated the anatomical resolving power of the eyes in wild-type mice at around 1.0 cyc/deg, using the equation: *estimated*

$visual\ acuity = (\sqrt{D/2}) * RMF$ where D = peak density of RGC (4500 cells/mm²) and RMF = retinal magnification factor (0.015mm/deg; $RMF = 2 * \pi * PND / 360$). In most species, the behavioral visual acuity is very close to the estimated acuity (i.e. horse, dog, cat, rabbit, dolphin and cat; see overview: Gianfranceschi et al., 1999). However, in mice and rats whose habits do not depend primarily upon vision, the behavioral acuity is lower.

The optomotor experiment in the present study provided a slightly lower spatial resolution limit (0.30–0.40 cyc/deg), compared to other behavioral paradigms. That the experimental procedures introduce different levels of noise was already stated by Prusky et al. (2004), who recognized that the spatial frequency threshold was lower in their virtual optomotor experiment (about 0.40 cyc/deg) than in other psychophysical experiments. In this study, reflexive head movements were tracked in unrestrained mice while they were facing a rotating cylinder covered with a vertical sine wave grating that was drawn in virtual three-dimensional space on four computer monitors that formed a square. An acuity of approximately 0.50 cyc/deg was found in wild-type mice in measurements of optokinetic eye movements (Sinex et al., 1979), or forced choice procedures ("visual water task", Prusky et al., 2000; and "T-maze behavioral task", Gianfranceschi et al., 1999). In addition, both pattern electroretinogram (PERG, Porciatti et al., 1996) and visual evoked potentials (VEPs, Porciatti et al., 1999; Rossi, Pizzorusso, Porciatti, Marubio, Maffei & Changeux, 2001; Gianfranceschi, Siciliano, Walls, et al, 2003), have been extensively used to measure spatial vision in both wild-type and mutant mice, even during development (Huang, Kirkwood, Pizzorusso, et al., 1999). Both VEP and PERG measurements provided spatial resolution thresholds (visual acuity) of approximately 0.60 cyc/deg. The lower spatial frequency cut-off found in the present study might be due to the fact that statistical significances were hidden in higher standard deviations.

In the present study, mice were most sensitive to square wave gratings between 0.10 and 0.20 cyc/deg. Lower spatial frequencies caused a reduced optomotor response. This result is in accordance with the observations in a behavioral study by Sinex et al. (1979) who reported the highest grating

sensitivity at 0.125 cyc/deg in mice. Porciatti et al. (1999) found the highest sensitivity to gratings at about 0.06 cyc/deg, using pattern VEP. This figure is comparable with the average receptive field size obtained from single unit recordings in the visual cortex of the mouse (Drager, 1975; Mangini & Pearlman, 1980; Gordon & Stryker, 1996).

By comparison, the peak sensitivity to sine-wave gratings for the cat is 1.0 cyc/deg (Blake, Cool, & Crawford, 1974), and is at 4.0 cyc/deg in the pigeon (Nye, 1976), 3.0 to 5.0 cyc/deg in the squirrel monkey (Merigan, 1976), 3.0 cyc/deg in the macaque (De Valois, Morgan, & Snodderly, 1974) and 0.20 cyc/deg in Long-Evans and nondystrophic RCS rats (McGill, Douglas, Lund, & Prusky, 2004).

3.3 Grating acuity at different light levels

The importance of visual input decreased monotonically with illuminance (400 lux: 100%, 20 lux: 76.4%, 2 lux: 45.9%, darkness -9%), suggesting that the "high acuity system" of the mouse requires relatively high light levels, similar to humans (>200 lux, Diepes, 1975). Porciatti et al. (1999) found that the VEP amplitude is maximal at a luminance of 25 cd/m² (low photopic range, comparable to about 400 lux in the present drum set-up, Figure 40). Similar to in the present study, a decreasing VEP response was observed when the light was dimmed down. No reliable response could be elicited in the scotopic range (<0.01 cd/m²) in the VEPs. This result is different from the present behavioral data since there was still visual input detected (approximately 45% of the maximal response) in the range where only rod vision was present (2 lux equivalent to about 0.005 cd/m²). The findings in the present study are supported by data from Herreros de Tejada, Munoz Tedo, & Costi (1997) who measured absolute visual threshold in albino and pigmented mice using an operant method (modified Skinner box), and found a threshold at -5.3 log cd/m² and -5.5 log cd/m², respectively. Abdeljalil et al. (2005) evaluated head movements in response to a rotating optomotor drum. In this new study, visual acuity increased from 0.26 cyc/deg at scotopic conditions to 0.52 cyc/deg at

photopic conditions. Even though the visual threshold in the present dissertation was lower (0.30 cyc/deg under photopic conditions), the finding that spatial acuity is increasing with illuminance was in line with the present study. As should be expected, no visual input was measurable in complete darkness. Also Mitchiner et al. (1976) did not observe any eye movements in an optokinetic paradigm when the stripes were rotated in the dark.

Figure 40 illustrates the luminance ranges for rod and cone vision. Since they depend on the ambient illuminance, luminance (cd/m^2) is plotted versus illuminance (lux) to permit comparisons.

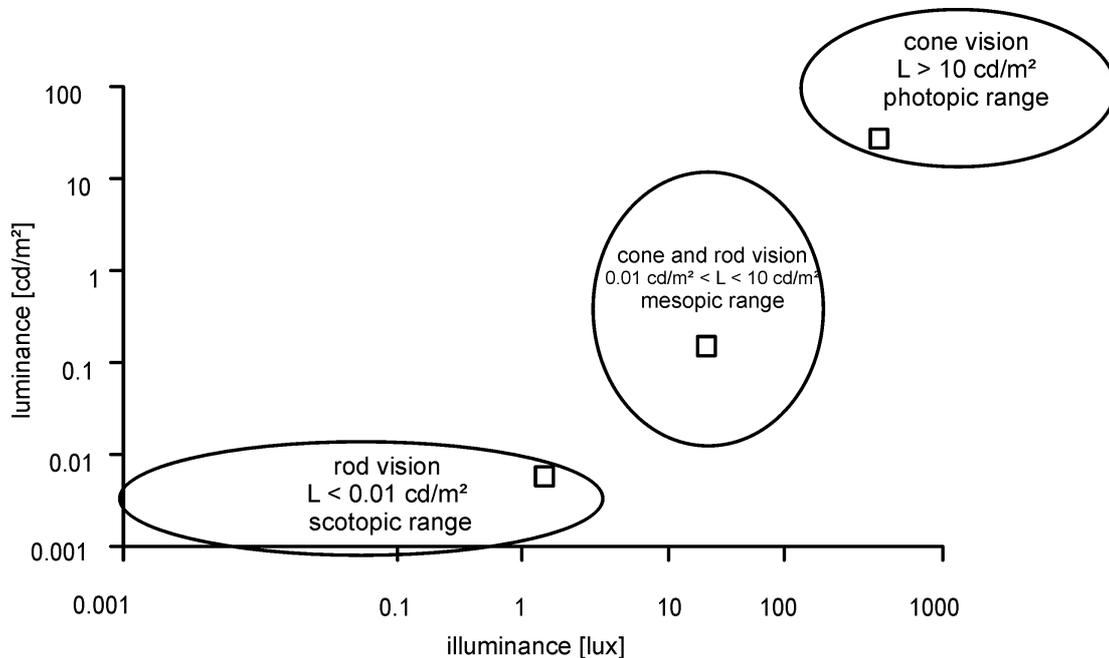


Figure 40. Luminance [cd/m^2] is plotted versus illuminance [lux], as measured in the optomotor drum with a luminance meter and a calibrated photocell in photometric mode, respectively. The ranges for scotopic and photopic vision in humans is also indicated (Zeiss, 1987). L: luminance.

3.4 Refractive state and visual acuity

Although there are extensive data on the refractive state in mice as measured by optical techniques (Chapter IV. 1. and 2. or Schmucker & Schaeffel, 2004a and 2004b), it is difficult to evaluate the small eye artifact, and accordingly, the

true subjective refractive state. There was a slight improvement in spatial acuity when a smaller drum was used (large drum: 0.30 cyc/deg, small drum: 0.50 cyc/deg; $P < 0.05$, variance ratio test). This observation could suggest that the mice were slightly myopic. However, since small eyes with high refractive power have a large dioptric depth of focus (Pennesi et al., 1998; Chapter IV. 4.3 or Schmucker & Schaeffel, 2005), the gratings used in the present study were probably close to best focus in both drums, and the exact refractive state was not limiting. Also electrophysiological recordings in mice did not require refractive corrections in order to map receptive fields in the visual cortex (Drager, 1978; Gordon & Stryker, 1996). Therefore, the slight improvement in spatial acuity in the small drum resulted more likely from the fact that the mice could approach the stripe pattern, thereby increasing their viewing angle.

3.5 Spatial acuity in mutant mice

It was found that spatial vision in juvenile $RHO^{-/-}$ and $CNGB1^{-/-}$ mice was limited to the photopic range (400 lux). The finding is in line with previous electrophysiological and anatomical work (Jaissle et al., 2001). These authors had shown that during the period of complete absence of rod input but normal or even supernormal cone responses between postnatal week four and six, the (cone only) ERG features a 'right shift' due to the lower sensitivity of cones compared to rods. The present behavioral data showed a reduced visual acuity in these cone-only models (0.10 cyc/deg in $RHO^{-/-}$ and 0.20 cyc/deg in $CNGB1^{-/-}$ compared to 0.30 cyc/deg in C57BL/6 wild-type mice; $P < 0.05$, variance ratio test). This suggests that, in the absence of a macula, the peak visual performance in mice is obtained when they use their rod system. The difference between the $RHO^{-/-}$ and the $CNGB1^{-/-}$ mutants could reflect a more natural morphological organization of cone outer segments in $CNGB1^{-/-}$ mice due to the presence of structurally supporting, but nonfunctional rods.

The "all-rod-mouse" ($CNGA3^{-/-}$) performed the behavioral test both under photopic and scotopic conditions similar to the wild-type. This observation suggests that the rod system (without dilation of pupils) is not entirely saturated

at illuminances of up to 400 lux. It may be speculated that rod vision originates in this case from a mid-peripheral ring between a central area of desensitization (too much light for the rod system) and a peripheral ring of subthreshold stimulation (too little light for the rod system).

In mice without any photoreceptor functionality in the outer retina (CNGA3^{-/-}RHO^{-/-}), no optomotor response could be elicited under the present test conditions. This suggests that the melanopsin-containing ganglion cell system does not contribute to spatial vision. A similar conclusion was reached, based on ERG recordings by Claes et al. (2004).

3.6 Conclusions

It was demonstrated that an automated optomotor paradigm with freely ranging mice could be used to study spatial visual functions in both wild-type and mutant mice. It was found that spatial vision in mice is more responsive in the photopic range. The results suggest that experiments in which visual input is important, for instance studies on myopia, should be done at 400 lux or even higher. Studies with mutants suggest that spatial acuity is governed by rod vision which appears -without dilation of pupils- to function properly even in the mesopic or low photopic range. Mice lacking both cones and rods have no detectable grating acuity, indicating that the retinal melanopsin system does not contribute to spatial vision.

4. Contrast thresholds of wild-type mice wearing diffusers or spectacle lenses, and the effect of atropine, a myopia inhibiting drug

4.1 Comparisons to contrast thresholds measured in previous studies

In the present study, the contrast thresholds in mice with normal vision were generally higher than in other studies (e.g. visual water task: Prusky & Douglas, 2004; optomotor response: Prusky et al., 2004; electrophysiological measurements: Porciatti et al., 1999). The threshold contrast was about 24% at the lowest spatial frequency tested (0.03 cyc/deg), and increased to 45% at 0.10 cyc/deg and to 91% at 0.30 cyc/deg. In a recent study by Prusky et al. (2004), the peak contrast sensitivity was found at a spatial frequency of 0.064 cyc/deg in mice at the age of 30 days (maximum sensitivity: 24.5 or contrast threshold: 4%), using a virtual optomotor drum. Furthermore, in this study, the contrast sensitivity decreased with increasing spatial frequencies as in the present study, but less so (at 0.10 cyc/deg, the contrast threshold was at 16% contrast; at 0.272 cyc/deg, it was at 25%). Using the visual water task (Prusky & Douglas, 2004), the contrast sensitivity curve peaked at 0.208 cyc/deg with a contrast threshold of 15.7%. As in the present study, contrast thresholds increased with increasing spatial frequencies (at 0.50 cyc/deg, the contrast threshold was at 50%). Porciatti et al. (1999) used VEPs to evaluate contrast sensitivity in mice. They found a contrast threshold of 5% for coarse gratings (0.06 cyc/deg) and of 17% for fine gratings (0.20 cyc/deg).

Why the contrast thresholds were higher in the present optomotor experiments, compared to other studies, remains elusive. It could be explained either by differences in the visual system of the different laboratory mouse strains (which appears less likely), or by differences in the behavioral paradigms. It is likely that freely ranging mice introduce more statistical noise since their natural cleaning behavior is superimposed in all the tracking records and causes considerable non-visually triggered movements (see also Chapter V. 3.2).

4.2 Contrast thresholds in dim light

Contrast thresholds in dim light have not been studied before. The present dissertation shows that, at 20 lux (where only rod vision is possible; Chapter IV. 3.3 or Schmucker et al., 2005), gratings were detected only at maximum contrast (91%). No spatial vision was detected at a contrast of 67%, or below. This suggests that experiments with diffusers to study deprivation myopia in mice should not be successful in dim light because the retinal processing is not very different with and without diffusers. In bright light, however, the diffusers had a solid effect on spatial vision (compare Figure 33 and Figure 36), confirming a previous conclusion that studies on deprivation myopia in mice should be done under photopic conditions.

4.3 Refractive state inferred from optomotor experiments with lenses

The data on the optomotor responses with different lenses (Figure 35) provide some information on refractive state in mice and also on their depth of field. Since no optomotor responses were elicited with ± 25 D lenses, the imposed defocus was probably outside the range of depth of field. However, there was also no obvious decline in the magnitude of the optomotor responses over the range of plus to minus ten diopters away from plano lenses, suggesting that the depth of field may be that large. A possible confounding factor, which tends to expand the apparent depth of field, may be the presence spurious resolution of the grating. Even minor hints may be sufficient to trigger an optomotor response. Nevertheless, the literature provides similar values: both in PERGs (Porciatti et al., 1996) and in VEPs (Porciatti et al., 1999), trial lenses in front of the eyes of ± 10 D in power did not alter the response amplitudes.

Finally, the decline in the optomotor responses was about symmetrical with respect to refraction zero, suggesting that the refractive state was around zero diopters. The fact that the stripe patterns were not presented at infinity but rather at about 3 D (drum radius: 31.5 cm) is of minor importance. A difference of 3 D in refraction cannot be resolved in Figure 35. But it is interesting that the

standard deviations in direct optical measurements of refractive state with infrared photoretinoscopy were only 2.7 D (Schaeffel et al., 2004) - much less than the behavioral depth of field.

4.4 Contrast thresholds after atropine eye drops

Surprisingly, despite the larger pupil diameter which resulted from atropine application and produced a decline in optical quality of the eye, the contrast threshold was lowered, at least at 0.03 cyc/deg. Since pupil dilatation should not improve the retinal image contrast, it is likely that the change in contrast sensitivity was neural and occurred in the retina or cortex. The mechanisms by which atropine can enhance contrast sensitivity is subject to speculation. It was previously shown that atropine boosts the release of dopamine from the retina (Schwahn, Kaymak, & Schaeffel, 2000) and it is known that dopamine reduces receptive field sizes and can increase contrast sensitivity at higher spatial frequencies (Bodis-Wollner & Tzelepi, 1998). The observed change in contrast sensitivity is in line with an idea by Diether & Schaeffel (1999). They suggested (derived from experiments in the chicken) that the increase in contrast sensitivity of the retina with atropine may reduce the error signal that is generated with diffusers and which is responsible for the stimulation of axial eye growth. An effect of atropine on retinal function, as measured with the multifocal electroretinogram, could not be detected in children who were treated with daily eye drops for two years (Luu, Lau, Koh, & Tan, 2005). However, it should be kept in mind that also the inhibitory effect of atropine on myopia declines over time (Chua et al., 2003; Chua, 2004) and it is likely that the retina had re-adjusted its contrast sensitivity function after such long treatment periods.

4.5 Conclusions

It was shown that the mouse eye has sufficient spatial vision to respond to treatment with spectacle lenses or diffusers. Accordingly, these treatments

should be effective in inducing refractive errors in this animal model since they degrade the retinal image quality by a detectable amount. The study also shows that the range of spatial frequencies at which the mouse responds to changes in contrast, is rather small (at 0.03 cyc/deg, the contrast threshold was 24% and at 0.30 cyc/deg the contrast threshold was 91%). Furthermore, at dim light, spatial vision declines rapidly which is an unexpected finding, given that the optics of the eye produces a very bright retinal image ($f/\text{number} \leq 1$) and that mice are considered nocturnal. Finally, atropine appears to improve contrast sensitivity at low spatial frequencies, a result that was previously obtained also in the chicken (Diether & Schaeffel, 1999).

VI. Summary

This dissertation provides evidence that mice may be a potentially valuable new model for studies on the visual and genetic control of eye growth and myopia. Although the mouse is not predominantly a visual animal, it was shown that visual functions and ocular biometry can be studied *in vivo* using optical techniques. In addition, the study provides a paraxial schematic eye model for the growing mouse and shows how spatial vision changes with illuminance, and how the rod and cone photoreceptors contribute. Finally, it was demonstrated, to which extent diffusers, spectacle lenses and atropine affect spatial vision.

1. A paraxial schematic eye model for the growing C57BL/6 mouse

The measured refractive errors were initially $+4.0 \pm 0.6$ D at approximately 30 days, and levelled off with $+7.0 \pm 2.5$ D at about 70 days. Corneal radius of curvature did not change with age (1.414 ± 0.019 mm). Both axial lens diameter and axial eye length grew linearly (regression equations: lens: $1619 \mu\text{m} + 5.5 \mu\text{m}$ per day, $R=0.92$; axial length: $2899 \mu\text{m} + 4.4 \mu\text{m}$ per day, $R=0.94$). The lens grew so fast that vitreous chamber depth declined with age (regression equation: $896 \mu\text{m} - 3.2 \mu\text{m}$ per day, $R=0.69$). The radii of curvature of the anterior lens surface increased during development (from 0.982 mm at day 22 to 1.208 mm at day 100), whereas the radii of the posterior lens surface remained constant (-1.081 ± 0.054 mm). The calculated homogeneous lens index increased linearly with age (from 1.568 to 1.605). The small eye artifact, as calculated from the dioptric difference of the positions of the vitreo-retinal interface and the photoreceptor plane, increased from +35.2 D to +39.1 D, which was much higher than the hyperopia measured with photorefractometry. Retinal image magnification increased from 31 to 34 $\mu\text{m}/\text{deg}$, and the f-number remained ≤ 1 at all ages, suggesting a bright retinal image. A calculated axial eye elongation of 5.4 to 6.5 μm was sufficient to make the schematic eye 1 D more myopic.

In conclusion, one of the reasons why the mouse eye is a challenging model to study the development of myopia is its relatively slow growth rate, making long treatment periods necessary to induce significant deprivation myopia.

2. *In vivo* biometry in the mouse eye with optical low coherence interferometry

The second part of the dissertation demonstrated that OLCI is a powerful technique to resolve tiny differences in ocular biometry in living mouse eyes. Axial length could be determined with an average standard deviation of 8.0 ± 2.9 μm , corneal thickness with 3.5 ± 2.1 μm and anterior chamber depth with 10.6 ± 12.3 μm . Neither axial length, nor corneal thickness, nor anterior chamber depth were significantly different in left and right eyes of individual mice that had normal visual experience (mean absolute difference between axial lengths: 17 ± 18 μm , between corneal thickness 5.1 ± 4.8 μm , and between anterior chamber depths 16.7 ± 14.8 μm). Compared to the variability that was previously found in frozen sections, the variability of axial length measurements with OLCI was 2.7 times less.

After two weeks of form deprivation, OLCI revealed a significant axial elongation in the occluded eyes, compared to the contralateral fellow eyes ($+38 \pm 36$ μm or 1.16%). In this sample, no accompanying myopic shift was observed in the occluded eyes, but this observation is not so unexpected, given the inherently variable responses of mouse eye growth to visual deprivation.

In conclusion, axial length changes of 8 μm , equivalent to a dioptric change of about 2 D, could be detected in mouse eyes. However, the natural variability of the inter-ocular differences between both eyes requires that axial changes are induced by deprivation in the range of 20 μm , equivalent to about 4 D, to be reliably detected.

3. Grating acuity at different illuminances in wild-type mice, and in mice lacking rod or cone function

The optomotor drum provided reliable data on the visual input to the mouse behavior and was convenient to use since the only experimenter's action was to place the mice individually in a perspex cylinder. Optomotor grating acuity of the wild-type mice was limited to 0.30 to 0.40 cyc/deg. Maximal optomotor responses were obtained at 0.10 to 0.20 cyc/deg. The importance of visual input declined monotonically with decreasing illuminance (400 lux: 100%, 20 lux: 76.4%, 2 lux: 45.9%, darkness -9%). Mice lacking functional rods were able to resolve gratings up to 0.10 cyc/deg at 400 lux. Surprisingly, mice lacking functional cones had an optomotor acuity that was similar to the wild-type. Double knock-out mice without rods and cones had no detectable grating acuity.

In conclusion, since the visual system of the mouse is more responsive at bright illumination, studies on the visual control of eye growth should be done at reasonable light levels (about 400 lux or even higher). Apparently, the rods represent the high acuity system in the mouse with little contribution from the cones. The retinal melanopsin system does not contribute to spatial vision, since double knock-outs without rods and cones did not respond to the optomotor drum.

4. Contrast thresholds of wild-type mice wearing diffusers or spectacle lenses, and the effect of atropine, a myopia inhibiting drug

The range of spatial frequencies, at which the mice responded to stripes with lowered contrast was rather small. At 0.03 cyc/deg, the mice responded to stripes with a contrast down to 24%. At 0.10 cyc/deg, the minimal contrast was 45%, and at 0.30 cyc/deg, only the maximum contrast (91%) elicited a significant optomotor response. In dim light, spatial vision was severely impaired and only the lowest spatial frequencies, presented at the highest contrast were detected. The magnitude of optomotor responses was similar

VI. Summary

over a wide range of spectacle lens powers (at least ± 10 D), indicating a large depth of focus. No visual input was detected when occluders blurred the retinal image. Finally, atropine improved contrast sensitivity, at least, at the lowest spatial frequency tested, a result that was previously obtained also in the chicken and could help to explain the inhibitory effect of atropine on myopia.

In conclusion, it was found that spatial vision in wild-type mice was sensitive to defocus, that diffusers completely removed visual input, that the contrast thresholds increased when illuminance declined and that atropine, shown to suppress myopia in other animal models, in fact enhanced contrast sensitivity.

VII. References

Abdeljalil, J., Hamid, M., Abdel-mouttalib, O., Stephane, R., Raymond, R., Johan, A., Jose, S., Pierre, C., & Serge, P. (2005). The optomotor response: A robust first-line visual screening method for mice. *Vision Research*, *45*, 1439-1446.

Acosta, E., Vazquez, D., Smith, G., & Garner, L. (2003). A comparison and analysis of various techniques for determining the gradient index distribution of non-symmetric crystalline lenses. available:
<http://research.opt.indiana.edu/Meetings/Mopane2003/Acosta/Acosta.pdf>.

Al-Bdour, M. D., Odat, T. A., & Tahat, A. A. (2001). Myopia and level of education. *European Journal of Ophthalmology*, *11*, 1-5.

Artal, P., Herreros de Tejada, P., Munoz Tedo, C., & Green, D. G. (1998). Retinal image quality in the rodent eye. *Visual Neuroscience*, *15*, 597-605.

Artal, P., Berrio, E., Guirao, A., & Piers, P. (2002). Contribution of the cornea and internal surfaces to the change of ocular aberrations with age. *Journal of the Optical Society of America A, Optics, Image Science and Vision*, *19*, 137-143.

Barnard, A. R., Appleford, J. M., Sekaran, S., et al. (2004). Residual photosensitivity in mice lacking both rod opsin and cone photoreceptor cyclic nucleotide gated channel 3 subunit. *Visual Neuroscience*, *21*, 675-683.

Bartmann, M., & Schaeffel, F. (1994). A simple mechanism for emmetropization without cues from accommodation or colour. *Vision Research*, *34*, 873-876.

Bear, J. C. (1991). Epidemiology and genetics of refractive anomalies. In: Grosvenor, T., & Flom, M. C. (eds), *Refractive anomalies: research and clinical applications*, (pp. 57-80). Boston: Butterworth-Heinemann.

Bedrossian, R. H. (1979). The effect of atropine on myopia. *Ophthalmology*, *86*, 713-719.

Beuerman, R. W., Barathi, A., Weon, S. R., & Tan, D. (2003). Two models of experimental myopia in the mouse. *Investigative Ophthalmology and Visual Science*, *44*, ARVO E-Abstract, 4338.

Biel, M., Seeliger, M., Pfeifer, A., et al. (1999). Selective loss of cone function in mice lacking the cyclic nucleotide-gated channel CNG3. *Proceedings of the National Academy of Sciences USA*, *96*, 7553-7557.

Biel, M., Zong, X., Ludwig, A., Sautter, A., & Hofmann, F. (1999). Structure and function of cyclic nucleotide-gated channels. *Reviews of Physiology, Biochemistry and Pharmacology*, *135*, 151-171.

Birch, D., & Jacobs, G. H. (1979). Spatial contrast sensitivity in albino and pigmented rats. *Vision Research*, *19*, 933-938.

VII. References

- Bitzer, M., & Schaeffel, F. (2002). Defocus-induced changes in ZENK expression in the chicken retina. *Investigative Ophthalmology and Visual Science*, *43*, 246-252.
- Blake, R., Cool, S., & Crawford, M. (1974). Visual resolution in the cat. *Vision Research*, *14*, 1211-1218.
- Bodis-Wollner, I., & Tzelepi, A. (1998). The push-pull action of dopamine on spatial tuning of the monkey retina: the effects of dopaminergic deficiency and selective D1 and D2 receptor ligands on the pattern electroretinogram. *Vision Research*, *38*, 1479-1487.
- Bradley, D. V., Fernandes, A., Lynn, M., Tigges, M., & Boothe, R. G. (1999). Emmetropization in the rhesus monkey: from birth to young adulthood. *Investigative Ophthalmology and Visual Science*, *40*, 214-229.
- Campbell, M. C. W. (1984). Measurement of refractive index in an intact crystalline lens. *Vision Research*, *24*, 409-415.
- Carter-Dawson, L. D., & La Vail, M. M. (1979). Rods and cones in the mouse retina I. Structural analysis using light and electron microscopy. *Journal of Comparative Neurology*, *188*, 245-262.
- Chan, O. Y., & Edwards, M. (1993). Refractive errors in Hong Kong Chinese pre-school children. *Optometry and Vision Science*, *70*, 501-505.
- Charman, W. N., & Tucker, J. (1973). Optical system of the goldfish eye. *Vision Research*, *13*, 1-8.
- Chaudhuri, A., Hallett, P. E., & Parker, J. A. (1983). Aspheric curvatures, refractive indices and chromatic aberration for the rat eye. *Vision Research*, *23*, 1351-1364.
- Cheng, X., Bradley, A., Hong, X., & Thibos, L. N. (2003). Relationship between refractive error and monochromatic aberrations of the eye. *Optometry and Vision Science*, *80*, 43-49.
- Chua, W. H., Balakrishnan, V., Tan, D., Chan, Y., & ATOM Study Group. (2003). Efficacy results from the atropine in the treatment of myopia (ATOM) study. *Investigative Ophthalmology and Visual Science*, *44*, ARVO E-Abstract, 3119.
- Chua, W. H. (2004) Presentation at a special interest group meeting on myopia at ARVO 2004.
- Claes, E., Seeliger, M., Michalakis, S., Biel, M., Humphries, P., & Haverkamp, S. (2004). Morphological characterization of the retina of a CNGA3^{-/-}RHO^{-/-} mutant mouse lacking functional cones and rods. *Investigative Ophthalmology and Visual Science*, *45*, 2039-2048.
- Coletta, N. J., Marcos, S., Wildsoet, C., & Troilo, D. (2003). Double-pass measurement of retinal image quality in the chicken eye. *Optometry and Vision Science*, *80*, 50-57.
- Cook, R. C., & Glasscock, R. E. (1951). Refractive and ocular findings in the newborn. *American Journal of Ophthalmology*, *34*, 1407-1413.

VII. References

- Cook, C. A., Koretz, J. F., Pfahnl, A., Hyun, J., & Kaufman, P. L. (1994). Aging of the human crystalline lens and anterior segment. *Vision Research*, *34*, 2945-2954.
- De Valois, R., Morgan, H., & Snodderly, D. (1974). Psychophysical studies of monkey vision III. Spatial luminance contrast sensitivity tests of macaque and human observers. *Vision Research*, *14*, 75-81.
- Diepes, H. (1975). Refraktionsbestimmung, (pp. 82-85). Pforzheim, Germany: Bode.
- Diether, S., & Schaeffel, F. (1997). Local changes in eye growth induced by imposed local refractive error despite active accommodation. *Vision Research*, *37*, 659-668.
- Diether, S., & Schaeffel, F. (1999). Long-term changes in retinal contrast sensitivity in chicks from frosted occluders and drugs: relations to myopia? *Vision Research*, *39*, 2499-2510.
- Diether, S., Schaeffel, F., Fritsch, C., Trendelenburg, A. U., Payor, R., & Lambrou, G. (2004). Contralateral inhibition of lens induced myopia in the chick by ipsilateral intravitreal atropine application: can a simple dilution model account for the effect? *Investigative Ophthalmology and Visual Science*, *45*, ARVO E-Abstract, 1238.
- Drager, U. C. (1975). Receptive fields of single cells and topography in mouse visual cortex. *Journal of Comparative Neurology*, *160*, 269-290.
- Drager, U. C. (1978). Observations on monocular deprivation in mice. *Journal of Neurophysiology*, *41*, 28-42.
- Drexler, W., Baumgartner, A., Findl, O., Hitzenberger, C. K., Sattman, H., & Fercher, A. F. (1997). Submicrometer precision biometry of the anterior segment of the human eye. *Investigative Ophthalmology and Visual Science*, *38*, 1304 - 1313.
- Feldkaemper, M. P., Wang, H. Y., & Schaeffel, F. (2000). Changes in retinal and choroidal gene expression during development of refractive errors in chicks. *Investigative Ophthalmology and Visual Science*, *41*, 1623-1628.
- Fernandes, A., Yin, H., Byron, E. A., Iuvone, P. M., Schaeffel, F., Williams, R. W., & Pardue, M. T. (2004). Effects of form deprivation on eye size and refraction in C57BL/6J mice. *Investigative Ophthalmology and Visual Science*, *45*, ARVO E-Abstract, 4280.
- Fincham, W. H. A., & Freeman, M. H. (1974). Optics, 8th edition, London: Butterworth.
- Fledelius, H. C., & Christensen, A. C. (1996). Reappraisal of the human ocular growth curve in fetal life, infancy, and early childhood. *British Journal of Ophthalmology*, *80*, 918-921.
- Foster, F. S., Zhang, M. Y., Duckett, A. S., Cucevic, V., & Pavlin, C. J. (2003). *In vivo* imaging of embryonic development in the mouse eye by ultrasound biomicroscopy. *Investigative Ophthalmology and Visual Science*, *44*, 2361-2366.
- Gee, S. S., & Tabbara, K. F. (1988). Increase in ocular axial length in patients with corneal opacification. *Ophthalmology*, *95*, 1276-1278.

VII. References

- Geiger, S. N., Jaissle, G. B., Zrenner, E., Biel, M., & Seeliger, M. W. (2003). Properties of rod-mediated flicker assessed in the CNGA3 mouse model lacking cone function. *Investigative Ophthalmology and Visual Science* 44, ARVO E-Abstract, 1871.
- Gianfranceschi, L., Fiorentini, A., & Maffei, L. (1999). Behavioral visual acuity of wild-type and bcl2 transgenic mouse. *Vision Research*, 39, 569-574.
- Gianfranceschi, L., Siciliano, R., Walls, J., Morales, B., Kirkwood, A., Huang, Z. J., Tonegawa, S., & Maffei, L. (2003). Visual cortex is rescued from the effects of dark rearing by overexpression of BDNF. *Proceedings of the National Academy of Sciences USA*, 100, 12486-12491.
- Gimbel, H. V. (1973). The control of myopia with atropine. *Canadian Journal of Ophthalmology*, 8, 527-532.
- Glickstein, M., & Millodot, M. (1970). Retinoscopy and eye size. *Science*, 168, 605-606.
- Gordon, R. A., & Donzis, P. B. (1985). Refractive development of the human eye. *Archives of Ophthalmology*, 103, 785-789.
- Gordon, J. A., & Stryker, M. P. (1996). Experience-dependent plasticity of binocular responses in the primary visual cortex of the mouse. *Journal of Neuroscience*, 16, 3274-3286.
- Graham, B., & Judge, S. J. (1999). Normal development of refractive state and ocular component dimensions in the marmoset *Callithrix jacchus*. *Vision Research*, 39, 177-187.
- Gur, M., & Sivak, J. G. (1979). Refractive state of the eye of a small diurnal mammal: the ground squirrel. *American Journal of Optometry and Physiological Optics*, 56, 689-695.
- Gwiazda, J., Thorn, F., Bauer, J., & Held, R. (1993). Emmetropization and the progression of manifest refraction in children followed from infancy to puberty. *Clinical Vision Science*, 8, 337-344.
- Gwiazda, J., Hyman, L., Hussein, M., et al. (2003). A randomized clinical trial of progressive addition lenses versus single vision lenses on the progression of myopia in children. *Investigative Ophthalmology and Visual Science*, 44, 1492-1500.
- Hammond, C. J., Snieder, H., Gilbert, C. E., & Spector, T. D. (2001). Genes and environment in refractive error: the twin eye study. *Investigative Ophthalmology and Visual Science*, 42, 1232-1236.
- Hattar, S., Lucas, R. J., Mrosovsky, N., et al. (2003). Melanopsin and rod-cone photoreceptive systems account for all major accessory visual functions in mice. *Nature*, 3, 76-81.
- He, J. C., Sun, P., Held, R., Thorn, F., Sun, X., & Gwiazda, J. E. (2002). Wavefront aberrations in eyes of emmetropic and moderately myopic school children and young adults. *Vision Research*, 42, 1063-1070.

VII. References

- Herreros de Tejada, P., Munoz Tedo, C., & Costi, C. (1997). Behavioral estimates of absolute visual threshold in mice. *Vision Research*, *37*, 2427-2432.
- Hitzenberger, C. K. (1991). Optical measurement of the axial eye length by laser doppler interferometry. *Investigative Ophthalmology and Visual Science*, *32*, 616-624.
- Hodos, W., & Kuenzel, W. J. (1984). Retinal-image degradation produces ocular enlargement in chicks. *Investigative Ophthalmology and Visual Science*, *25*, 652-659.
- Howlett, M. C., & McFadden, S. A. (2002). A fast and effective mammalian model to study the visual regulation of eye growth. *Investigative Ophthalmology and Visual Science*, *43*, ARVO E-Abstract, 2928.
- Hoyt, C. S., Stone, R. D., Fromer, C., & Billson, F. A. (1981). Monocular axial myopia associated with neonatal eyelid closure in human infants. *American Journal of Ophthalmology*, *91*, 197-200.
- Huang, Z. J., Kirkwood, A., Pizzorusso, T., Porciatti, V., Morales, B., Bear, M. F., Maffei, L., & Tonegawa, S. (1999). BDNF regulates the maturation of inhibition and the critical period of plasticity in mouse visual cortex. *Cell*, *98*, 739-755.
- Hughes, A. (1977). The topography of vision in mammals of contrasting life style: comparative optics and retinal organization. In: Crescitelli, F. (ed), *Handbook of Sensory Physiology*, Vol. VIII/5 (pp. 613-756). Berlin, Heidelberg, New York: Springer.
- Hughes, A. (1979). A schematic eye for the rat. *Vision Research*, *19*, 569-588.
- Humphries, M. M., Rancourt, D., Farrar, G. J., et al. (1997). Retinopathy induced in mice by targeted disruption of the rhodopsin gene. *Nature Genetics*, *15*, 216-219.
- Hung, L. F., Crawford, M. L., & Smith, E. L. (1995). Spectacle lenses alter eye growth and the refractive status of young monkeys. *Nature Medicine*, *1*, 761-765.
- Irving, E. L., Callender, M. G., & Sivak, J. G. (1991). Inducing myopia, hyperopia, and astigmatism in chicks. *Optometry and Vision Science*, *68*, 364-368.
- Irving, E. L., Sivak, J. G., & Callender, M. G. (1992). Refractive plasticity of the developing chick eye. *Ophthalmic Physiological Optics*, *12*, 448-456.
- Irving, E. L., Sivak, J. G., Curry, T. A., & Callender, M. G. (1996). Chick eye optics: zero to fourteen days. *Journal of Comparative Physiology A*, *179*, 185-194.
- Jacobs, G. H., Neitz, J., & Deegan, J. F. (1991). Retinal receptors in rodents maximally sensitive to ultraviolet light. *Nature*, *353*, 655-656.
- Jacobs, G. H., Williams, G. A., & Fenwick, J. A. (2004). Influence of cone pigment coexpression on spectral sensitivity and color vision in the mouse. *Vision Research*, *44*, 1615-1622.
- Jaissle, G. B., May, C. A., Reinhard, J., et al. (2001). Evaluation of the rhodopsin knock-out mouse as a model of pure cone function. *Investigative Ophthalmology and Visual Science*, *42*, 506-513.

VII. References

- Jeon, C. J., Strettoi, E., & Masland, R. H. (1998). The major cell populations of the mouse retina. *Journal of Neuroscience*, *18*, 8936-8946.
- Jester, J. V., Lee, Y. G., Li, J., Chakravarti, S., Paul, J., Petroll, W., & Cavanagh, H. D. (2001). Measurement of corneal sublayer thickness and transparency in transgenic mice with altered corneal clarity using in vivo confocal microscopy. *Vision Research*, *41*, 1283-1290.
- Katz, J., Tielsch, J. M., & Sommer, A. (1997). Prevalence and risk factors for refractive errors in an adult inner city population. *Investigative Ophthalmology and Visual Science*, *38*, 334-340.
- Kiely, P. M., Crewther, S. G., Nathan, J., Brennan, N. A., Efron, N., & Madigan, M. A. (1987). A comparison of ocular development of the cynomolgus monkey and man. *Clinical Vision Science*, *1*, 269-280.
- Kroger, R. H., Campbell, M. C., Fernald, R. D., & Wagner, H. J. (1999). Multifocal lenses compensate for chromatic defocus in vertebrate eyes. *Journal of Comparative Physiology A*, *184*, 361-369.
- Krumpaszy, H. G., Haas, A., Klauss, V., & Selbmann, H. K. (1997). New blindness incidents in Wurttemberg-Hohenzollern. *Ophthalmologe*, *94*, 234-236.
- Larsen, J. S. (1971a). The sagittal growth of the eye. III. Ultrasonic measurement of the posterior segment (axial length of the vitreous) from birth to puberty. *Acta Ophthalmologica (Copenhagen)*, *49*, 239-262.
- Larsen, J. S. (1971b). The sagittal growth of the eye. II. Ultrasonic measurement of the axial diameter of the lens and the anterior segment from birth to puberty. *Acta Ophthalmologica (Copenhagen)*, *49*, 427-440.
- Luu, C. D., Lau, A. M. I., Koh, A. H. C., & Tan, D. (2005) Multifocal electroretinogram in children on atropine treatment for myopia. *British Journal of Ophthalmology*, *89*, 151-153.
- Mangini, N. J., & Pearlman, A. L. (1980). Laminar distribution of receptive field properties in the primary visual cortex of the mouse. *Journal of Comparative Neurology*, *193*, 203-222.
- Marshall, J., Mellerio, J., & Palmer, D. A. (1973). A schematic eye for the pigeon. *Vision Research*, *13*, 2449-2453.
- Martin, G. (1986). Limits of visual resolution. *Nature*, *319*, 540.
- Mathis, U., Schaeffel, F., & Howland, H. C. (1988). Visual optics in toads (*Bufo americanus*). *Journal of Comparative Physiology A*, *163*, 201-213.
- McBrien, N. A., & Millodot, M. (1987). A biometric investigation of late onset myopic eyes. *Acta Ophthalmologica (Copenhagen)*, *65*, 461-468.
- McBrien, N. A., Moghaddam, H. O., New, R., & Williams, L. R. (1993a). Experimental myopia in a diurnal mammal (*Sciurus carolinensis*) with no accommodative ability. *Journal of Physiology*, *469*, 427-441

VII. References

- McBrien, N. A., Moghaddam, H. O., & Reeder, A. P. (1993b). Atropine reduces experimental myopia and eye enlargement via a nonaccommodative mechanism. *Investigative Ophthalmology and Visual Science*, *34*, 205-215.
- McBrien, N. A., Moghaddam, H. O., Cottrill, C. L., Leech, E. M., & Cornell, L. M. (1995). The effects of blockade of retinal cell action potentials on ocular growth, emmetropization and form deprivation myopia in young chicks. *Vision Research*, *35*, 1141-1152.
- McFadden, S. A., Howlett, M. H., & Mertz, J. R. (2004). Retinoic acid signals the direction of ocular elongation in the guinea pig eye. *Vision Research*, *44*, 643-653.
- McGill, T. J., Douglas, R. M., Lund, R. D., & Prusky, G. T. (2004). Quantification of spatial vision in the royal college of surgeons rat. *Investigative Ophthalmology and Visual Science*, *45*, 932-936.
- McLean, R. C., & Wallman, J. (2003). Severe astigmatic blur does not interfere with spectacle lens compensation. *Investigative Ophthalmology and Visual Science*, *44*, 449-457.
- Merigan, W. H. (1976). The contrast sensitivity of the squirrel monkey. *Vision Research*, *16*, 375-379.
- Mertz, J. R., Nickla, D., & Troilo, D. (2000). Choroidal retinoic acid synthesis in a primate model of eye growth: the common marmoset. In: Thorn, F., Troilo, D., & Gwiazda, J. (eds), *Proceedings of the VIII International Conference on Myopia*, (pp. 200-204). Boston: The New College of Optometry.
- Millodot, M., & Blough, P. (1971). The refractive state of the pigeon eye. *Vision Research*, *11*, 1019-1022.
- Mitchiner, J. C., Pinto, L. H., & Venable, J. W. (1976). Visually evoked eye movements in the mouse. *Vision Research*, *16*, 1169-1171.
- Morgan, I., & Rose, K. (2005). How genetic is school myopia? *Progress in Retinal eye Research*, *24*, 1-38.
- Mouse Genome Sequencing Consortium (2002). Initial sequencing and comparative analysis of the mouse genome. *Nature*, *420*, 520-562.
- Mutti, D. O., Ver Hoeve, J. N., Zadnik, K., & Murphy, C. J. (1997). The artifact of retinoscopy revisited: comparison of refractive error measured by retinoscopy and visual evoked potential in the rat. *Optometry and Vision Science*, *74*, 483-488.
- Mutti, D. O., Mitchell, G. L., Moeschberger, M. L., Jones, L. A., & Zadnik, K. (2002). Parental myopia, near work, school achievement, and children's refractive error. *Investigative Ophthalmology and Visual Science*, *43*, 3633-3640.
- Napper, G. A., Brennan, N. A., Barrington, M., Squires, M. A., Vessey, G. A., & Vingrys, A. J. (1995). The duration of normal visual exposure necessary to prevent form deprivation myopia in chicks. *Vision Research*, *35*, 1337-1344.

VII. References

- Norton, T. T. (1990). Experimental myopia in tree shrews. In: Bock, G. R., & Widdows, K. (eds). *Myopia and the control of eye growth*, Vol. 155 (pp. 178-194). West Sussex: John Wiley & Sons Ltd.
- Norton, T. T., & McBrien, N. A. (1992). Normal development of refractive state and ocular component dimensions in the tree shrew. *Vision Research*, 32, 833-842.
- Norton, T. T., Essinger, J. A., & McBrien, N. A. (1994). Lid-suture myopia in tree shrews with retinal ganglion cell blockade. *Visual Neuroscience*, 11, 143-153.
- Norton, T. T., Wu, W. W., & Siegwart, J. T. (2003). Refractive state of tree shrew eyes measured with cortical visual evoked potentials. *Optometry and Vision Science*, 80, 623-631.
- Nye, P. W. (1976). The binocular acuity of the pigeon measured in terms of the modulation transfer function. *Vision Research*, 8, 1041-1053.
- Ohngemach, S., Hagel, G., & Schaeffel, F. (1997). Concentrations of biogenic amines in fundal layers in chickens with normal visual experience, deprivation, and after reserpine application. *Visual Neuroscience*, 14, 493-505.
- Ott, M., & Schaeffel, F. (1995). A negatively powered lens in the chameleon. *Nature*, 373, 692-694.
- Oyster, C. W. (1999). *The human eye: structure and function*. Sunderland, Massachusetts: Sinauer Associates.
- Pacella, R., McLellan, J., Grice, K., Del Bono, E. A., Wiggs, J. L., & Gwiazda, J. E. (1999). Role of genetic factors in the etiology of juvenile-onset myopia based on a longitudinal study of refractive error. *Optometry and Vision Science*, 76, 381-386.
- Panda, S., Provencio, I., Tu, D. C., et al. (2003). Melanopsin is required for non-image forming photic responses in blind mice. *Science*, 25, 525-527.
- Park, T., Winawer, J., & Wallman, J. (2001). In a matter of minutes the eye can know which way to grow. *Cited by: Wallman, J., & Winawer, J. (2004). Homeostasis of eye growth and the question of myopia (Review). Neuron*, 43, 447-468.
- Park, T., Winawer, J., & Wallman, J. (2003). Further evidence that chick eyes use the sign of blur in spectacle lens compensation. *Vision Research*, 43, 1519-1531.
- Pennesi, M. E., Lyubarsky, A. L., & Pugh, E. N. (1998). Extreme responsiveness of the pupil of the dark-adapted mouse to steady retinal illumination. *Investigative Ophthalmology and Visual Science*, 39, 2148-2156.
- Pennie, F. C., Wood, I. C., Olsen, C., White, S., & Charman, W. N. (2001). A longitudinal study of the biometric and refractive changes in full-term infants during the first year of life. *Vision Research*, 41, 2799-2810.
- Perry, V. H., & Cowey, A. (1985). The ganglion cell and cone distributions in the monkey's retina: implications for central magnification factors. *Vision Research*, 25, 1795-1810.

VII. References

- Pettigrew, J. D., Dreher, B., Hopkins, C. S., McCall, M. J., & Brown, M. (1988). Peak density and distribution of ganglion cells in the retinae of microchiropteran bats: implications for visual acuity. *Brain, Behavior and Evolution*, *32*, 39-56.
- Pickett-Seltner, R. L., Weerheim, J., Sivak, J. G., & Pasternak, J. (1987). Experimentally induced myopia does not affect post-hatching development of the chick lens. *Vision Research*, *27*, 1779-1783.
- Pickett-Seltner, R. L., Sivak, J. G., & Pasternak, J. J. (1988). Experimentally induced myopia in chicks: morphometric and biochemical analysis during the first 14 days after hatching. *Vision Research*, *28*, 323-328.
- Porciatti, V., Pizzorusso, T., Cenni, M. C., & Maffei, L. (1996). The visual response of retinal ganglion cells is not altered by optic nerve transection in transgenic mice overexpressing Bcl-2. *Proceedings of the National Academy of Sciences USA*, *93*, 14955-14959.
- Porciatti, V., Pizzorusso, T., & Maffei, L. (1999). The visual physiology of the wild-type mouse determined with pattern VEPs. *Vision Research*, *39*, 3071-3081.
- Prusky, G. T., West, P. W., & Douglas, R. M. (2000a). Behavioral assessment of visual acuity in mice and rats. *Vision Research*, *40*, 2201-2209.
- Prusky, G. T., Reidel, C., & Douglas, R. M. (2000b). Environmental enrichment from birth enhances visual acuity but not place learning in mice. *Behavioural Brain Research*, *114*, 11-15.
- Prusky, G. T., & Douglas, R. M. (2003). Developmental plasticity of mouse visual acuity. *European Journal of Neuroscience*, *17*, 167-173.
- Prusky, G. T., Alam, N. M., Beekman, S., & Douglas, R. M. (2004). Rapid quantification of adult and developing mouse spatial vision using a virtual optomotor system. *Investigative Ophthalmology and Visual Science*, *45*, 4611-4616.
- Prusky, G. T., & Douglas, R. M. (2004). Characterization of mouse cortical spatial vision. *Vision Research*, *44*, 3411-3418.
- Rabin, J., Van Sluyters, R. C., & Malach, R. (1981). Emmetropization: a vision-dependent phenomenon. *Investigative Ophthalmology and Visual Science*, *20*, 561-564.
- Rajan, U., Saw, S. M., Lau, C., O'Brien, L., Chan, T. K., Lam, D. S. C., & Chew, S. J. (1998). Prevalence of myopia in school children and risk factors for its progression. In: Tokoro, T. (ed), *Myopia Updates*, (pp. 69-80). Tokyo, Berlin, Heidelberg, New York: Springer.
- Raviola, E., & Wiesel, T. N. (1985). An animal model of myopia. *The New England Journal of Medicine*, *312*, 1609-1615.
- Remtulla, S., & Hallett, P. E. (1985). A schematic eye for the mouse and comparison with the rat. *Vision Research*, *25*, 21-32.

VII. References

- Ridder, W., & Nusinowitz, S. (2002). Sweep VEP acuity in mice. *Investigative Ophthalmology and Visual Science*, 43, ARVO E-Abstract, 1802.
- Rohrer, B., Schaeffel, F., & Zrenner, E. (1992). Longitudinal chromatic aberration and emmetropization: results from the chicken eye. *The Journal of Physiology*, 449, 363-376.
- Rohrer, B., Iuvone, P. M., & Stell, W. K. (1995). Stimulation of dopaminergic amacrine cells by stroboscopic illumination or fibroblast growth factor (bFGF, FGF-2) injections: possible roles in prevention of form-deprivation myopia in the chick. *Brain Research*, 686, 169-181.
- Rose, K., Smith, W., Morgan, I., & Mitchell, P. (2001). The increasing prevalence of myopia: implication for Australia. *Clinical Experimental Ophthalmology*, 29, 116-120.
- Rossi, F. M., Pizzorusso, T., Porciatti, V., Marubio, L. M., Maffei, L., & Changeux, J. P. (2001). Requirement of the nicotinic acetylcholine receptor $\beta 2$ subunit for the anatomical and functional development of the visual system. *Proceedings of the National Academy of Sciences USA*, 98, 6453-6458.
- Saw, S. M., Hong, R. Z., Zhang, M. Z., Fu, Z. F., Ye, M., Tan, D., & Chew, S. J. (2001). Near-work activity and myopia in rural and urban schoolchildren in China. *Journal of Pediatric Ophthalmology and Strabismus*, 38, 149-155.
- Saw, S. M. (2003). A synopsis of the prevalence rates and environmental risk factors for myopia. *Clinical and Experimental Optometry*, 86, 289-294.
- Schaeffel, F., Howland, H. C., & Farkas, L. (1986). Natural accommodation in the growing chicken. *Vision Research*, 26, 1977-1993.
- Schaeffel, F., Glasser, A., & Howland, H. C. (1988). Accommodation, refractive error and eye growth in chickens. *Vision Research*, 28, 639-657.
- Schaeffel, F., & Howland, H. C. (1988a). Visual optics in normal and ametropic chickens. *Clinical Vision Science*, 3, 83-98.
- Schaeffel, F., & Howland, H. C. (1988b). Mathematical model of emmetropization in the chicken. *Journal of the Optical Society of America A*, 5, 2080-2086.
- Schaeffel, F., Troilo, D., Wallman, J., & Howland, H. C. (1990). Developing eyes that lack accommodation grow to compensate for imposed defocus. *Visual Neuroscience*, 4, 177-183.
- Schaeffel, F., & Howland, H. C. (1991). Properties of the feedback loops controlling eye growth and refractive state in the chicken. *Vision Research*, 31, 717-734.
- Schaeffel, F., & Wagner, H. (1996). Emmetropization and optical development of the eye of the barn owl (*Tyto alba*). *Journal of Comparative Physiology A*, 178, 491-498.
- Schaeffel, F., & Diether, S. (1999). The growing eye: an autofocus system that works on very poor images. *Vision Research*, 39, 1585-1589.

VII. References

- Schaeffel, F., & Burkhardt, E. (2002). Measurement of refractive state and deprivation myopia in the black wildtype mouse. *Investigative Ophthalmology and Visual Science*, 43, ARVO E-Abstract, 182.
- Schaeffel, F., & Howland, H. C. (2003). Axial length changes in myopic mouse eyes. *Investigative Ophthalmology and Visual Science, Electronic letter*, April 25, 2003.
- Schaeffel, F., Burkhardt, E., Howland, H. C., & Williams, R. W. (2004). Measurement of refractive state and deprivation myopia in two strains of mice. *Optometry and Vision Science*, 81, 99-110.
- Schaeffel, F., & Burkhardt, E. (2005). Pupillographic evaluation of the time course of atropine effects in the mouse eye. *Optometry and Vision Science*, 82, 215-220.
- Schmid, K. L., & Wildsoet, C. F. (1997). Contrast and spatial-frequency requirements for emmetropization in chicks. *Vision Research*, 37, 2011-2021.
- Schmid, K. L., & Wildsoet, C. F. (2004). Inhibitory effects of apomorphine and atropine and their combination on myopia in chicks. *Optometry and Vision Science*, 81, 137-147.
- Schulz, D., Iliev, M. E., Frueh, B. E., & Goldblum, D. (2003). In vivo pachymetry in normal eyes of rats, mice and rabbits with the optical low coherence reflectometer. *Vision Research*, 43, 723-728.
- Schwahn, H. N., & Schaeffel, F. (1994). Chick eyes under cycloplegia compensate for spectacle lenses despite six-hydroxy dopamine treatment. *Investigative Ophthalmology and Visual Science*, 35, 3516-3524.
- Schwahn, H. N., & Schaeffel, F. (1997). Flicker parameters are different for suppression of myopia and hyperopia. *Vision Research*, 37, 2661-2673.
- Schwahn, H. N., Kaymak, H., & Schaeffel, F. (2000). Effects of atropine on refractive development, dopamine release and slow retinal potentials in the chick. *Visual Neuroscience*, 17, 165-176.
- Sharpe, L. T., & Stockman, A. (1999). Rod pathways: the importance of seeing nothing. *Trends in Neuroscience*, 22, 497-504.
- Sherman, S. M., Norton, T. T., & Casagrande, V. A. (1977). Myopia in the lid-sutured tree shrew (*Tupaia glis*). *Brain Research*, 124, 154-157.
- Siegwart, J. T., & Norton, T. T. (1998). The susceptible period for deprivation-induced myopia in tree shrew. *Vision Research*, 38, 3505-3515.
- Sinex, D. G., Burdette, L. J., & Pearlman, A. L. (1979). A psychophysical investigation of spatial vision in the normal and reeler mutant mouse. *Vision Research*, 19, 853-857.
- Sivak, J. G. (1974). The refractive error of the fish eye. *Vision Research*, 14, 209-213.
- Smith, E. L. 3rd, Harwerth, R. S., Crawford, M. L., & von Noorden, G. K. (1987). Observations on the effects of form deprivation on the refractive status of the monkey. *Investigative Ophthalmology and Visual Science*, 28, 1236-1245.

VII. References

- Smith, E. L. 3rd, Bradley, D. V., Fernandes, A., & Boothe, R. G. (1999). Form deprivation myopia in adolescent monkeys. *Optometry and Vision Science*, *76*, 428-432.
- Smith, E. L. 3rd, & Hung, L. F. (1999). The role of optical defocus in regulating refractive development in infant monkeys. *Vision Research*, *39*, 1415-1435.
- Smith, E. L. 3rd, & Hung, L. F. (2000). Form-deprivation myopia in monkeys is a graded phenomenon. *Vision Research*, *40*, 371-381.
- Smith, E. L. 3rd, Hung, L. F., Kee, C. S., & Qiao, Y. (2002). Effects of brief periods of unrestricted vision on the development of form-deprivation myopia in monkeys. *Investigative Ophthalmology and Visual Science*, *43*, 291-299.
- Stone, R. A., Lin, T., Laties, A. M., & Iuvone, P. M. (1989). Retinal dopamine and form-deprivation myopia. *Proceedings of the National Academy of Sciences USA*, *86*, 704-706.
- Stone, R. A., Sugimoto, R., Gill, A. S., Liu, J., Capehart, C., & Lindstrom, J. M. (2001). Effects of nicotinic antagonists on ocular growth and experimental myopia. *Investigative Ophthalmology and Visual Science*, *42*, 557-565.
- Sundberg, J. P., Smith, R. S., & John, S. W. M. (2002). Selection of controls. In: Smith, R. S. (ed), *Systematic evaluation of the mouse eye: anatomy, pathology and biomethods*, (pp. 77-80). Boca Raton, FL: CRC press.
- Tejedor, J., & de la Villa, P. (2003). Refractive changes induced by form deprivation in the mouse eye. *Investigative Ophthalmology and Visual Science*, *44*, 32-36.
- Thorn, F., Gollender, M., & Erickson, P. (1976). The development of the kitten's visual optics. *Vision Research*, *16*, 1145-1150.
- Thorn, F., Grice, K., Held, R., & Gwiazda, J. (1998). Myopia: Nature, nurture, and the blur hypothesis. In: Lin, L. L.-K., Shih, Y.-F., & Hung, P. T. (eds), *Myopia Updates II*, (pp. 89-93). Tokyo, Berlin, Heidelberg, New York: Springer.
- Tigges, M., Iuvone, P. M., Fernandes, A., Sugrue, M. F., Mallorga, P. J., Laties, A. M., & Stone, R. A. (1999). Effects of muscarinic cholinergic receptor antagonists on postnatal eye growth of rhesus monkeys. *Optometry and Vision Science*, *76*, 397-407.
- Troilo, D., Gottlieb, M. D., & Wallman, J. (1987). Visual deprivation causes myopia in chicks with optic nerve section. *Current Eye Research*, *6*, 993-999.
- Troilo, D., & Judge, S. J. (1993). Ocular development and visual deprivation myopia in the common marmoset *Callithrix jacchus*. *Vision Research*, *33*, 1311-1324.
- Troilo, D., & Nickla, D. L. (2002). The response to form deprivation by occluder in the marmoset differs with age of onset. *Investigative Ophthalmology and Visual Science*, *43*, ARVO E-Abstract, 186.

VII. References

- Truong, H. T., Cottrill, C. L., Gentle, A., & McBrien, N. A. (2002). Pirenzepine affects scleral metabolic changes in myopia through a non toxic mechanism. *Experimental Eye Research*, *74*, 103-111.
- Waessle, H. (1971). Optical quality of the cat eye. *Vision Research*, *11*, 995-1006.
- Wallman, J., Turkel, J., & Trachtman, J. (1978). Extreme myopia produced by modest change in early visual experience. *Science*, *29*, 1249-1251.
- Wallman, J., Adams, J. I., & Trachtman, J. N. (1981). The eyes of young chickens grow toward emmetropia. *Investigative Ophthalmology and Visual Science*, *20*, 557-561.
- Wallman, J., & Adams, J. I. (1987). Developmental aspects of experimental myopia in chicks: susceptibility, recovery and relation to emmetropization. *Vision Research*, *27*, 1139-63.
- Wallman, J., Gottlieb, M. D., Rajaram, V., & Fugate-Wentzek, L. A. (1987). Local retinal regions control local eye growth and myopia. *Science*, *237*, 73-77.
- Wallman, J. (1993). Retinal control of eye growth and refraction. *Progress in Retinal Eye Research*, *12*, 133-153.
- Wallman, J., Wildsoet, C., Xu, A., Gottlieb, M. D., Nickla, D. L., Marran, L., Krebs, W., & Christensen, A. M. (1995). Moving the retina: choroidal modulation of refractive state. *Vision Research*, *35*, 37-50.
- Wallman, J., & Winawer, J. (2004). Homeostasis of eye growth and the question of myopia (Review). *Neuron*, *43*, 447-468.
- Whatham, A. R., & Judge, S. J. (2001). Compensatory changes in eye growth and refraction induced by daily wear of soft contact lenses in young marmosets. *Vision Research*, *41*, 267-273.
- Wiesel, T. N., & Raviola, E. (1977). Myopia and eye enlargement after neonatal lid fusion in monkeys. *Nature*, *266*, 66-68.
- Wildsoet, C. F., & Pettigrew, J. D. (1988). Experimental myopia and anomalous eye growth patterns unaffected by optic nerve section in chickens: evidence for local control of eye growth. *Clinical Vision Science*, *3*, 99-107.
- Wildsoet, C. F., Howland, H. C., Falconer, S., & Dick, K. (1993). Chromatic aberration and accommodation: their role in emmetropization in the chick. *Vision Research*, *33*, 1593-1603.
- Wildsoet, C. F., & Wallman, J. (1995). Choroidal and scleral mechanisms of compensation for spectacle lenses in chicks. *Vision Research*, *35*, 1175-1194.
- Wildsoet, C. F., & Schmid, K. I. (2001). Emmetropization in chicks uses optical vergence and relative distance cues to decode defocus. *Vision Research*, *41*, 3197-3204.

VII. References

- Wildsoet, C. F. (2003). Neural pathways subserving negative lens-induced emmetropization in chicks - insights from selective lesions of the optic nerve and ciliary nerve. *Current Eye Research*, 27, 371-385.
- Winawer, J., & Wallman, J. (2002). Temporal constraints on lens compensation in chicks. *Vision Research*, 42, 2651-2668.
- Woods, R. L., Bradley, A., & Atchinson, D. A. (1996). Monocular diplopia caused by ocular aberrations and hyperopic defocus. *Vision Research*, 36, 3597-3606.
- Woolf, D. (1956). A comparative cytological study of the ciliary muscle. *Anatomical Record*, 124, 145-163.
- Wu, S. Y., Nemesure, B., & Leske, M. C. (1999). Refractive errors in a black adult population: the Barbados eye study. *Investigative Ophthalmology and Visual Science*, 40, 2179-2184.
- Yinon, U., Rose, L., & Shapiro, A. (1980). Myopia in the eye of developing chicks following monocular and binocular lid closure. *Vision Research*, 20, 137-141.
- Young, T. L., Ronan, S. M., Drahozal, L. A., et al. (1998). Evidence that a locus for familial high myopia maps to chromosome 18p. *American Journal of Human Genetics*, 63, 109-119.
- Zadnik, K., & Mutti, D. O. (1987). Refractive error changes in law students. *American Journal of Optometry and Physiological Optics*, 64, 558-561.
- Zadnik, K., Mutti, D. O., Fusaro, R. E., & Adams, A. J. (1995). Longitudinal evidence of crystalline lens thinning in children. *Investigative Ophthalmology and Visual Science*, 36, 1581-1587.
- Zeiss, C. (1987). Physiologische Optik des Auges. In: Handbuch fuer Augenoptik, Vol. 3 (pp. 61-98). Stuttgart: Maurer.
- Zhou, G., & Williams, R. W. (1999a). Eye1 and Eye2: gene loci that modulate eye size, lens weight, and retinal area in the mouse. *Investigative Ophthalmology and Visual Science*, 40, 817-825.
- Zhou, G., & Williams, R. W. (1999b). Mouse models for the analysis of myopia: an analysis of variation in eye size of adult mice. *Optometry and Vision Science*, 76, 408-418.

VIII. Publications and presentations in connection with this research work

Publications:

Schmucker, C., & Schaeffel, F. (2004a). A paraxial schematic eye model for the growing C57BL/6 mouse. *Vision Research*, 44(16), 1857-1867.

Schmucker, C., & Schaeffel, F. (2004b). In vivo biometry in the mouse eye with low coherence interferometry. *Vision Research*, 44(21), 2445-2456.

Schmucker, C., Seeliger, M., Humphries, P., Biel, M., & Schaeffel, F. (2005). Grating acuity at different luminances in wild-type mice and in mice lacking cone or rod function. *Investigative Ophthalmology and Visual Science*, 46(1), 398-407.

Schmucker, C., & Schaeffel, F. (2005). Contrast sensitivity of wild-type mice wearing diffusers or spectacle lenses, and the effect of atropine. *Vision Research*, submitted.

Presentations at National and International Meetings:

Schmucker, C., & Schaeffel, F. (2003). Die Maus als Modell für Myopie - Entwicklung der optischen Eigenschaften des Mausauges. *Arbeitskreis Ophthalmische Optik. Würzburg*.

Schmucker, C., & Schaeffel, F. (2004). In vivo biometry in the mouse eye with optical low coherence interferometry. *Arbeitskreis Ophthalmische Optik. Köln*.

Schmucker, C., & Schaeffel, F. (2004). A paraxial schematic eye model for the growing C57BL/6 mouse. *Investigative Ophthalmology and Visual Science 45, ARVO E-Abstract 4279*.

Schmucker, C., & Schaeffel, F. (2004). A battery of optical test to measure visual function and myopia in alert mice. *II EOS topical meeting on physiological optics. Granada*.

Garcia de la Cera, E., Rodriguez, G., Llorente, L., Schmucker, C., Schaeffel, F., & Marcos, S. (2005). Optical aberrations in the normal and anesthetized mouse eye. *Investigative Ophthalmology and Visual Science, ARVO E-Abstract 2009*.

IX. Acknowledgements

Als erstes möchte ich meinen Doktorvater Professor Dr. Frank Schaeffel danken, dass er mir die Gelegenheit gegeben hat, als „Exote“ eine Doktorarbeit in seiner Abteilung anzufertigen. Besonders möchte ich ihn für seine hervorragende Unterstützung, sein enormes Wissen und den unzähligen wissenschaftlichen Anregungen danken. Ich möchte ihn auch für das hervorragende Arbeitsklima danken, und dass er mir verschiedene Kongressbesuche ermöglichte.

Herrn Professor Dr. E. Zrenner danke ich, dass er mir die Möglichkeit gegeben hat, diese Arbeit an seiner Klinik anzufertigen.

Herrn Dr. M. Seeliger möchte ich danken, dass er verschiedene *knock-out* Mäuse zur Verfügung gestellt hat.

Herrn Willmann und seinen Kollegen aus der Feinmechanik-Werkstatt der Augenklinik danke ich für das Mit-Anfertigen der Optomotor Trommel.

Meinen Kollegen danke ich, dass sie immer hilfsbereit und aufmunternd waren, und das man wirklich gut mit ihnen zusammenarbeiten kann. Ganz besonders danke ich Eva Burkhardt für ihre ausgezeichnete technische Unterstützung.

Besonders möchte ich meinen Eltern und Bruder danken, dass sie mich stets unterstützt und ermutigt haben.

Con möchte ich für seine Geduld und sein Verständnis danken - und natürlich auch dafür, dass er meine Englisch Kenntnisse verbesserte.

X. Curriculum Vitae

NAME

Christine Maria Schmucker

GEBURTSDATUM / ORT

04. November 1974 in Weiden i. d. Opf.

SCHULAUSBILDUNG

Sept. 87 – Juli 91	Sophie-Scholl-Realschule Abschluss: Mittlere Reife	Weiden i. d. Opf.
Sept. 95 – Juli 97	Berufsoberschule Abschluss: Fachgebundene Hochschulreife	Regensburg

BERUFSAUSBILDUNG

Sept. 91 – Juli 94	Optik Stober Ausbildung zur Augenoptikerin	Weiden i. d. Opf.
--------------------	---	-------------------

HOCHSCHULAUSBILDUNG

März 98 – April 02	Fachhochschule Diplomstudiengang Augenoptik Diplomarbeit bei Dr. M. Woodhouse, Cardiff University "Dynamische und statische Akkommodation bei Kindern mit zerebralen Paresen"	Aalen
März 03 – gegenwärtig	Univ.-Augenklinik Promotion bei Prof. Dr. F. Schaeffel „Eye growth, optics and visual performance of the mouse, a new mammalian model to study myopia"	Tübingen

BERUFSERFAHRUNG

Aug. 94 – Aug. 95	Optik Gufler Augenoptikerin	Weiden i. d. Opf.
März 00 – April 00	Kontaktlinseninstitut Haunreiter Praktikum in der Kontaktlinsenanpassung	München
Mai 00 – Juni 00	Univ.-Augenklinik Klinisches Praktikum bei Prof. Lorenz	Regensburg
Aug. 02 – Feb. 03	Univ.-Augenklinik Wissenschaftliche Mitarbeiterin bei Prof. Lieb Betreuung einer Studie über akkommodative IOLs	Würzburg

AUSLANDSERFAHRUNG

Juli 00 – Sept. 00	Augenklinik Hilfsprojekt zur Versorgung Sehbehinderter	Malawi/Afrika
Sept. 01 – März 02	Department of Optometry and Vision Sciences Diplomarbeit	Cardiff